Contractile Properties of Striated Muscle in Development and Disease

Alice Ward Racca

A dissertation

submitted in partial fulfillment of the

requirements for the degree of

Doctor of Philosophy

University of Washington

2015

Reading Committee:

Michael Regnier, Chair

Michael Bamshad

Charles Asbury

Program Authorized to Offer Degree:

Department of Bioengineering

University of Washington

Abstract

Contractile Properties of Striated Muscle in Development and Disease

Alice Ward Racca

Chair of the Supervisory Committee:

Dr. Michael Regnier, Vice Chair and Washington Research Foundation Endowed Professor

Department of Bioengineering

In utero development is a key time for muscle formation, and muscle-related birth defects are sometimes linked to mutations in muscle contractile proteins expressed in utero. Even in heart disease, the development of the disease pre-dates the clinical symptoms; however, studying the developing muscle before it presents in clinic is difficult. Muscle contractility can be studied directly, and the use of multiple assays has allowed me to examine muscle development and disease at the protein, subcellular, and cellular level. Distal arthrogryposis is a skeletal muscle birth defect that can be caused by a mutation in embryonic myosin; herein, I have found that the continued muscle dysfunction is linked to a delay in relaxation, likely from slower cross-bridge detachment, and that this is not from an overexpression of embryonic myosin. Fetal muscle in which embryonic myosin is highly expressed is slow to activate and relax, and generates very little force, even compared to fetal cardiac muscle of a similar age. Fetal cardiac muscle develops more force as gestation increase, showing an increase in activation and relaxation rates, though the cross-bridge cycling rates appear to fluctuate, potentially as a function of structure. The fetal cardiac muscle is a good milestone for assessing the maturity of human induced pluripotent stem cell derived cardiomyocytes, which are used to model heart disease and therapeutics, and produce force at rates of activation and relaxation that are close to those of fetal cardiac myofibrils and not adult cardiac myofibrils. The human induced pluripotent stem cell derived cardiomyocytes from patients with known mutations show potentially early onset factors in cardiomyopathy. Finally, failing adult cardiac muscle demonstrates that the activation rate and force production of the myofilament can be enhanced without slowing the relaxation through using 2-deoxy-ATP.

Table of Contents

LIST of FIGURES

LIST of TABLES

Acknowledgements

I would like thank the study subjects for their participation.

Dedication

To Raymond Reynolds, who inspired me to pursue medical research

CHAPTER 1.   INTRODUCTION

During development, striated muscle undergoes vast changes in protein isoform and density. By identifying the key changes in muscle contraction that occur during fetal development, the mechanisms by which disease takes root are better elucidated and treated. Some diseases, such as the skeletal muscle syndromes collectively titled distal arthrogryposis, present *in utero*, making the study of *in utero* skeletal muscle key to understanding the disease development, while others, such as congenital heart failure, may present only in the tragedy of sudden cardiac death. Herein, I have examined the contractile kinetics of normal human fetal skeletal and cardiac muscle, diseased human adult skeletal and cardiac muscle, and finally, human induced-pluripotent-stem-cell-derived cardiomyocytes, and used these different groups to draw parallels between development, disease modelling, and therapeutic effects.

1.1 Background

1.1.1 The function of thick filament protein myosin

Force generation is a multi-step chemo-mechanical process, as described in Figure 1-1[1]. Myosin S-1 heads that have hydrolyzed ATP (M.ADP.Pi; step 3) bind to actin in a calcium dependent manner (steps 4 and 5). Myosin then undergoes a conformational change known as the power stroke (step 6), generating tension and releasing phosphate (step 7), then ADP (step 8, rate-limiting[2]), then will release from actin upon binding a new ATP (steps 1 and 2) and repeat this cycle. This process has been well-characterized by the Regnier lab (and others) for multiple myosin isoforms. The rate and the strength of contraction are heavily influenced by the composition of myosin isoforms within the tissue[3].

Myosin motor protein consists of six proteins: two myosin heavy chains and four myosin light chains. Myosin heavy chains are large proteins (~200 kDa, or 2000 amino acids), and contain several floppy regions, making them difficult to crystallize and resolve structure with a high degree of certainty. Striated muscle myosins bind two light chains per head, one "essential" light chain and one "regulatory" light chain, each which a molecular mass of ~20 kDa. Myosin

motor protein wraps together in the thick filament, creating a helix pattern of head placement along the filament.

There are several regions of interest within this protein, which functions as a mechanical enzyme, hydrolyzing ATP into ADP and Pi and generating force[4,5]. Currently, only slime mold myosin (*Dictyostelium discoideum*) is available in crystal structure with sufficiently high (>2.5 Angstrom) resolution for *in silico* experimentation in the 4 key power stroke states (Pre-power stroke M.ATP.Pi-analogue Vanadate[6,7], post-power stroke M.ADP + inhibitor beryllium fluoride[8], Rigor (APO) M, and ATP-bound M.AMP.Pi) [9–12]; nonetheless, a cross-species comparison of myosin isoforms does contain many conserved regions[13] .
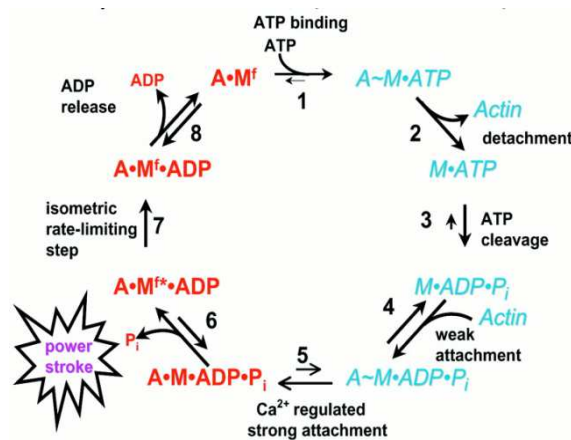
Figure 1-1: The actin-myosin crossbridge cycle.

The cross bridge cycle shown in chemical formula with weak or no acto-myosin binding states in blue and strong acto-myosin binding states in red (Gordon (2001)).

Actin (A), Myosin (M), Adenosine Trip-Phosphase (ATP), Adenosine Di-Phosphate (ADP), Phosphate (Pi)

The head region contains four domains, two of which bind to actin and are commonly called the upper 50 kDa domain and the lower 50 kDa domain. The actin binding domain spreads across both, and the cleft opens (weakly binding to actin) and closes (strongly binding to actin). Cardiomyopathy can be caused by mutations in β myosin heavy chain within these domains, such as mutation R403Q (in the upper 50 kDa domain) and L908V (in the lower 50 kDa domain). Moving away from the actin binding site within the head is the ATP binding pocket,

nestled between the upper domain that binds to actin and the N-terminal and central (also known as the converter) domains. Severe birth defects related to skeletal muscle can be caused by mutations at R672, Y583, and T178 of embryonic myosin (and paralogous mutation R671C in β-myosin heavy chain that causes cardiomyopathy) point to a cavity near this ATP binding pocket and may alter pocket conformation and binding site function[14]. Moving on to the neck region, essential light chain and regulatory light chain sites are found in the lever domain; other skeletal muscle defect-causing mutations are near the regulatory light chain interaction sites (V825, K498, del L841 of embryonic myosin)[15].

1.1.2   State of Field in study of myosin mutations

Changes in force production and cross bridge kinetics can be caused by point mutations in myosin through a variety of mechanisms[16]. However, the exact mechanism by which a small amount myosin mutant in a muscle fiber, such as the distal arthrogryposis embryonic myosin mutation in adult muscle, results in dysfunction is yet unknown. It may be that the mutant protein produces significant drag on thin filaments such that it significantly alters the kinetics of the sarcomere as a whole.

Some mutations in myosin heavy chains are known to cause drastic changes in structure and function of the affected tissue and have been studied in multiple ways. Cardiac diseases are known to be caused by mutations in gene *MYH6* and gene *MYH7*. Mutations in human α cardiac myosin isoform (gene *MYH6*) have been characterized by phenotypic studies and can cause atrial septal defects in the heart[17]. Mutations in β-myosin heavy chain (gene *MYH7*), including R671C, can cause familial hypertrophic cardiomyopathy[15,18,19], though their effects on the heavy chain vary. Mutations R403Q and L908V show shorter actin attachment times, but quicker actin filament velocities[18,20–22]. *MYH7* R403Q in particular has further been studied in myofibrils, showing an increase in tension generation and relaxation rates[23]. The R723G mutation in β-myosin heavy chain has even been shown to affect calcium sensitivity in cardiomyocytes[24]. A series of mutations in the neck region of the myosin heavy chain may affect how the macrostructure of cardiomyocytes, causing myopathy from force generation imbalances[25]. Finally, a mutation near the actin binding site (L342Q) in the gene for skeletal myosin type IIb

(gene *MYH4*), leads to an increase in the fraction of strongly bound cross bridges in heterozygote mice skinned cell studies[26].

Human embryonic and neonatal skeletal myosins, however, remain understudied, yet mutations in these heavy chains cause debilitating and persistent skeletal muscle disorders.

1.1.3   The function of thin filament proteins

The regulation of striated muscle contractile activation is dependent on calcium. Cytosolic calcium level are normally kept below 0.1 µM [27]; while calcium sensitivity greatly varies between muscle types, depending largely on the regulatory thin filament proteins present, generally, concentrations of calcium exceeding 1 µM (pCa 6.0) will allow for force generation. Several reviews of thin filament protein interactions and muscle activation are worth noting and were used in this summary[28,29].

Briefly, calcium released from the sarcoplasmic reticulum[*] binds to the troponin subunit troponin C (TnC). In skeletal muscle, calcium is bound to two sites at the NH_2 terminus, and binding at one site enhances the potential for calcium binding at the second site; in cardiac muscle, calcium only binds to one site, as the second site is unable to bind calcium. The binding of calcium to TnC opens a hydrophobic patch on TnC that results in increased interaction with Troponin I (TnI), though for cardiac TnC this interaction is far less strong than in skeletal TnC. The mobile region of TnI (Md-TnI) is believed to work as a fail-safe latch[30], as it inhibits myosin S1 ATPase activity[31], and may only be structured when it is fulfilling its inhibitory role docked into actin[30,31]. Increased TnC-TnI interaction causes TnI dissociation from actin. TnT lies along the C-terminal end of Tropomyosin (Tm), binding to TnC, TnI, and Tm, and greatly influences Tm flexibility. In the presence of calcium, TnT changes the way in which it binds to TnC and Tm[29,32], and Tm's binding to actin weakens, allowing for increased movement of the Tropomyosin (Tm) strand on the actin backbone. Tm movement allows initial myosin binding and further displaces Tm, allowing additional, cooperative myosin binding, resulting greater thin filament 'activation' and myofibril force development. Post-contraction, calcium dissociates from the TnC subunit, allowing a conformational change of the troponin that restricts acto-myosin binding, and calcium is sequestered back to the sarcoplasmic reticulum. Changes in

---

[*] A special type of smooth endoplasmic reticulum found in muscle cells that stores and releases Ca^{2+}

calcium sensitivity and cooperativity can be caused by mutations in troponin subunit amino acids. Calcium sensitivity is dependent on troponin conformational changes, which may be altered by point mutations in TnT and TnI. Additionally, troponin mutations may cause upstream alterations in the calcium signaling process, but studies in this project will be confined to phenotypic characterization of myofilament protein contraction and relaxation properties.

Cooperativity, or the nonlinear increase in force resulting from a linear increase in calcium, is a remarkable phenomenon shared by skeletal and cardiac muscle.

In skeletal muscle, cooperativity may manifest from neighboring tropomyosin-troponin interactions, by which one activated tropomyosin-troponin partially activates its neighboring tropomyosin-troponin, as supported by *in vitro* knock-out studies, which showed that calcium sensitivity and cooperativity both decrease in proportion to decreasing amounts of functional tropomyosin-troponin[33]. In cardiac muscle, force production depends on strongly bound cross-bridges, as bound and cycling cross-bridges enhance calcium binding to troponin. Using NEM-S1, a modified myosin fragment which binds to the thin filament, enhancing cross-bridge binding, results in faster force redevelopment rate and greater sensitivity to calcium in skinned myocardium samples[34]. The use of 2-deoxy-ATP (dATP) also increases the total force and rate of force redevelopment[35], as well as the calcium sensitivity of force production[36] in cardiac samples.

1.2   Problem Statement – Distal Arthrogryposis (DA)

1.2.1   Genetic mutations in sarcomere proteins can cause lifelong contractures

Distal arthrogryposis is a congenital contracture syndrome that affects 1 of 3000 live births[37,38]. Though phenotypically similar to clubfoot in its contractures of the distal leg and foot, it can be far more severe because it affects the upper limbs, torso, and face[37,38]. Previously believed to be an effect of tendon and ligament malformation, distal arthrogryposis is a syndrome largely caused by mutations in the genes of sarcomere proteins[14,39–42].

Current treatments for distal arthrogryposis include major tendon realignment and reconstructive surgery that, while done early in life, cannot fully restore function. Such

treatments can also impose economic strains to families and increase the risk of early onset degenerative joint diseases such as osteoarthritis[43–51].

1.2.2 DA is caused by genetic mutations in sarcomere proteins

Causes of most congenital contractures are unknown; one of the more common, distal arthrogryposis, has been linked to several mutations in genes for sarcomere proteins. The distal arthrogryposis syndromes are a group of ten dominantly inherited disorders characterized by multiple congenital contractures such as clubfoot and camptodactyly Thus far, the Bamshad lab and others have identified mutations in at least 6 genes in families with distal arthrogryposis which code for proteins in the thick and thin filament that are directly involved in skeletal muscle contraction[4,14,52–61].

The majority of mutations found to date to cause distal arthrogryposis syndromes are located in *MYH3*, the gene that encodes embryonic myosin[14]. Non-overlapping mutations in *MYH3* cause both the most common, Sheldon-Hall syndrome (DA2B, SHS, OMIM #601680), and the most severe, Freeman-Sheldon syndrome (DA2A, FSS, OMIM #193700), of the distal arthrogryposis syndromes. This observation suggests that *MYH3* mutations causing DA2A have different functional consequences than those causing DA2B.

Thick filament mutations account for 54 of 193 probands studied by the Bamshad lab[14,52,53,62]; however, assessments of how these mutations affect contractile function have not been reported due to difficulty in obtaining specimens the techniques involved in assessing them. However, the phenotype does persist throughout life.

While the genetic causes of distal arthrogryposis are in discovery, the biophysical mechanisms of how the known mutations cause life-long contractures remains unknown. Different types of distal arthrogryposis often have similar phenotypes, yet are associated with various distinct pathologies that often have significant impact on proposed treatment[38].

1.2.3 The molecular effects of DA mutations are unknown

While the list of identified mutations that cause distal arthrogryposis is growing, only a few studies have investigated if/how contractile properties of affected muscles are altered[63–65]. There are a few reports investigating mutations in thin filament proteins, which are also known

6

to cause distal arthrogryposis, where the mechanism may be altered calcium sensitivity of contraction[41,63,64,66]. However, how this change in calcium sensitivity occurs remains unknown. To date, no studies of muscle cell contractility in individuals with defects of embryonic myosin have been reported.

My preliminary work, with a manuscript accepted at Human Molecular Genetics, shows a marked increase in relaxation time of human muscle cells and myofibrils containing an R672C mutation of embryonic myosin heavy chain[67]. Our data suggest this may occur via altered cross bridge cycling kinetics. As such, there is much to be learned from contractile assessments from patient biopsies containing mutations in both thin and thick filament sarcomere proteins.

Together our studies and others suggest that a <u>widespread array of functional changes</u> may cause congenital contractures[63–65].

The goal of this project is to investigate the underlying mechanisms of contractile apparatus dysfunction caused by distal arthrogryposis - associated mutations of myofilament proteins.

1.2.4 <u>State of field</u>

fsTnI R174Q is in the COOH-terminal end of TnI, believed to interact with actin and/or tropomyosin (Tm)[68,69]. In previous studies, cardiac TnI R174Q has been shown to reduce calcium sensitivity of contraction[70,71]. Another isoform of the TnI protein, cTnI from the gene *TNNI3* for cardiac troponin, has mutations near the an paralogous site (R204) at both G203 and K206 which cause familial hypertrophy; these mutations cause a shift in the backbone structure of cTnI and affect the cross bridge cycling rate[18,72][†]. In a previous study with recombinant proteins exchanged into skinned rabbit psoas cells, this mutation increased the calcium sensitivity and cooperativity of contraction[22].

The fsTnT R63H mutation is in a highly variable region just outside the Tm binding region, which begins at residue 72[73]. Both cardiac (gene *TNNT2*) and fast skeletal (gene *TNNT3*)[‡]

[†] *TNNI1* codes for slow skeletal troponin I, though it is present in fetal human heart.
[‡] *TNNT1* codes for slow skeletal troponin T. Mutations in *TNNT1* can cause Nemaline Myopathy, a congenital disorder resulting in muscle weakness and rod-shaped inclusions in skeletal muscle cells.

isoforms contain developmentally regulated and alternatively spliced exons, resulting in slightly different adult and fetal protein sequences[18,74]. Mutations at the paralogous site in *TNNT2*, R93, cause hypertrophic cardiomyopathy[75]. In transgenic mice expressing the cardiac TnT (*TNNT2)* R92Q mutation, cardiac fiber bundles showed increased calcium sensitivity and an increase in cooperativity, but a decrease in maximal force production[76]. In a previous study with recombinant proteins exchanged into skinned rabbit psoas cells, the fast skeletal TnT (*TNNT3*) R63H mutation increased the calcium sensitivity of contraction[22].

Myosin mutations remain difficult to study, due to their large size and complex folding. Studies on other myosins indicate changes to the head region of the myosin, and in particular at this site, can lead to cardiomyopathies (1.1.2, State of Field in study of myosin mutations). However, in-depth studies as to the specific effects of this mutation in any muscle myosin are lacking.

1.2.5 <u>Approach</u>

The goal of studying the mutations which cause distal arthrogryposis was to determine 1) if the mutation continues to affect the contraction of the adult muscle and 2) if there are functional difference in how specific mutations result in altered contractures that may be relevant for future potential therapeutics. I have studied skeletal muscle biopsies from two unrelated patients carrying an identical thick filament mutation, embryonic myosin R672C. These biopsies had changes in myosin (cross bridge) binding, detachment, and interaction with actin. The embryonic myosin R672C mutation leads to a severe form of distal arthrogryposis, Freeman-Sheldon Syndrome (DA2A). By determining functional changes and the causal mechanisms, we can begin to develop targeted therapies that would restore function on the molecular and cellular level. The studies presented in CHAPTER 3 characterize the thick filament mutations' manifestation in skinned muscle and myofibril studies, with promising preliminary data from thin filament mutation *in vitro* motility and *in silico* studies. These studies allow control of cross bridge cycling through substrate and solution changes; future studies may build on this study using additional muscle biopsies and mutations to form a cohesive picture of the cause of contraction in distal arthrogryposis.

1.3   Problem Statement – Fetal Skeletal and Cardiac Muscle

1.3.1   Human fetal striated muscle contraction & understanding disease

Many skeletal muscle diseases, such as distal arthrogryposis (DA), develop *in utero*. DA has many types[38], some of which are caused by mutations in fetal muscle specific protein isoforms of myosin, such as embryonic myosin heavy chain (gene *MYH3*)[15]. However, little is known about the contractile and chemo mechanical properties of these myosins, which are expressed predominantly *in utero*. Additionally, the contractile properties of human fetal skeletal muscle have not been observed and published. Without understanding the underlying physiology of the state in which these contractures develop, we cannot accurately hypothesize and understand the nuances of the adult presentation of distal arthrgyposis. A better understanding of the mechanics of the contractile apparatus in fetal muscle may provide important information about the mechanisms that cause congenital contractures. Samples for the fetal skeletal muscle project come from fetal skeletal muscle tissue of ~15 weeks gestation, during which time, embryonic myosin gene expression dominates other myosin genes (81% total *MYH* gene expression is *MYH3* expression (Figure 4-1)). Therefore while we will get a better understanding of the physiology of fetal muscle from this specific time period, this study is limited to better understanding fetal muscle contraction and chemo mechanics, specifically when expressing embryonic myosin. This study is published with the Journal of Physiology.

In contrast, cardiomyopathies such as those in Familial Cardiomyopathy and Duchenne's Muscular Dystrophy, develop far earlier than when intervention is needed at a clinical level, but rarely show overt clinical symptoms at birth. To understand how mutations alter development of contractile properties requires comparison with normal human fetal cardiac muscle, but these data, like those for skeletal, are missing from the literature. Additionally stem cell derived cardiomyocytes are often used as a model for studying heart disease and modeling potential therapeutics *in vitro*, yet the maturity of these cells is difficult to gauge without human fetal cardiac muscle as a comparison.

1.3.2   State of field

While their functional and contractile characteristics are not well-defined for the human isoforms, developing skeletal muscles from feline, rat, and even sheep have shown age-related

changes. For example, contractility measurements of neonatal feline and rat skeletal muscle have found that the energetics and mechanical characteristics, notably the duration and speed of twitch-activated tension and release, are similar to that of adult slow muscles[77–79]. Force production significantly increases as development progresses, even after birth, but neither calcium sensitivity of force (pCa_{50}) nor cooperativity of thin filament activation (n_H) change significantly[77–79]. Increases in force may be due to increased sarcomere alignment and myofibril density[80]. Additionally, a change in twitch contraction time between early and late gestation has been attributed to changes in myosin heavy chain isoform, with suppression of fast-twitch properties and elevation of slow-twitch properties [80].

1.3.3   Approach

Little is known about the contractile and chemo mechanical properties of embryonic myosin in human skeletal muscle. Human fetal skeletal muscle contraction is largely unstudied, yet the development of muscle-related birth defects originates in this muscle. I have observed the properties of muscle containing wild-type embryonic myosin and have written a published manuscript on this subject, which is summarized in CHAPTER 4.

Similarly, while there are limited studies looking at protein expression and density in the human fetal myocardium, there have been no studies to date on the contractility of the developing human fetal myocardium. I have observed the contractile properties of the human fetal myocardium from 7 to 20 weeks gestation, which is summarized in CHAPTER 5.

I have observed maximal force production, activation kinetics, and relaxation kinetics from single isolated myofibrils from human fetal muscle biopsies. I have also performed *in vitro* motility assay experiments to quantify the substrate sensitivity and ATPase rate of fetal myosins from both skeletal and cardiac tissues. Finally, I have compared human fetal cardiac tissue to human induced pluripotent stem cell derived cardiomyocytes, and age-matched the kinetics and force production.

1.4 Problem Statement – Human Adult Heart Failure

1.4.1 Heart failure has many causes

Heart failure is a growing epidemic in the United states and around the world[81], but its pathological origins vary widely, including congenital heart disease, which is often of genetic origins[82], and cardiomyopathy that develops after a primary pathology such as Duchenne's Muscular Dystrophy[83]. Heart failure reduces life expectancy[84].

1.4.2 Therapeutics for heart failure

Altering intracellular calcium through inotropic agents is one of a number of treatment strategies used for targeted treatments of heart failure; however, prominent therapies do not directly target the myofilament protein myosin[85].

Over the past 15 years, the Regnier lab has published multiple studies on the ability of striated muscle to use dATP as a myosin substrate for contraction, and that dATP increases steady state force and stiffness (S_{max}), the rate of force development (k_{TR}) and unloaded shortening velocity (Vu), and calcium sensitivity (pCa_{50}) of force development[35,36,86–91]. Furthermore, the Regnier lab has shown the feasibility of using dATP to restore function in damaged cardiomyocytes (Figure 1-2, unpublished). In this experiment, cardiomyocytes from infarcted hearts showed slowed contraction and relaxation, but these kinetic parameters were recovered with elevated dATP.

These effects are believed to occur via increased myosin (M.dADP.Pi) affinity for actin (cross bridge binding; determined from stiffness) coupled with a faster rate of dADP release from myosin and cross bridge detachment (following NTP binding) while myosin affinity for actin is the same as for ATP (unpublished Regnier lab data). Thus, dATP provides a mechanism whereby increases in magnitude and rate of contraction could be improved in muscle where these mechanical properties are compromised. Importantly, after dATP is hydrolyzed by myosin, it can be rapidly re-phosphorylated by creatine kinase, so an increase in dATP should confer long-lived effects on contractility.

1.4.3   Approach

The goal of studying dATP in heart failure was to determine if the dATP can increase the force and rate of force production in heart failure without negatively affecting the relaxation kinetics. To achieve this, ventricle samples from patients in stage IV heart failure were subjected to a battery of tests using dATP and ATP; those included here are parts which I have contributed to directly. These studies show that dATP increases the rate of activation, the rate of cross-bridge cycling, and the total force production, which might improve systole, or the contracting phase of the ventricle. Importantly, dATP did not slow relaxation kinetics and thus might not impair diastole, or the filling phase of the ventricle.
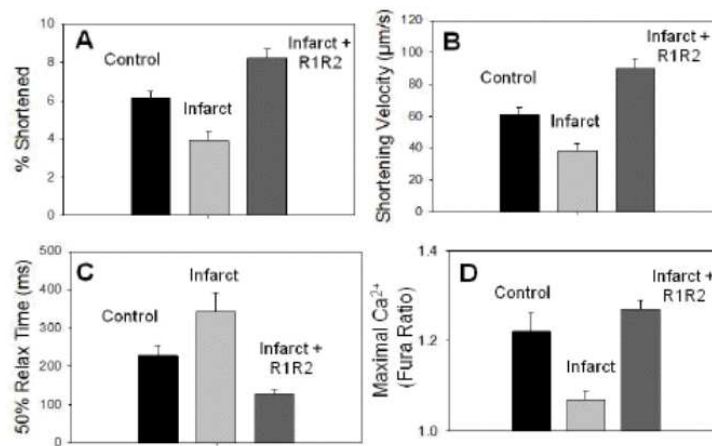
Figure 1-2: dATP rescues contractile deficits in single cells from damaged hearts.

Overexpression of dATP rescues extent (A) and rate of shortening (B), time to 50% relaxation (C) and maximal Ca^{2+} release (D) of cardiomyocytes from infarcted hearts. (unpublished data, Regnier lab)

CHAPTER 2.   METHODS and MATERIALS

2.1   Sources of tissue for study

2.1.1   Compliance Statements

Normal human adult tissue was obtained with Institutional Review Board (IRB) approval from Seattle Children's Hospital. Normal human fetal tissue was obtained by the Laboratory of Developmental Biology at the University of Washington with IRB approval from the University of Washington and Seattle Children's Hospital. All animal procedures were conducted in accordance with the US National Institutes of Health Policy on Humane Care and Use of Laboratory Animals and were approved by the UW Institutional Animal Care and Use Committee (IUCAC). Rabbits and mice were housed in the Department of Comparative Medicine at UW and cared for in accordance with UW IUCAC policies.

2.1.2   Adult Human Tissues

Skeletal muscle biopsies were obtained from needle biopsy of DA or control subjects, flash frozen in liquid nitrogen, and stored at -80°C. Control experiments on skinned muscle cells using rabbit psoas muscle demonstrated no appreciable change in contractile properties between fresh and flash frozen muscle samples.

Muscle biopsies from 2 patients with the embryonic myosin R672C mutation, 1 patient with the neonatal myosin (gene *MYH8*) R674Q, and several control biopsies, some obtained through needle biopsy and flash frozen in liquid nitrogen, and some of which were obtained through an IRB-exempt transfer from the Department of Pathology and were biopsied and frozen in cooled liquid isopentane. Each provided single muscle fibers and myofibril preparations for the proposed studies. It is common for patient biopsy studies to be limited to a small group, usually family, of affected patients[60,64,66,92,93]. The clinical relevance of these studies is limited; however, the functional analysis allows for a better understanding the pathogenesis underlying the disease and offers new possibilities for treatment.

Human cardiac muscle biopsies were obtained from either a left-ventricular assist device (LVAD) core sample or dissected from the left ventricle by a practicing cardiologist.

2.1.3 Fetal Human Tissues

Laboratory personnel from the Laboratory of Developmental Biology collect specimens at clinics, where a short time after passage, the specimens were examined, sexed, and aged by calculating the age in post-conception days. Samples were stored on PBS at 4C until dissection, for a period of 2 to 6 hours. Thereafter, individual skeletal tissues were dissected and flash frozen in liquid nitrogen, and stored at -80°C until use. Individual tissues for histology were also prepared. All fetal skeletal muscle for this project was of 12-15 weeks gestation. The age range of fetuses for this project was 52 – 134 days gestation. The heart was identified and piece of the outer wall of the left ventricle removed and used fresh. Other pieces of the heart and non-muscle tissues were removed and flash frozen in liquid-nitrogen-cooled isopentane, and then stored at -80°C. For a subset of samples, left ventricle wall tissue was placed in 4% formaldehyde solution.

2.1.4 Animal Tissues

Male New Zealand white rabbits were anaesthetized with an intravenous injection of pentobarbital (40mg kg^{-1}) in the marginal ear vein and when the animals had no reflexive response, were exsanguinated. The psoas muscle was exposed and small bundles of psoas fibers were excised at native length, demembranated and stored at −20°C for up to 6 weeks as previously described[33]. Psoas and gastrocnemius muscled were also extracted and flash frozen in liquid nitrogen and stored at -80°C. Mouse hearts were extracted shortly after euthanizing and used fresh.

2.2 Human Stem Cells

Human induced-pluripotent-stem cell-derived cardiomyocytes for this project were provided by Jose Manuel Pioner. Briefly, human induced-pluripotent stem cells (provided by the Neuromuscular Disease Group and the lab of Charles Murry) were differentiated into cardiomyocytes[94]and matured up to 20 days, then transferred to a Nano patterned surface with 800 nm grooves (provided by the lab of Doek-ho Kim), then allowed to mature an additional 60

days. For a subset of samples, fully matured cells were incubated in 4% formaldehyde solution for electron microscopy.

2.3 Mechanical studies

This project included mechanics at multiple levels of muscle integration, including isolated proteins (*in vitro* motility assay), sub-cellular myofibrils, and skinned single muscle cells. These are the preparations that allow analysis of chemo-mechanical transduction and how it is changed in development and disease. This is because ATP substrate and products, calcium, and a variety of inhibitor/activator compounds can all be finely controlled. Intact muscle cells do not provide the detailed mechanistic information of our multi-level muscle preparations.

2.3.1 Solutions

Experimental solutions for muscle mechanics contained (mM): EGTA 1, MOPS 1, free Mg^{2+} 1, $(Na^+ + K^+)$ 135, ATP 5, Dithiothreitol (DTT) 1, and 4% (w/v) Dextran T-500 (Pharmacia). The pH was adjusted to 7.0 at 15°C, the ionic strength was 0.17 M. The concentrations of free calcium were 10^{-9} M (relaxing solution) and $10^{-6.4}$, $10^{-6.2}$, $10^{-6.1}$, $10^{-6.0}$, $10^{-5.9}$, $10^{-5.8}$, $10^{-5.7}$, $10^{-5.6}$, $10^{-5.4}$, $10^{-5.2}$, $10^{-5.0}$ and $10^{-4.0}$ M **(**activating solutions), expressed as pCa values (i.e., -log $[Ca^{2+}]$).

Experimental solutions for myofibril mechanics were calculated as previously described [95] and contained (mM): phosphocreatine 10, EGTA 10 (ratio of CaEGTA/EGTA set to obtain free calcium concentration values between 10^{-9} and 10^{-4} M, as described above), Mops 10, free Mg^{2+} 1, $(Na^+ + K^+)$ 155, MgATP 5, and propionate and sulphate to adjust the final solution ionic strength to 0.2 M. Rigor solution for myofibril mechanics contained the following (mM): Tris 50, KCl 100, $MgCl_2$ 2, EGTA 1, DTT 2, and diluted (1:200) protease inhibitor cocktail (Sigma-Aldritch), and were adjusted to a pH of 7.0.

For experiments in muscle cells or myofibrils in which ADP was tested, both ATP and ADP activating and relaxing solutions were made without phosphocreatine. For some experiments, 30 mM 2,3-butanedione monoxime (BDM, Sigma-Aldrich) was added to pCa 9.0 or pCa 4.0 solutions to inhibit strong cross bridge binding[96,97]**.** Experimental solutions for myofibril mechanics which compared ATP to dATP were calculated as previously described [95] and contained (mM): phosphocreatine 10, EGTA 10 (ratio of CaEGTA/EGTA set to obtain free

calcium concentration values between 10^{-9} and 10^{-4} M, as described above), Mops 10, free Mg^{2+} 1, $(Na^+ + K^+)$ 155, MgATP 2, and propionate and sulphate to adjust the final solution ionic strength to 0.2 M.

2.3.2   Skinned Muscle cells

Single skinned muscle fiber experiments allowed for several activations, with relatively little deterioration of preparations, for detailed analysis of calcium dependent contraction. Additionally, these studies did not destroy the experiment preparation, which was saved and used for additional proteomic analysis, such as fiber typing and myosin heavy chain content.

2.3.2.1   *Preparation of Muscle cells*

Frozen biopsies were thawed at 4°C for 4 hours in relaxing solution (pCa 9.0, see 2.3.1) with 1% triton and 50% glycerol. Individual skinned muscle cell segments were dissected from muscle bundles and ends are wrapped in aluminum foil T-clips, mounted, and moved between different activating solution troughs as previously described[98–101].

2.3.2.2   *Equipment*

Briefly, individual skinned muscle cell segments were mounted on a Nikon (Japan) inverted microscope with pin hooks attached to an Aurora Scientific force transducer (Model 400A, Ontario, Canada) and a General Scanning servo-motor (model G120DT, Watertown, MA, U.S.A.) in a temperature-controlled solution well as described previously[98]. Muscle cell segment length was set to "just-above-slack" plus 10% and monitored during activation and relaxation. Sarcomere length at "just-above-slack" plus 10% was measured in muscle cells in which sarcomeres were clearly visible using video microscopy (IonOptix) , confirming this stretch brought the muscle to a sarcomere length of 2.3 to 2.5 µm. Muscle cell preparations were moved between individual troughs that held solutions containing different concentrations of calcium. At 5 second intervals, muscle cell segments were shortened by 15%, then rapidly restretched to the initial muscle cell segment length to maintain fiber integrity[102]. Force and shortening measurements were collected and analyzed digitally as previously described[88] and on a Gould 2400 chart recorder or digitally for long-timescale measures of relaxation. Calcium concentrations were varied to observe maximal force, the calcium sensitivity of force, and the degree of cooperativity in calcium activation.

2.3.2.3   Analysis

In order to control for muscle cell diameter, the reported force was normalized to muscle cell cross-sectional area. Cross-sectional area was determined by averaging three diameter measurements across each muscle cell length set at "just-above-slack" plus 10% (at approximately 25, 50, and 75% of the muscle cell length) and using a circular cross-sectional area estimate of πr^2. Dextran T-500 was included in all solutions to minimize variation of myofilament lattice spacing (and fiber diameter) with force[100,101].

Force measurements were plotted using Sigma Plot, and steady-state force-pCa relationships were fitted with the Hill equation (Equation 2.1), to obtain the concentration of calcium at half-maximal force (pCa_{50}, to determine calcium sensitivity) and the slope of the linear portion of the curve (the Hill coefficient n_H, to determine the apparent cooperativity of contractile activation) .

$$F = F_o/(1 + 10^{n_H(pCa^- pCa^{50})})$$

Equation 2.1

For each cell, the concentration of calcium in activation solutions was varied for measures of isometric tension, muscle cell stiffness, and the rate of tension redevelopment (k_{TR}) following a rapid release-restretch transient[101].   Through these measurements, I determined maximal force (F_{max}) and k_{TR} (k_{TR-max}), and the calcium sensitivity (pCa_{50}) and apparent cooperativity (n_H) of force development. Changes in $k_{TR\,max}$ also indicate changes in cross bridge cycling rate[40,41]. A force-pCa curve is shown in Figure 3-2 and a k_{TR} trace is shown in Figure 3-5.

Changes in pCa_{50} and n_H are indicative of altered cross bridge binding and troponin/tropomyosin (Tn/Tm) mobility. Relaxation was monitored, but studied in depth with myofibrils. Fiber diameter was measured to determine muscle cross-sectional area (CSA) for determination of specific force production (force/CSA). Fiber diameter provided evidence for hypertrophy by comparing the absolute force *vs.* specific force.

Force tracings were manually analyzed to determine the time required for activation and relaxation. Time required for activation was taken from when the muscle cell was first immersed

17

in the pCa 4.0 solution until maximal force was reached. Time required for relaxation was taken from when a muscle cell was removed from the pCa 4.0 solution and transferred into pCa 9.0 solution to the time that either 50% or 90% of maximal relaxation was reached (Figure 3-2).

2.3.3   Myofibrils

The rate of muscle contraction and relaxation are important aspects of motor skill and control. These rate measurements were essential for an understanding how development and disease may alter myofilament level mechanisms of myosin cycling and its regulation by thin filament proteins. The ability to quantitatively assess activation and relaxation in skinned muscle fibers is likely limited by the rate calcium diffuses to the outside of the cell and is chelated by the EGTA buffer[103–106].   These kinetic properties of muscle, and how they are affected by changing calcium, ATP, ADP, and Pi, were studied using single myofibril preparations in a custom built mechanics apparatus.

Myofibril preparations provided more detailed and accurate information of kinetics of contractile activation and relaxation due to thin filament activation and cross bridge cycling rates. This was achieved using rapid solution switching through the small myofibril diameter. The influence of diffusion was limited on the rates of tension development and tension release (relaxation) because the preparations measured <10 μm wide.

2.3.3.1   Separation

Pieces of flash frozen muscle were thawed and demembranated for 24 hours at 4°C in relaxing solution (Section 2.3.1) containing 50% glycerol (by volume) and1% Triton-100 detergent, as previously described [35,107]. Human fetal heart tissues aged 7 to 20 weeks (52 – 134 days) and human adult heart tissue were placed immediately into the demembranating solution described above and stored overnight at 4°C.

Demembranated muscle cell bundles were stored at -20°C in 50% glycerol-relaxing solution for use up to one week. Muscle bundles were manually dissected into pieces smaller than 500 μm long and wide at 10X magnification, placed into rigor solution and shredded with a high speed homogenizer for 1 or 2 bursts of 10-30 seconds. Cardiomyocytes were skinned on the nano-patterned surface using a rigor solution containing 1% triton X-100 for 5 minutes on ice,

before harvesting the supernatant, centrifuging, and then re-suspending in rigor buffer. The sample was briefly vortexed. The centrifuging, re-suspending, and vortexing of the sample were repeated 3 times.

Myofibrils were stored at 4°C and used within 3 days.

2.3.3.2 Equipment

Myofibril experiments were performed as previously described[108]. Briefly, myofibrils were mounted between two needles micro-forged from borosilicate glass capillary tubes (OD 1.0 mm, ID 0.5 mm, Sutter Instruments, Novato, CA). One of these needles was a cantilever force probe, deflecting in a predictable manner upon application of force[108]. Needle stiffness was determined by first deflecting the needle with a known amount of force using a galvanometer and measuring its deflection under a 40x lens. This yielded stiffness in nN μm^{-1}, and needles typically ranged between 2 and 50 nN μm^{-1}. This needle was positioned over a dual diode system, which recorded needle displacement and correlates displacement to force development. A calibration curve was performed at the end of each experiment in which this needle was moved in 1 μm steps over the range of the diodes using micromanipulators (MP-285, Sutter Instruments, Novato, CA). A second, straight needle was attached to the other end of the myofibril.

A double-barreled borosilicate theta glass pipette (Capillary glass tubing OD 2.0 mm, ID 1.4 mm, SEP 0.2 mm, modified in house to OD of 0.55 mm, Warner Instruments, Hamden, CT) was used to stream low (10^{-9} M, pCa 9.0) and high (10^{-4} M, pCa 4.0) calcium-containing solutions to the mounted preparation. This pipette was controlled by a computerized motor (SF-77B Perfusion Fast step, Warner Instruments Corporation, Hamden, CT) to step-switch solutions over the preparation. The solution change was complete in ~10 ms[109,110].

2.3.3.3 Analysis

Activation and relaxation data was collected at 15°C and fitted with either single-exponential curves or linear coefficients as previously described[111]. Briefly, the activation rate (k_{ACT}; with rapid increase in calcium) was estimated from a single-exponential rise to a maximum (3-variable, reporting rate only). Relaxation rate for slow phase ($k_{REL,slow}$) was reported as the slope of a regression line fit to the tension trace and normalized to the tension amplitude, and the

duration of slow phase was measured from the onset of solution change at the myofibril to the shoulder marking the beginning of fast phase. Transition from slow to rapid phase was determined through multiple factors. An apparent change in the slope of the data or a change in the signal-to-noise ratio was often apparent at the transition. The relaxation rate for fast phase ($k_{REL,fast}$) was measured from a single exponential decay fitted to the data (3-variable, reporting rate only). A $t_{1/2}$ estimation was made in cases where the decay was not well-described by a single exponential, and this was converted to a rate (Equation 2.2). This was done through a semi-automated analysis program which I built in Microsoft VBA (see APPENDIX).

$$k = \ln (2)/t_{1/2}$$

Equation 2.2

Single myofibril preparations were prepared, attached, and tested as previously described[112,113]. Myofibrils were activated at maximal (pCa 4.0) or submaximal (pCa 6.0-pCa 5.0) calcium concentrations for measurements of force production, the rate of force development (k_{ACT}), the duration of the slow phase of relaxation ($t_{REL,slow}$), and the slow ($k_{RELslow}$) and fast ($k_{RELfast}$) rates of relaxation (Figure 4-3). The rate of force development includes the rate of thin filament activation and the rate of cross bridge cycling[114]. Relaxation in myofibrils occurs in a biphasic manner characterized by a slow and a fast phase[113]. The rate of the fast phase of relaxation is thought to reflect the phenomenon of sarcomere give, independent of the calcium binding properties of troponin[114]. In contrast the rate of the slow phase of relaxation is thought to be determined by the rate of cross bridge detachment[113]. Finally, the duration of the slow phase of relaxation is influenced by the calcium dissociation rate (k_{off}) from troponin[113], and may be a reflection of the amount of time the thin filament remains "open" or activated.

Additional experiments exploring differences in k_{ACT} and/or k_{REL} used solutions with altered concentrations of ATP and ADP, to look for reduced myosin affinity for ATP or reduced rate of hydrolysis product (Pi, ADP) release. For example, if an experimental sample exhibited slower ADP release, increasing the concentration of ADP in the relaxation solution would have a greater effect on control sample relaxation than that of the experimental sample.

2.3.4   *In vitro* motility

2.3.4.1   *Proteins*

Rabbit skeletal myosin was prepared according to previously described methods and stored at
−20°C in a high phosphate solution (0.5 mM KCl, 10 mM NaHPO$_4$, 2 mM MgCl$_2$, 1 mM DTT)
mixed with 50% glycerol[115]. Aliquots of the glycerinated myosin stock were digested to heavy
meromyosin (HMM) by enzymatic digestion[116,117] with tosyl lysine chloromethyl ketone
(TLCK)–chymotrypsin (Sigma-Aldritch, St. Louis, MO). HMM was stored at 4°C and used for
up to one week. Daily aliquots of HMM were centrifuged with actin to remove denatured HMM
as previously described[115,118]. Human myosins were prepared according to previously described
methods and used within 3 days[118,119]. Purity was assessed by SDS-PAGE. HMM and myosin
concentrations were determined using spectrophotometry as previously described[119]. Rabbit
skeletal F-actin was prepared from acetone powder, labeled with rhodamine–phalloidin
(Molecular Probes, Eugene, OR, USA) as previously described, stored at 4°C, and used within 6
weeks[116,117,120,121].

2.3.4.2   *Solutions*

Solutions for varying the concentration of ATP and ADP were made in advance and stored at -
20°C for up to 6 months, as previously described[118]. ATP and ADP solutions were used up to
one week after thawing and stored at 4°C. dATP solutions were made daily. Mixtures with ADP
were made so that the total concentration of the NTP remained at 2 mM.

2.3.4.3   *Equipment and Data Acquisition*

Flow cells were prepared as previously described[118,122]. Experimental procedures were
performed as previously described[123]. Briefly, two glass coverslips, one 22 mm x 60 mm (VWR
Scientific, West Chester, PA) and one 18 mm^2 (Corning, Horseheads, NY) were separated by 2
mm adhesive foam spacers. The larger coverslip surface was cleaned and coated with 1%
nitrocellulose in amyl acetate (Sigma-Aldritch, St. Louis, MO) and allowed to dry. The channel
was coated sequentially with solutions containing: HMM, bovine serum albumin, unlabeled
shredded actin, ATP, a rigor wash, rhodamine-phalloidin labelled actin, and motility buffer[124].
Unregulated F-actin filament motility was measured at 30°C unless otherwise noted. At least 6
unique areas of each assay chamber were recorded for 10 seconds each at 10 Hz.

2.3.4.4 Data Analysis

Recordings were analyzed digitally, using custom software developed in house. The Homsher-Sellers ratio was determined by analyzing recordings with a [ATP] = 2 mM, and determining which ratio included all filaments that moved non-erratically [125]. Filaments were excluded as erratic if they 1) did not move during part of the recording (stalled), 2) crossed paths with another filament, 3) tangled on their own filament tail, or 4) pulled apart into separate pieces.

Additional statistical analysis was performed on *in vitro* motility data to propagate uncertainties associated with filament speeds. This statistical analysis was based on prior reporting [119,125].

First, filaments (f) which met the above-stated exclusion criteria were analyzed individually to determine a mean filament 'i' speed (u_{fi}) and standard deviation (σ_{fi}) of that speed.

Then, filaments were grouped into their respective video segments (v), and a mean speed for individual video segment 'j' (u_{vj}) was determined by performing a weighted average of individual filament mean speeds (u_{fi}), with a weight (w_i) assigned according to the number of frames (f_i) a filament was present in the 'j' video. A standard deviation (σ_{vi}) for each weighted mean speed was determined by propagating the standard deviation associated with each filament mean speed (σ_{fi}), weighted to the number of frames a filament was present in the video (Equation 2.3, whereas $w_i = f_i$).

$$\bar{u} = \sum \left(u_i * \frac{w_i}{\sum w_i} \right); \; \sigma = \sqrt[2]{\sum \sigma_i * \left(\frac{w_i}{\sum w_i} \right)^2}$$

Equation 2.3

Third, video segments were grouped by each slide (s), and the mean speed for individual slide 'k' was determined through use of a weighted mean (u_{sk}) and standard deviation (σ_{sk}), with a weight calculated according to the number of filaments in each video (n_j) (Equation 2.3, whereas $w_j = n_j$).

Finally, slides were grouped by condition (c), and the mean speed for individual condition 'l' was determined through use of a weighted mean (u_{cl}) and standard deviation (σ_{cl}), with a weighting according to the sum of all filaments which met the criteria in each slide (n_{sk}) (Equation 2.3, whereas $w_k = n_{sk}$). A summary of the results of these statistical analyses is listed in Table 2-1.

Table 2-1: Influence of weighting strategy on filament speed and error.

'Embryonic' human fetal skeletal myosin had slightly higher V_{MAX} and much smaller standard error (SE) when data was weighted to percentage of time filaments were present on the recording and number of filaments on each recording and for each slide (SE was calculated based on multiple slides of measurements. * indicates that no actin filaments met the requirements for smoothly moving filaments in that category.

Condition in mM		'Embryonic' human fetal skeletal smoothly moving filaments				Adult rabbit psoas skeletal smoothly moving filaments			
		non-weighted		weighted		non-weighted		weighted	
[ATP]	[ADP]	mean	SE	mean	SE	mean	SE	mean	SE
0	0	0*	0*	0*	0*	0*	0*	0*	0*
0.01	0	0.60	0.07	0.68	0.01	1.02	0.42	0.77	0.06
0.02	0	1.57	0.89	1.50	0.07				
0.03	0	1.15	0.16	1.18	0.01	1.64	0.08	1.64	0.07
0.04	0	1.41	n/c	1.40	0.07				
0.05	0	1.54	0.32	1.66	0.01	2.29	0.14	2.23	0.06
0.10	0	1.75	0.47	1.84	0.05	3.46	0.05	3.48	0.08
0.20	0	2.08	0.51	2.34	0.02	4.55	0.83	4.37	0.09
0.50	0	2.25	0.47	2.41	0.02	4.80	0.44	4.93	0.12
1.00	0	2.49	0.58	2.80	0.02	6.07	0.39	6.03	0.15
2.00	0	2.34	0.62	2.64	0.02	6.74	0.84	6.72	0.09
2.0	0.0	2.34	0.62	2.64	0.02	6.74	0.84	6.72	0.09
1.5	0.5	1.68	0.17	1.74	0.05	6.40	0.42	6.16	0.09
1.0	1.0	1.46	0.09	1.51	0.03	4.74	0.14	4.74	0.06
0.5	1.5	0.86	0.03	0.85	0.03	2.34	0.19	2.48	0.06
0.2	1.8	0.51	0.02	0.51	0.03	0.98	0.15	1.04	0.05

2.4 Imaging and Structural Analysis

Analysis by visualization of muscle cells and finer subcellular structures provides key insight into morphological changes cause by the mutations. Physical changes caused through growth or maladaptation and dysfunction were visualized of cross and longitudinal sections of muscles, showing differences in the structure and organization of the sarcomere.

2.4.1 Light microscopy with cross-sections

In the case that a biopsy was extracted at clinic, a small section of the biopsied tissue was thawed and quickly refrozen in the mounting medium as follows. A cross-section of human muscle tissues was first frozen to a base of -80°C mounting medium (optimal cutting temperature compound (OCT) Sakura Finetek, Torrance, CA) with a rapidly freezing aerosol (Cytocool II, Richard-Allan Scientific, Kalamazoo, MI). This tissue block on OCT was frozen in liquid isopentane (Sigma-Aldrich, St. Louis, MO) cooled to -80°C in liquid nitrogen and stored at -80°C until use. Frozen samples were cut in cross-section (across muscle fibers) into 5 µm sections. Adjacent slices of the cross-section cut sample were processed by hematoxylin and eosin (H&E) staining or incubated in either low pH (4.3) or high pH (10.3) solution to perform an ATPase assay, as previously described [126]. Photos were taken with an Olympus BX41 microscope (Olympus, Center Valley, PA) 40x objective and a Leica DFC290 digital camera (Leica, Allendale, New Jersey).

To perform immunohistochemistry, a cross-sectional muscle segment was immediately frozen upon dissection as described above or fixed in 10% neutral-buffered formalin solution (Sigma-Aldrich, St. Louis, MO) and stored at -80°C or room temperature, respectively, until processing. Frozen or fixed 5 µm sections were used for hybridization. The two myosin antibodies used for skeletal muscle were an adult skeletal, fast type II & neonatal antibody (M4276, clone MY-32, Sigma-Aldrich, St. Louis, MO) and a 'fetal skeletal' embryonic myosin heavy chain antibody. The hybridoma used to generate the fetal skeletal embryonic myosin heavy chain antibody used for immunohistochemistry (F1.652) was obtained from the Developmental Studies Hybridoma Bank at the University of Iowa (Iowa City, Iowa, USA, http://dshb.biology.uiowa.edu/). Purified myosin from a 15 week human fetus was originally

used as the antigen to generate this antibody[127]. The hybridoma line was cultured in Iscove's Modified Dulbecco's Medium (IDEM) with 10% fetal calf serum and gentamicin.

2.4.2 Light & Electron Microscopy with Longitudinal sections

For ultrastructural observation, fresh tissues were promptly fixed in ½ strength Karnovsky's fixative (2.5% glutaraldehyde and 2% paraformaldehyde in 0.1M phosphate buffer) and stored at 4°C until processing. The tissues were then post fixed in osmium tetroxide, dehydrated with ethanol, and embedded in Poly/Bed 812 epoxy resin. Thick longitudinal (along muscle fiber direction) sections were stained with Richardson's stain and viewed and photographed on a Nikon E400 upright microscope (Nikon Instruments Inc., Melville, NY), using a 100x oil immersion objective and an Olympus DP72 digital camera (Olympus, Center Valley, PA). Ultrathin longitudinal sections were stained with uranyl acetate and lead citrate and viewed and photographed on a FEI Tecnai G2 spirit biotwin electron microscope (FEI Company, Hillsboro, OR).

2.4.3 *MYH* transcript analysis

Total RNA was been isolated from multiple tissues of human fetuses and the gastrocnemius tissue of human adult using the RNeasy Fibrous Tissue kit (QIAGEN, Valencia, CA) according to the manufacturer's protocol. Briefly, total RNA was extracted from the dissected tissues by homogenizing the tissues, incubating in Proteinase K for 20 minutes at 55°C, and purified using on-column isolation. RNA was then eluted from the column using sterile deionized and distilled water. Following RNA isolation, the samples were quantitated and analyzed on a BioAnalyzer (Agilent Technologies, Santa Clara, CA). Preliminary expression profiling of the samples on a whole-genome expression array, each with two technical replicates, was performed using the Illumina Human HT-12 V3 BeadChips (Illumina Inc.) according to the protocol supplied by Illumina.

The percentage expression of a particular gene relative to other similar genes was calculated by dividing the expression level of a single gene (e.g. *MYH6*) by the summed expression levels of all the genes in the specific class (e.g. *MYH*).

2.4.4 Protein expression quantification

To determine whether *MYH3* mRNA was expressed in control adult human skeletal muscle, total RNA from control fetal and adult human skeletal muscle (Stratagene, La Jolla, CA) was reverse-transcribed to cDNA using an oligo(dT)$_{20}$ primer (Invitrogen Superscript III First-strand Synthesis Supermix kit, Carlsbad, CA), and *MYH3* and *MYH2* (as a control) were amplified using intron-spanning human primers that were designed to generate unique amplicons that were size-specific for either cDNA or genomic DNA. The sequences of these primers were:

MYH3_RT_exon 38_F (5'- GATTGCAGGATCTGGTGGAT-3'),

MYH3_RT_exon 39_R (5'- CCTGCTGGAGGTGAAGTCTC-3'),

MYH2_RT_exon 36_F (5'- GAGCTGGAAGGAGAGGTTGA-3'), and

MYH2_RT_exon 37_R (5'- CCAAATCTTGAAGCCTGAGAA-3').

Sequences from all bands of the expected sizes were used to confirm the specificity of the primers.

To determine whether embryonic myosin was expressed in control adult human skeletal muscle, individual control muscle cells were boiled in standard 1x SDS-PAGE sample buffer and ¼ of the sample was loaded per lane on a 12.5% SDS-PAGE gel. Mixed human fetal skeletal muscle cells were prepared from a 163 day of gestation fetal gastrocnemius muscle snap-frozen in liquid nitrogen immediately after dissection, and stored at -80°C. Then, this muscle was digested in 1 mg/5 µl lysis buffer (25mM Tris-HCl pH 7.5, 150mM NaCl, 5mM EDTA, 1% Triton, 5mM Benzamidine, 1mM PMSF, 1% β-Mercaptoethanol) plus a 1:200 dilution of "Protease Inhibitor Cocktail" (Sigma-Aldrich). Following homogenization for ~15 seconds with a TissueRuptor homogenizer, the sample was sonicated for 10 minutes. An equal volume of 2x standard SDS-PAGE sample buffer was added, and the sample was again sonicated for 2 minutes prior to being boiled for 2 minutes.

A second quantitative assessment was performed on small bundles of the remaining samples. ~ 1mg pieces of tissue were placed in ~ 4x volume (20 µL) extraction buffer (in molar: 0.3 NaCl, 0.1 NaH$_2$PO$_4$, 0.05 Na$_2$HPO$_4$, 0.01 sodium pyrophosphate, 0.001 MgCl$_2$, and 0.002 DTT, adjusted to pH 6.5) on ice, then diluted in 9X volume (180 µL) of a 50% glycerol solution containing 40 mM sodium pyrophosphate (adjusted to pH 8.5) [128]. A Bradford assay was used to determine protein concentration. A 12.5% SDS-PAGE gel was run with equal amounts of protein

from the five samples. This was initially probed for embryonic myosin heavy chain, then stripped (Restore Western blot stripping buffer, Thermo Scientific), and probed for anti-α-actin (A2103, Sigma-Aldritch). Densities of bands were analyzed using ImageJ (National Institutes of Health).

2.5   Statistical Analysis

Statistical analyses which reflect literature were used[112,113,129–133]. Statistical analyses used to compare myofibril fits was conducted using ANOVA between groups, followed with Tukey post-hoc analysis, and where appropriate, student t-tests between means, as described in our lab's previous work[132] and in similar work[113,134]. The small patient group size was similar to what has been previously reported[92,99], and as reported, the observed changes only reflect the given group's manifestation of the given mutation and may not reflect all manifestation of that mutation. Genetics has varying degrees of penetrance associated with mutations, and no study can encompass all possible penetrance effects.

Following myofibril experiments, samples were immediately frozen and stored at -20°C. Differences in troponin and myosin expression were performed on some of these samples using a 12.5% SDS-PAGE gel, which was then stained and analyzed as reported. A subset was also transferred to nitrocellulose paper for Western blot.

CHAPTER 3.   HUMAN SKELETAL MUSCLE in DISTAL ARTHROGRYPOSIS

3.1 **Items of Note**

Parts of this section have been published[67] and are reproduced here with permission from _____ (see APPENDIX, Licenses for reprint, Racca *et. al.* 2015)

3.1.1 Aim – To observe the effect of the embryonic myosin R672C mutation on contractile properties of human adult skeletal muscle.

Contractile changes caused by thick filament protein distal arthrogryposis-associated mutations have not been studied and reported in the literature previously. I have found that one such mutation, the embryonic myosin R672C mutation which causes DA2A, has a persistent effect on adult skeletal muscle contractility in two affected patients. Specifically, this mutation leads to a retarding of the cross-bridge cycle rate and decreases in the rates of activation and relaxation.

3.1.2 Key Points

- DA2A affected muscle cells have shown decreased maximum force per cross sectional area and increased passive force following an initial activation. In cell studies, apparent changes in time to reach full activation and full relaxation are also observed.

- DA2A affected muscle myofibrils show no significant changes in maximum force per cross sectional area, but do exhibit slowed activation and relaxation kinetics.

- Cross-bridge detachment and cycling appears to be prolonged in DA2A.

3.1.3 Summary

Distal arthrogryposis is the most common known heritable cause of congenital contractures (e.g., clubfoot) and results from mutations in genes that encode proteins of the contractile complex of skeletal muscle cells. Mutations are most frequently found in *MYH3* and are predicted to impair the function of embryonic myosin. We measured the contractile properties of individual skeletal muscle cells and the activation and relaxation kinetics of isolated myofibrils from two adult individuals with a R672C substitution in embryonic myosin and distal arthrogryposis syndrome

29

2A (DA2A) or Freeman-Sheldon syndrome. In R672C-containing muscle cells, we observed reduced specific force, a prolonged time to relaxation, and incomplete relaxation (elevated residual force). In R672C-containing muscle myofibrils, the initial, slower phase of relaxation had a longer duration and slower rate, and time to complete relaxation was greatly prolonged. These observations can be collectively explained by a small sub-population of myosin cross bridges with greatly reduced detachment kinetics, resulting in a slower and less complete deactivation of thin filaments at the end of contractions. These findings have important implications for selecting and testing directed therapeutic options for persons with DA2A and perhaps congenital contractures in general.

3.1.4   Relevance to fetal skeletal work

This mutation is in a skeletal protein which is primarily expressed during fetal development, thus understanding the differences between fetal skeletal muscle and adult skeletal muscle has helped in outlining the potential causes of dysfunction seen in this muscle. Additionally, as in all types of distal arthrogryposis, the individuals with DA2A included in this study exhibited contractures at birth, indicating *in utero* development of contractures. By knowing that fetal skeletal muscle expressing mostly embryonic myosin is much slower and weaker than adult skeletal muscle, we knew there was a possibility that the DA2A muscle kinetics would likely be strongly influenced by a change in expression of embryonic myosin as compared to control samples.

3.2   Introduction

Congenital contractures (i.e., restricted movement around a joint(s)) such as clubfoot affect ~1 of every 200-500 live births in the United States, and are caused by a combination of genetic and environmental risk factors[43–51,136]. The distal arthrogryposis syndromes are a group of ten autosomal dominant disorders characterized by congenital contractures, most notably clubfoot and camptodactyly (i.e., flexion contractures of the fingers or toes)[38]. To date, we and others have discovered that distal arthrogryposis syndromes can be caused by mutations in each of at least six genes that encode proteins of the skeletal muscle contractile complex including: troponin I, troponin T, β-tropomyosin, embryonic myosin, perinatal myosin, and myosin binding protein C [4,14,52–60].

Despite the identification of genes underlying distal arthrogryposis syndromes, the mechanism(s) by which perturbation of the contractile complex results in contractures has remained unclear. Several studies have examined the functional consequences of either troponin or tropomyosin mutants[63,64], which together account for less than 20% of cases[52–57,62,137]. The outcomes of these studies have been mixed and difficult to reconcile, much less generalize across these disorders. Further inferences about possible mechanisms have been made from studies of homologous proteins found in individuals with conventional myopathies (e.g., nemaline myopathy)[41]. However, unlike conventional myopathies, weakness is not a prominent feature of distal arthrogryposis syndromes. This suggests that mutations that cause distal arthrogryposis syndromes have distinct and novel effects on the contractile apparatus.

Both the most common (i.e., DA2B or Sheldon-Hall syndrome (SHS; OMIM#601680) and the most severe (i.e., DA2A or Freeman-Sheldon syndrome (FSS; OMIM#193700)) DA syndromes are associated with mutations in *MYH3*, which encodes embryonic myosin. Utilizing a variety of complementary techniques to measure parameters of muscle contractility, we evaluated skeletal muscle from two unrelated persons with DA2A (i.e., DA2A-1 and DA2A-2; see Methods for a detailed description of the clinical characteristics of both individuals) caused by a R672C substitution in embryonic myosin. We report that in DA2A muscle cells specific force is reduced and the time to full relaxation is significantly increased compared to controls. Additionally, in DA2A muscle myofibrils, we demonstrate alterations in the early, slow phase of relaxation and the relaxed muscle cell state. Moreover, while the expression of *MYH3* has been considered to be limited to fetal development and shortly thereafter, we found that *MYH3* mRNA and embryonic myosin protein are present in both normal adult and fetal skeletal muscle. This finding suggests that mutations in *MYH3* could affect contractility and relaxation in both prenatal and adult human skeletal muscles.

3.3 Results

3.3.1 *MYH3* & embryonic myosin protein are expressed in adult skeletal muscle

The expression of myosin isoforms is developmentally regulated, and *MYH3* expression is down regulated in skeletal muscle toward the end of gestation in rat, mouse and human[138–140]. Additionally, contractures in persons with distal arthrogryposis are, in general, not progressive

after birth suggesting any perturbation of contractility is mitigated postnatally. Consistent with these observations, we and others have hypothesized that *MYH3* transcript and the resulting embryonic myosin protein are not expressed in adults and that the major effects of defects of embryonic myosin on muscle cell contractility occur prenatally. To test this hypothesis, we examined the expression of *MYH3* RNA and embryonic myosin protein in normal adult muscle cells, and found that both *MYH3* RNA and embryonic myosin were expressed (Figure 3-1A-B). While embryonic myosin heavy chain is a substantially slower myosin than adult isoforms[135,141], quantitative assessments of the control and DA2A samples showed DA2A does not express more embryonic myosin than controls (Figure 3-1C-D). These results suggested that mutant embryonic myosin could continue to influence contractile function postnatally and set the stage for functional testing of muscle cells and myofibrils sampled postnatally.

3.3.2   Force production is lower in demembranated DA2A muscle cells

To test the effect of the presence of the mutant embryonic myosin on force production and passive stiffness in the DA2A muscle cells, we performed *in vitro* force measurements on demembranated single muscle cell segments. The initial, pre-activated passive force (in the absence of calcium) was not different between DA2A-1 muscle cells (5.7 ± 1.1 mN•mm^{-2} (n = 16)) and control muscle cells from two individuals (6.8 ± 1.1 mN•mm^{-2} (23), p = 0.22). Active absolute force was obtained by subtracting this passive force (pCa 9.0) from the total steady-state force. For measures of active contraction, maximal calcium activated force (F_{max}; pCa 4.0) was typically determined first, cells were relaxed (pCa 9.0), then cells were placed in activation solutions containing progressively higher calcium concentrations (decreasing pCa) for determination of the calcium sensitivity of force. Muscle cells were then relaxed again, followed by a final measurement of F_{max} (in pCa 4.0). The initial and final F_{max} were compared, and loss of maximal force was less than 10% during the experimental protocol for all muscle cells except one.

The maximum absolute force per muscle cell was greater for DA2A-1 (0.29 ± 0.04 mN (17)) than for the two controls (0.19 ± 0.02 mN (n = 22), p = 0.019; Figure 3-2A). The average diameter of the DA2A-1 muscle cells (159 ± 8 μm) was significantly larger than that of control muscle cells (104 ± 7 μm, p = 0.0000010; Figure 3-2B). Since all solutions contained 4%

weight-by-volume Dextran (See Methods), which maintains the lattice spacing between thick and thin filaments of myofibrils at approximately the same spacing as intact muscle cells [142,143], the much larger diameter of DA2A-1 muscle cells suggests they were hypertrophied compared to control muscle cells. Because of the much larger diameters, the maximum specific force (i.e., force per cross sectional area) of DA2A-1 muscle cells (13.8 ± 1.6 mN•mm^{-2} (17)) was significantly less than that of control muscle cells (29.0 ± 5.5 mN•mm^{-2} (22), p = 0.0067; Figure 3-2C). In muscle cells from DA2A-2, we observed a depression in specific active force (8.7 ± 0.9 mN•mm^{-2} (9), p = 0.0007) compared to control cells, but this depression was not linked to a larger cell diameter (86 ± 4 µm (22), p = 0.024).

The calcium sensitivity of active contractile force was also determined for muscle cells from DA2A-1 and one control. The force-pCa relationship for individual cells is shown in Figure 3-2D (DA2A-1) and 2E (control), respectively. Calcium sensitivity of force was determined as the concentration of calcium at which half-maximal force was produced (pCa$_{50}$) for each muscle cell, determined from Hill equation fits of the data (Methods). When the pCa$_{50}$ values for individual muscle cells were averaged they did not differ significantly between DA2A-1 (pCa$_{50}$ 5.53 ± 0.07 (11)) and control (pCa$_{50}$ 5.58 ± 0.03 (11)) muscle cells. There was also no difference in the average slope (cooperativity; n_H) of the force *vs.* pCa curves. However, there was far greater variation in both of these parameters in DA2A-1 cells compared to control cells. This was not likely due to differences in muscle cell types *per se*, as both DA2A-1 and the control samples contained a similar mix of fast and slow twitch muscle cells.

DA2A-1 muscle cells had a profoundly slower relaxation when moved from the well containing maximal calcium activation solution (pCa 4.0) to one containing relaxation solution (pCa 9.0) compared to control cells (Figure 3-2H). DA2A-1 muscle cells required four-fold longer to reach 50% relaxation (p = 0.000049) and ten-fold longer to reach 90% relaxation (p = 0.00019; Figure 3-2I), compared to control muscle cells. However, as relaxation kinetics are not accurately determined via exchange baths because the length of time required for calcium to leave the cell is limited by diffusion, we next studied relaxation in more detail with isolated myofibrils. One possibility for the much longer relaxation times of DA2A muscle cells could be slower buffering of calcium by EGTA in relaxation solution (pCa 9.0) due to the much larger diameter of these muscle cells. The markedly longer relaxation times for DA2A muscle cells

could be a function of muscle cell diameter; however, regression analysis showed that activation and relaxation times are not a function of muscle cell diameter (Figure 3-3). Additionally, if diffusion was a major determinant in the differences between DA2A and normal muscle cell relaxation, we would expect it to have a similar effect on activation times. However, while activation was significantly slower for DA2A muscle cells, the difference was not nearly as profound.

3.3.3 DA2A myofibril activation & relaxation kinetics are slower than control

Relaxation kinetics of DA2A and control muscle were then more accurately measured with myofibril preparations and rapid solution switching technology, where diffusion rates do not limit the assessment of the millisecond timescale of force generation and relaxation kinetics (Figure 3-4A-H). DA2A myofibrils produced a similar level of maximum specific force (DA2A-1: 14.8 ± 4.6 mN•mm^{-2} (13), $p = 0.70$; DA2A-2: 8.5 ± 1.6 mN•mm^{-2} (12), $p = 0.19$) as control myofibrils (12.7 ± 2.7 mN•mm^{-2} (30); Figure 3-4C). However, the force generation and relaxation kinetics differed for DA2A $vs.$ control muscle myofibrils (Figure 3-4A). The rate of force generation following a step change in calcium (k_{ACT}) from pCa 9.0 to pCa 4.0 was significantly slower for myofibrils from DA2A-1 (0.21 ± 0.02 s^{-1} (12)) compared to control myofibrils (0.41 ± 0.07 s^{-1} (29), $p = 0.0088$; Figure 3-4F). Additionally, the rate of force generation was more consistent among DA2A myofibrils with a narrow unimodal distribution ranging from $0.08 – 0.43$ s^{-1}, than among myofibrils from control muscle with a bimodal distribution ranging from $0.03 – 0.90$ s^{-1} (Figure 3-4A-B). The bimodal distribution of force generation rate measurements for control myofibrils is consistent with myofibrils sampled from both fast and slow twitch muscle cells [80,141,144], whereas the tight clustering of force generation rate measurements from DA2A suggest that the embryonic myosin R672C mutation could be limiting the rate of contractile activation in fast twitch muscle cells (i.e., making fast-twitch muscle cells behave more like slow twitch muscle cells).

Isolated myofibril preparations also allowed us to observe the biphasic nature of relaxation. Myofibril relaxation was characterized by an initial "slow" phase ($k_{REL,slow}$ and $t_{REL,slow}$; Figure 3-4A, top inset), which constitutes <10% of the force loss in relaxation, and a secondary "fast" phase ($k_{REL,fast}$, $t_{REL,90}$; Figure 3-4A), which constitutes the majority of the force

loss in relaxation. While a single exponential decay model ($F = F_{initial} \bullet e^{-k_{REL,fast} \bullet t}$) described the fast phase of relaxation for control myofibrils, the fast phase of relaxation in DA2A myofibrils did not fit this model. To compare the fast phase of relaxation between control and DA2A myofibrils, we estimated the rate of the fast phase relaxation ($k_{REL,fast}$) from the time to 50% relaxation (see Methods) and also measured the time to 90% relaxation. The fast phase relaxation rate was twice as slow for DA2A myofibrils ($k_{REL,fast}$: 0.49 ± 0.05 s^{-1} (26)) compared with control myofibrils ($k_{REL,fast}$: 1.08 ± 0.18 s^{-1} (29), p = 0.0028; Figure 3-4D)). The time to 90% relaxation was also about twice as long for DA2A myofibrils compared with control myofibrils ($t_{REL,90}$: DA2A 20.0 ± 1.2 s (26) *vs*. control myofibrils 11.4 ± 1.2 s (27), p < 0.00001; Figure 3-4E).

While the force loss during the initial, "slow" phase of relaxation is small in comparison to the magnitude of force loss in the fast phase of relaxation, it provides information about the deactivation of myofibrils. The slope of this initial slow relaxation phase ($k_{REL,slow}$) is thought to reflect the rate of crossbridge detachment during relaxation [114,145,146], which is required for thin filament deactivation. The slow phase relaxation rate was >3-fold smaller in DA2A myofibrils ($k_{REL,slow}$: 0.14 ± 0.02 s^{-1} (24)) compared to controls ($k_{REL,slow}$: control 0.47 ± 0.09 s^{-1} (28), p = 0.0011; Figure 3-4G). The duration of the slow phase relaxation ($t_{REL,slow}$) was also ~50% longer for DA2A-1 (264 ± 20 ms (14) *vs*. control (181 ± 15 ms (27)) (p = 0.0023; Figure 3-4H). Even so, the slow phase constituted significantly less of the total amplitude of relaxation in DA2A compared to controls myofibrils (slow phase amplitude over total amplitude of relaxation: control 5.4 ± 0.7 % (26) *vs*. DA2A-2 3.1 ± 0.7% (10) (p = 0.028) and *vs*. DA2A-1 2.4 ± 0.5% (14) (p = 0.0018)). Collectively, these results support the idea that a sub-population of crossbridges in DA2A myofibrils have a slower detachment rate that retards the slow phase specifically and relaxation overall.

3.3.4 R672C-containing muscle may have abnormally long-lived crossbridges

To study relaxation in more detail we next subjected both muscle cells and myofibrils to a series of experiments to determine the effects of slower crossbridge detachment by a sub-population of long lasting crossbridges (presumably those with the R672C mutation). Following calcium activation, relaxation in a pCa 9.0 solution appeared incomplete for individual DA2A muscle cells but not control muscle cells. Passive force for DA2A-1 muscle cells increased nearly two-

fold (3.8 ± 1.3 mN•mm^{-2} vs. 7.1 ± 2.6 mN•mm^{-2} (9), p=0.011) after the first activation, a gain not seen in control muscle cells. We relaxed the DA2A-1 muscle cells in BDM to inhibit strong crossbridge binding (Methods). Following the initial pCa 4.0 activation and pCa 9.0 relaxation, cells were activated a second time in pCa 4.0 and then relaxed in pCa 9.0 solution containing 30 mM BDM. Relaxation in the presence of BDM was more complete, with 32 ± 17 % (n=4) greater reduction in passive force compared to relaxation in pCa 9.0 without BDM, indicating crossbridge inhibition could modulate the increase in passive force. As a further demonstration, for a sub-set of isolated myofibril preparations (DA2A-2, n=12), after the initial activation (pCa 4.0) and relaxation (pCa 9.0) myofibrils were exposed to a second relaxation solution that contained 30 mM BDM, which further reduced force compared to the first relaxation solution without BDM (Figure 3-5A). Force rebounded when myofibrils were switched back to original relaxation solution without BDM, indicating the presence of long-lived crossbridges that did not detach in the presence of BDM. There was no further reduction in force, indicating that these long-lived crossbridges did not detach, when myofibrils were switched from pCa 9.0 to a second pCa 9.0 solution without BDM (Figure 3-5A, inset). These results support the hypothesis that after periods of muscle activity, a small set of "long-lived" attached crossbridges continue to exist at rest.

Additional evidence for long-lived attached crossbridges was found upon measuring the rate of isomeric tension redevelopment (k_{TR}) following a quick release-restretch of single muscle cells. In normal muscle cells, the k_{TR} protocol shortens the muscle cell's length during the release (slack) phase during which the low strain condition greatly accelerates the rate of crossbridge detachment. When re-stretched, myosin heads re-attach and generate force [88,147,148]. While control muscle cells demonstrated low residual force upon re-stretch (indicating high crossbridge turnover during the slack phase), DA2A-1 muscle cells demonstrated abnormally high residual starting force (75 ± 6 % (16)) (Figure 3-5B). This result is indicative of a high number of crossbridges remaining attached during the shortening phase of the protocol that produce force immediately upon the strain of re-stretch[86].

3.3.5 <u>Histological analysis of muscle from persons with DA2A</u>

It is plausible that the muscle cell structure is abnormal in DA2A, which could affect the contraction. However, H&E, NADH and modified Gomori trichrome staining showed relatively

normal muscle architecture (data not shown). While rare small muscle cells with a slight increase in central nuclei suggested a trace amount of necrosis and regeneration, there was no other overt evidence of necrosis or inflammation.

An ATPase assay of histological sections, verified using an antibody specific for adult fast-twitch myosin heavy chains, showed a similar proportion of cell types in DA2A muscles, (DA2A-1: Type I 40% by ATPase, Type II 60% by ATPase or 61% by immunohistochemistry; DA2A-2: Type I 56% by ATPase, Type II 44% by ATPase or 45% by immunohistochemistry; controls: 22%, 57%, and 83% fast/Type II by ATPase or immunohistochemistry) and a similar non-grouped mosaic arrangement pattern to that found in control muscle samples.
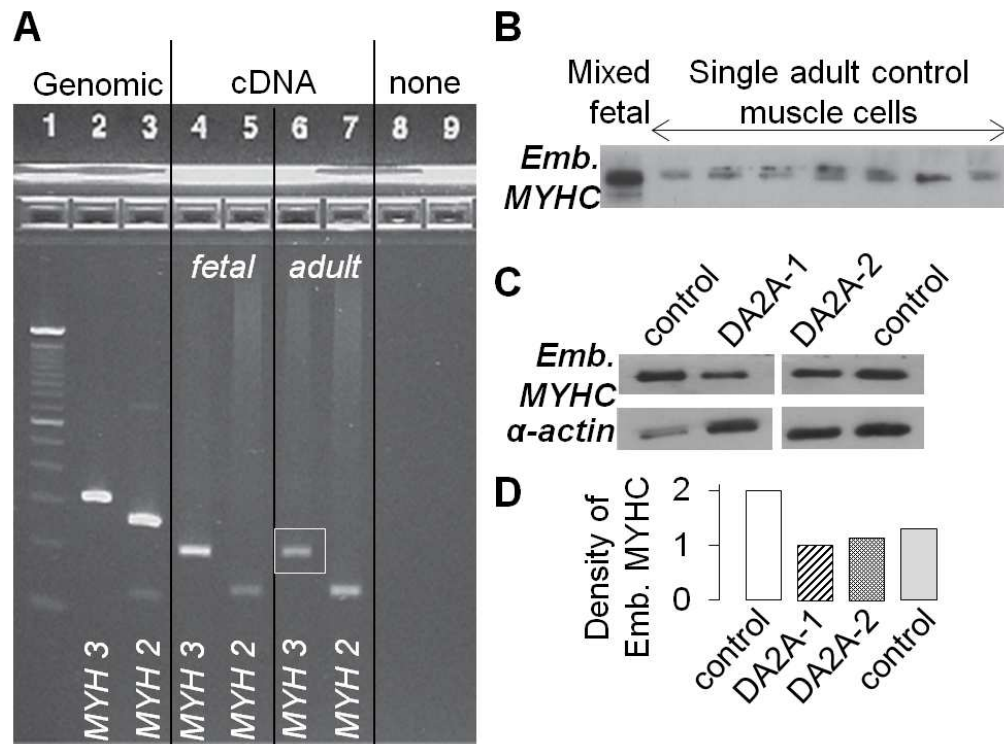
Figure 3-1: *MYH3* mRNA and embryonic myosin protein are expressed in both fetal and adult human skeletal muscle.

(**A**) Ethidium bromide stained agarose gel: 100bp ladder (Lane 1); amplicons of *MYH3* (Lane 2) and *MYH2* (Lane 3) from genomic DNA; amplicons of *MYH3* (Lane 4) and *MYH2* (Lane 5) from human fetal skeletal muscle (19-22 week estimated gestational age) cDNA; amplicons of *MYH3* (Lane 6) and *MYH2* (Lane 7) from human adult skeletal muscle cDNA. Genomic amplicons included an intron so as to distinguish amplification of cDNA from genomic DNA. Expected product sizes were as follows: *MYH3* genomic (313 bp), *MYH3* mRNA/cDNA (206 bp), *MYH2* genomic (264 bp) and *MYH2* mRNA/cDNA (142 bp). (**B**) Western blot of proteins separated by SDS-PAGE hybridized with an anti-embryonic myosin antibody, showing presence of embryonic myosin in adult control skeletal muscle cells. Control skeletal muscle from the gastrocnemius of a 163 day fetus, mixed muscle cells (Lane 1); single control adult muscle cells (Lanes 2 – 8). (**C**) Western blot of proteins separated by SDS-PAGE hybridized with an anti-embryonic myosin antibody, showing expression differences of embryonic myosin in adult DA2A (2 individuals) and control (2 individuals) skeletal muscle extracts, with anti- **α** -actin as a loading control. (**D**) Densitometry analysis of embryonic myosin expression between samples.
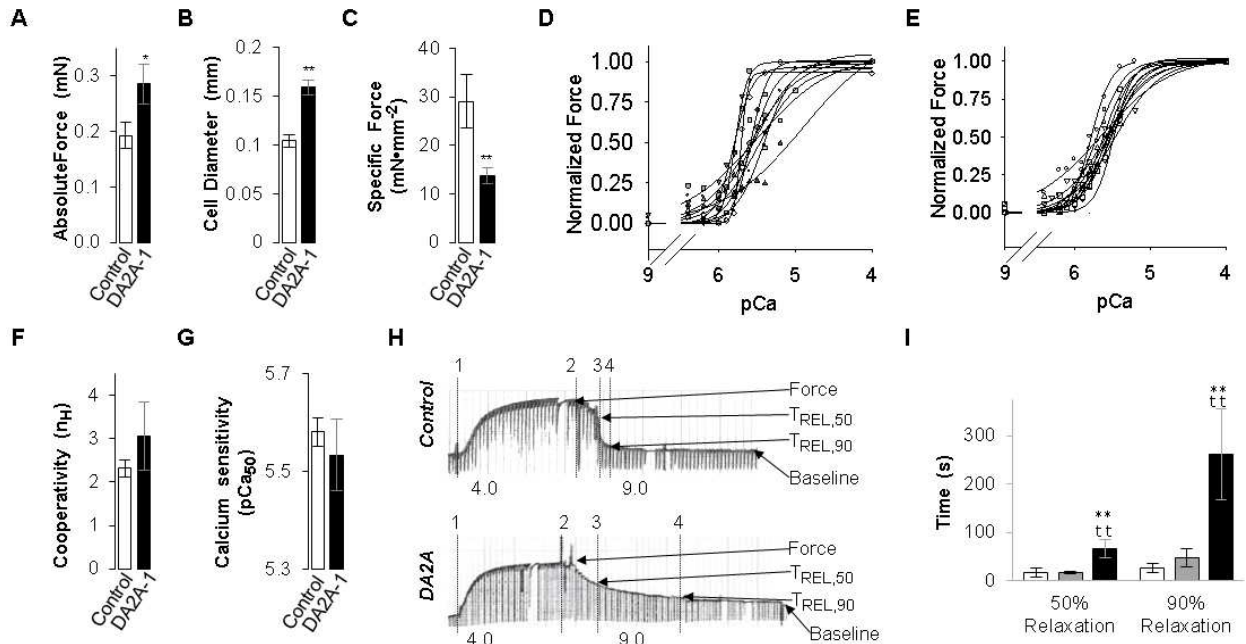
Figure 3-2. DA2A-1 muscle cells (grey) hypertrophy and produce less specific force and relax more slowly than controls (white/grey), while cooperativity and calcium sensitivity remain unchanged.

Student's t-tests were used to compare DA2A-1 and control groups: double stars indicate $p<0.01$, single stars indicate $p<0.05$. (**A**) Maximum absolute force (per muscle cell) is significantly higher in DA2A-1 cells. (**B**) However, cell diameters are significantly wider in DA2A-1 muscle cells. (**C**) Therefore, maximum specific force (force per cross sectional area) is drastically lower in DA2A-1 cells. (**D**) Force- pCa curves for all DA2A-1 cells *vs*. (**E**) control cells, demonstrating increased variability in DA2A-affected cells. (**F**) Averaged cooperativity (n_H) in DA2A-1 curves = 3.07 ± 0.8 (11) *vs*. control curves = 2.31 ± 0.20 (11). These differences were not significant for the $p<0.05$ level. (**G**) Average pCa $_{50}$ DA2A curves = 5.53 ± 0.07 (11) *vs*. control curves = 5.58 ± 0.03 (11). These differences were not significant for the $p<0.05$ level. Relaxation of muscle cells is much slower in DA2A-1. (**H**) Recordings of force generation of a control (top) and a DA2A-1 (bottom) muscle cell at maximal Ca^{2+} activation (pCa 4.0) followed by immersion in relaxing solution (pCa 9.0) with start of contraction (vertical line 1), start of relaxation (2), 50% relaxed ($T_{REL,50}$)(3), and 90% relaxed ($T_{REL,90}$) (4) indicated. (**I**) Average time ($\pm$ SEM) required to achieve 50% relaxation and 90% relaxation for control muscle cells (white bars, n=9; grey bars, n=2) and DA2A-1 muscle cells (green bars, n=8). Both controls required significantly less time to fully relax ($p < 0.01$).

39

A. Time to 100% Activation

$R^2 = 0.0175$

$R^2 = 0.2996$

seconds

Diameter in μm

B. Time to 50% Relaxation

$R^2 = 0.2276$

$R^2 = 0.0217$

seconds

Diameter in μm

C. Time to 90% Relaxation

$R^2 = 0.0529$

$R^2 = 0.019$

seconds

Diameter in μm
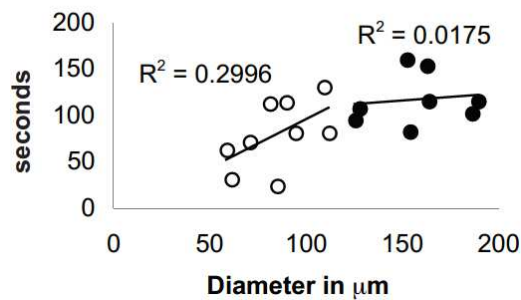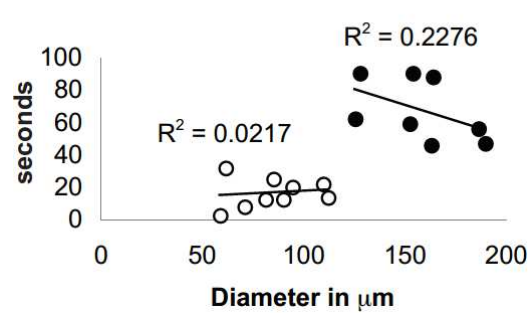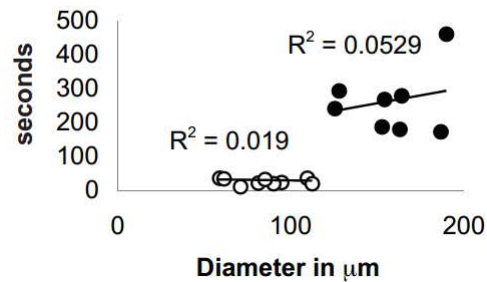
Figure 3-3. Activation and relaxation times in DA2A muscle cells.

Linear regression of time to 100% activation (**A**), 50% relaxation (**B**) and 90% relaxation (**C**) *vs.* muscle cell diameter for each individual muscle cell from control (open circles) and DA2A muscle cell (filled circles). No significant relationship was observed between time to relaxation and muscle cell diameter.
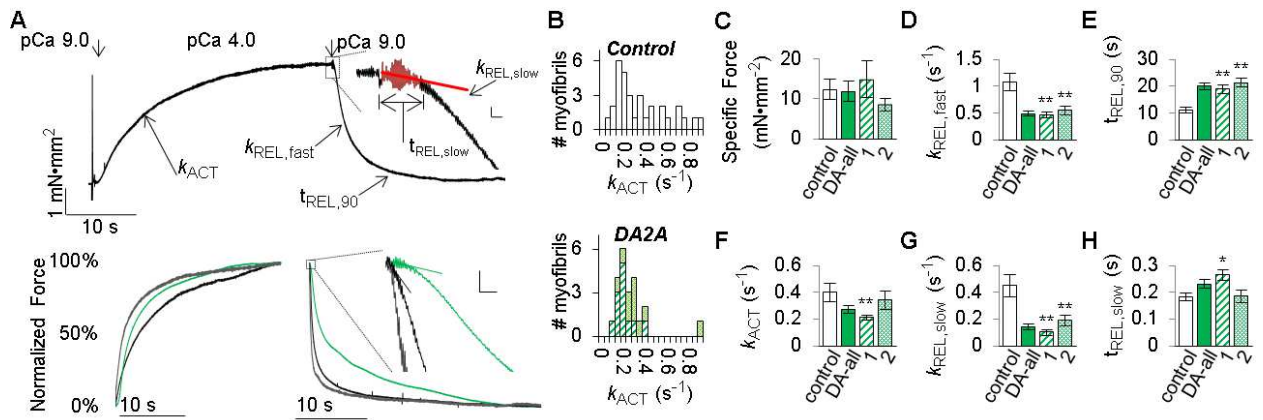
Figure 3-4: DA2A myofibrils exhibit significantly slowed kinetics.

(**A**, **top**) Diagram of activation and relaxation kinetics on human adult traces. (**A, top insert**) First second of relaxation, with red data indicating the data which was analyzed for slow phase kinetics. The vertical bar indicates 0.1 mN•mm^{-2} force; the horizontal bar indicates 100 ms. (**A, bottom**) Example normalized force traces of human adult control fast (grey), adult normal slow (black), and human adult DA2A (green) myofibrils. (**A, bottom insert**) DA2A slow phase of relaxation is significantly slower than heterogeneous control myofibrils. The vertical bar indicates 5% of force; the horizontal bar indicates 100 ms.

(**B**) Histograms of myofibril activation times. Shown are k_{ACT} (in s^{-1}) rates for control (top, grey) *vs*. DA2A-1 (bottom, striped green) and DA2A-2 (bottom, hatched green) myofibrils. Bin size was chosen to be roughly the SEM of both groups = 0.05 s^{-1}.

(**C-H**) Pronounced effect on DA2A myofibril kinetics and force generation. Shown are control (white), both DA2A patients together (solid green), DA2A-1 (striped green), and DA2A-2 (hatched green). (**C**) Maximum specific force produced was not significantly different between control and DA2A myofibrils. (**D**) The rate of total relaxation ($k_{REL,fast}$) was significantly slower in both DA2A-1 and DA2A-2 myofibrils. (**E**) The time to 90% relaxation ($t_{REL, 90}$) was drastically longer in both DA2A myofibril populations. (**F**) The rate of force production (k_{ACT}) was significantly slower in DA2A-1 myofibrils. (**G**) The rate of the slow phase of relaxation ($k_{REL,slow}$) was significantly slower in both DA2A populations. (**H**) The duration of the slow phase of relaxation ($t_{REL,slow}$)was significantly slower in DA2A-1.
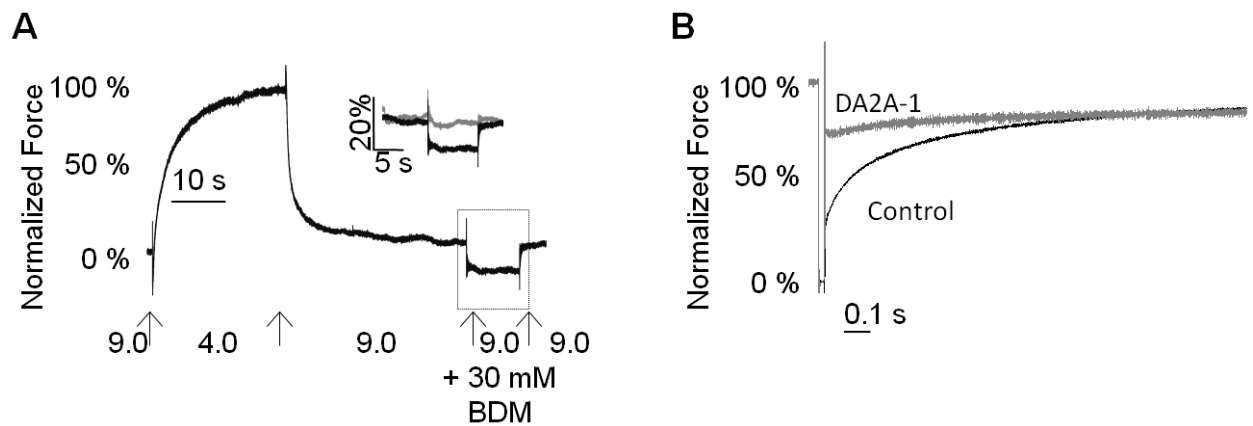
Figure 3-5: DA2A muscle shows prolonged crossbridge attachment.

(**A**) Following a full relaxation, the amount of passive force in myofibrils was further reduced in BDM solution (black) compared to pCa 9.0 solution (grey, inset) in DA2A-2 myofibrils.

(**B**) The slack-restretch maneuver in DA2A-1 (grey) and control (black) muscle cells.

3.4   Discussion

We have demonstrated that muscles of individuals with DA2A caused by a R672C substitution in embryonic myosin show a markedly increased time to relaxation. This increased relaxation time and the elevation of passive tension following calcium activation of contraction are novel observations among individuals with distal arthrogryposis, and congenital contractures in general, and suggest that the rate of turnover of crossbridges can be slowed by a small population of mutant myosins. The exact mechanism underlying diminished crossbridge turnover remains to be determined.

The R672 residue is located near the groove between the two 50kDa domains in the embryonic myosin head that forms the ATP binding site. Accordingly, the arginine to cysteine substitution could perturb nucleotide transition in and out of the binding pocket[14]. The difference in magnitude and distribution of activation rates between DA2A myofibrils and control myofibrils highlight a role mutant embryonic myosin may play in the activation of the muscle. The mutant myosin, with a drastically slower crossbridge release rate, could add a drag to sarcomere shortening by remaining attached to actin and preventing filament sliding[3,149]. The changes in slow phase relaxation kinetics in DA2A myofibrils provide evidence for a significantly slower crossbridge release rate ($k_{REL,slow}$)[144] and a potential secondary affect. The slow phase relaxation duration ($t_{REL,slow}$), which is related to the time that thin filaments remain "on" allowing crossbridge cycling to continue[144], was also significantly longer in DA2A-1 myofibrils. The longer duration and diminished slope of the slow phase of relaxation in DA2A myofibrils could be explained by the mutant myosin remaining bound to actin and preventing tropomyosin from moving back to an inhibitory position on F-actin following the release of calcium from troponin. Taken together, these results suggest there may be substantial differences in kinetics of myosin crossbridge chemo-mechanical cycling that affect thin filament state transitions[150] of DA2A myofibrils. A substantial change in crossbridge cycling is supported by the observed high residual force in DA2A muscle cells following the slack portion of the slack/re-stretch maneuver. This effect is also seen in demembranated normal muscle cells activated in solutions with low concentrations of ATP such that crossbridge detachment was slowed [86].

Alternatively, a higher percentage of embryonic myosin present in skeletal muscle of DA2A myofibrils could also explain slower crossbridge turnover, as embryonic myosin is slower[135,141] and the presence of a small amount of slow myosin can substantially change the kinetics of the muscle as a whole[3,149]. However, our results suggest there are at most minor differences in the amount of embryonic myosin present between the DA2A and control samples, with the DA2A samples potentially carrying less embryonic myosin than controls.

Whether delayed and incomplete relaxation is a general mechanism underlying the development of congenital contractures in individuals with this and other mutations in *MYH3* is unclear. To date, no other studies of muscle cell contractility in individuals with defects of embryonic myosin have been reported. The effects on muscle cell contractility of mutations in several other genes that underlie distal arthrogryposis disorders, including troponin T (*TNNT3*)[63], troponin I (*TNNI2*)[63], tropomyosin (*TPM2*)[63–65], and myosin binding protein C(MyBP-C)[137], have been investigated. These studies suggest a common feature of congenital contractures may be dysregulation of thin filament regulation, either through direct changes in regulatory protein function, or indirect effects on the ability to regulate through dysfunction of myosin or myosin binding protein C (MyBP-C). In some cases, such as herein, this may also result in elevated resting tension, especially following periods of muscle activity.

The presence of an abnormal contractile protein during fetal development can leave a long-lasting change in adult muscle cells[151], either through structural changes in the sarcomere or abnormal stoichiometry in the remaining thick or thin filament proteins. However, the physical presence of the embryonic myosin in the muscle cells studied leads us to hypothesize that the presence of mutant embryonic myosin, even at much lower quantitative levels than other myosins, can create a dominant negative effect on the contractile properties of the adult muscle cells.

Whether our findings can be generalized to other DA2A mutations in *MYH3*, or to DA-causing mutations in other genes that encode contractile components of skeletal muscle, is unclear. Indeed, there is some evidence that such mutations can cause congenital contractures by several different mechanisms. An *in vitro* study of demembranated rabbit muscle cells containing recombinant mutant troponin and tropomyosin molecules showed increased calcium sensitivity and force generation[63]. This increase in force and calcium sensitivity suggests that DA

syndromes are, in some cases, caused by increased muscle cell contractility[63]. On the other hand, *ex vivo* contractility studies using demembranated human muscle cells with mutant tropomyosin showed diminished maximal force production with no change in calcium sensitivity of force[64,65]. Whether these dissimilar results are the result of differences in experimental approach, the particular protein containing the mutation, and/or real differences in the mechanisms that cause contractures remains unknown.

Interventions based on specific muscle contractile deficits can show improved outcomes in muscle abnormalities that arise from both genetic mutations and muscle damage[152,153]. To date, we have studied genetic therapies that alter calcium sensitivity and crossbridge cycling[154–156]. While others have observed increases in contractility and changes to calcium sensitivity in DA[63,64], in this study we have demonstrated a deficit of the contractile apparatus, in the crossbridge cycle and detachment, which highlights a potential targeted therapeutic strategy moving forward. 2-deoxy-ATP has been shown to improve cross-bridge detachment and increase the rate of cross-bridge cycling in muscle[35,86,88] and would be an excellent candidate in future studies to develop a therapeutic for patients who show this specific contractile deficit.

Studies of contractile function in human tissues sampled from persons with rare conditions are frequently constrained by the availability of samples. Samples acquired in this study were also stored at -80°C prior to beginning experiments, which may affect the sample quality. The small sample number and cold storage was a limitation of our studies. Yet, samples from the two unrelated individuals with DA2A studied herein demonstrated similar departures from the contractility parameters of control muscle.

This is the first study to compare the contraction and relaxation properties of muscle cells and myofibrils from individuals with an *MYH3* mutation that causes congenital contractures. The combination of single cell and myofibril preparations has allowed us to examine muscular dysfunction *ex vivo* at cellular and subcellular levels. In muscle from two individuals with DA2A, we demonstrated abnormal contractile kinetics including remarkably prolonged relaxation. Such drastic changes in relaxation kinetics have not been observed previously[63–65]. Furthermore, we find that crossbridge detachment rate is reduced and could explain both the observed elevation in passive force and the prolonged relaxation. Our experiments highlight the importance of studying not only the force production, but the kinetics of force production and

relaxation to fully ascertain the cause(s) of mechanical dysfunction and to distinguish with greater precision potential therapeutic options.

3.5   Conclusions

Myosin mutation *MYH3* R672C appears to significantly reduce the amount of force generated by muscle cells, and indeed, affects the force generation at the myofibril level. Myofibrils from muscles of patients with the *MYH3* R672C mutation not only show reduced force, but they appear to be slower to activate and relax, indicating that cross bridge cycling is inhibited. Changes in relaxation are even apparent on a skinned cell level of testing.

3.6   Continuing and Future Work

3.6.1   Introduction to thin filament mutations

Though mutations in fast skeletal troponin I (gene *TNNI2*[63]), troponin T (*TNNT3*[63]) and β-tropomyosin (*TPM2*[57,63–65]) explain only a small fraction of DA cases, as mentioned above, these mutations afford more possibilities for experiments *in vitro*, which do not all produce similar force production deficits as the embryonic myosin R672C mutation. Whether these varied effects are the result of differences in experimental approach or differences in the mechanisms by which mutations in genes encoding contractile proteins cause contractures is unknown.

In contrast to thick filament mutations, thin filament mutations are likely to have altered contraction and relaxation kinetics that become apparent at sub-maximum calcium concentrations. Troponin mutations TnI and TnT mutations have been shown to alter calcium sensitivity and cooperativity[63]. The TnI R174Q mutation creates increased calcium sensitivity, with a possible increase in the cooperativity of the thin filament. The TnT R63H mutation also increased calcium sensitivity without changing the cooperativity of the thin filament. Changes to Troponin-Tropomyosin conformation and mobility may affect the rate at which myosin-binding sites on actin become available and become unavailable (the thin filament on/off transition).

3.6.2   Myofibril setup with troponin mutations

The myofibril setup would be able to show changes in kinetics of the troponin-tropomyosin on/off switching caused by these mutations in TnI and TnT, through the myofibril activation rate

and the duration of the slow phase of relaxation. Recent experiments in the use of myofibrils have shown that calcium sensitivity of the troponin regulatory unit can be detected in the kinetics of the relaxation of the myofibril, and these rates have been attributed to tropomyosin movement[112,132].

Force measured at low concentrations of calcium, combined with a rapid stretch-releases, was used to determine passive elastic element properties and cross bridge binding at rest. If strain at low calcium concentrations is increased relative to control because of cross bridge binding, addition of cross bridge inhibitors (BDM[97] or Vanadate[6]) would return the strain to normal levels. The rapid stretch-release protocol determines the strength of cross bridge binding at rest, and provides clues to the resting distribution of cross bridge chemo mechanical 'states', which can change with altered regulation[88].

I expect myofibrils containing myosin mutations will not slow cross bridge detachment kinetics, as seen in the data for cells containing *MYH3* R672C, but instead will slow the "off" rate for the troponin complex and thin filament, forcing a longer duration of the slow phase and possibly leading to a prolonged relaxation.

3.6.3 Future Directions *in silico* modeling with TnI

A glaring hole has existed in understanding the structural changes brought about by distal arthrogryposis mutations, including those in TnI and myosin. A potential continuation of my project could span into working with *in silico* modeling to explain how the changes seen in myofibrils, muscle cells, and overall phenotype change protein-to-protein interactions and help highlight avenues for intervention.

Some forms of distal arthrogryposis are caused by missense and nonsense mutations of the "mobile domain" (Md) region of TnI. While it is possible that TnI nonsense mutations result in mRNA policing and recycling of mutant copies, this hypothesis remains unsubstantiated. *In vitro*, the R174Q missense mutation causes reduced calcium sensitivity[63]; however, TnI is not directly responsible for calcium-binding in the sarcomere. Indeed, the mutation seen in distal arthrogryposis is not even within the region of TnI that directly interacts with TnC, the calcium-binding troponin subunit.

I suspect troponin mutations to this region of TnI change the availability of cross bridge binding sites on actin. fsTnI R174Q is in the COOH-terminal end of TnI, believed to interact with actin and/or tropomyosin[68,69]. In previous studies, cardiac mutations in the same region of TnI have been shown to reduce calcium sensitivity of contraction[70,71].

I have explored the possibility of modeling TnI mutation R174Q using molecular dynamics simulations, as described below. This study is limited to the small fragment of TnI known as the mobile domain region of TnI. This region has not been crystallized in conjunction with the rest of troponin I, nor other parts of the troponin, tropomyosin, or actin proteins, though it is believed to interact with actin[30,31,68].

The mobile region of TnI is believed to work as a fail-safe latch[30], and it has been shown to inhibit myosin-s1 ATPase activity[31]. This region is of TnI may only be structured when it is fulfilling its inhibitory role, docked into actin[30,31]. Key features of this region of TnI include a β-bulge at residues 146-150, which is held together by a 2 stranded β sheet (residues 143-145, 151-153), with small loops and α-helices at either end. Many residues in this β-sheet and bulge region are believed to be important to Md-TnI to actin docking[30,31,68]

Gross changes were observed in overall RMSD between the native and mutant (R173Q) Md-TnI. The average RMSD values of the whole protein for the last 5 ns of simulation were as follows: for native starting structure without calcium 4.8 ± 0.8 angstroms (n = 6), for the R173Q mutant starting structure without calcium 5.1 ± 0.8 angstroms (n = 6), for native starting structure with calcium 5.5 ± 1.0 angstroms (n = 6), and for R174Q mutant starting structure with calcium 8.7 ± 2.5 angstroms (n = 6). Loop 1 (141 - 142) and loop 3 (168- 169) are highly flexible and may favor binding to actin in low calcium, perpetuating the pre-activation state and preventing strong-myosin-actin binding[30] . Loop 1 and 2 (154-157) made significantly less contacts in the mutant forms than the WT forms. Indeed, contact times for side chains on residue 142 to residues 146-150 ranged from 0-5% of simulation time for the mutant Md-TnI from high calcium, whereas the same residues in the native form boasted contacts >2-fold higher ranged between 13-22% of time over 3 or more simulations. This change in contacts can be attributed to the change in overall conformation of the protein, where it is apparent that the two α helices in the mutant form have pulled apart (Figure 3-6).

These preliminary studies have found that the R174Q mutation changed the conformation the mobile domain of TnI, eliminating key contacts that were important for the β-bulge region (K145-E151) and changing to overall shape of the Md-TnI fragment. The mutation resulted in changes in structure from both the low calcium state and the high calcium starting state, regardless of which starting NMR structure was used; however, changes from the starting structure of the high calcium state were more pronounced.

These simulations are limited by the lack of surrounding structure, which may offer more stability through hydrophobic interactions and hydrogen-bonding. However, evidence exists of the Md-TnI being highly mobile in the presence of high calcium, implicating that other structures may not be in close contact for long enough periods of time to substantially affect the structure of this region[30,31].

The increased calcium sensitivity found through experiments could be explained by the behavior we see in our limited system as follows. The flexibility of the Md-TnI contributes to its binding to actin in the low calcium state[30,31,68,69]. If this mutation results in an Md-TnI fragment that is less stable and responsive to conformational changes from a Ca^{2+} - bound TnC subunit, then steric hindrance of the Md-TnI subunit would fail to inhibit tropomyosin movement at low calcium concentrations. This failed inhibition of tropomyosin movement would slow down the closing of the myosin-actin binding site, allowing force generation at lower calcium concentrations. Further work to test whether the R174Q mutation prevents actin to Md-TnI docking is warranted. First, a binding assay should be performed to see if the mutation prevents the mutant TnI domain from binding to actin would be a good first step, followed by experiments using FRET or additional *in silico* models, which would have to estimate the position of the mobile domain and dock it to the actin binding site.
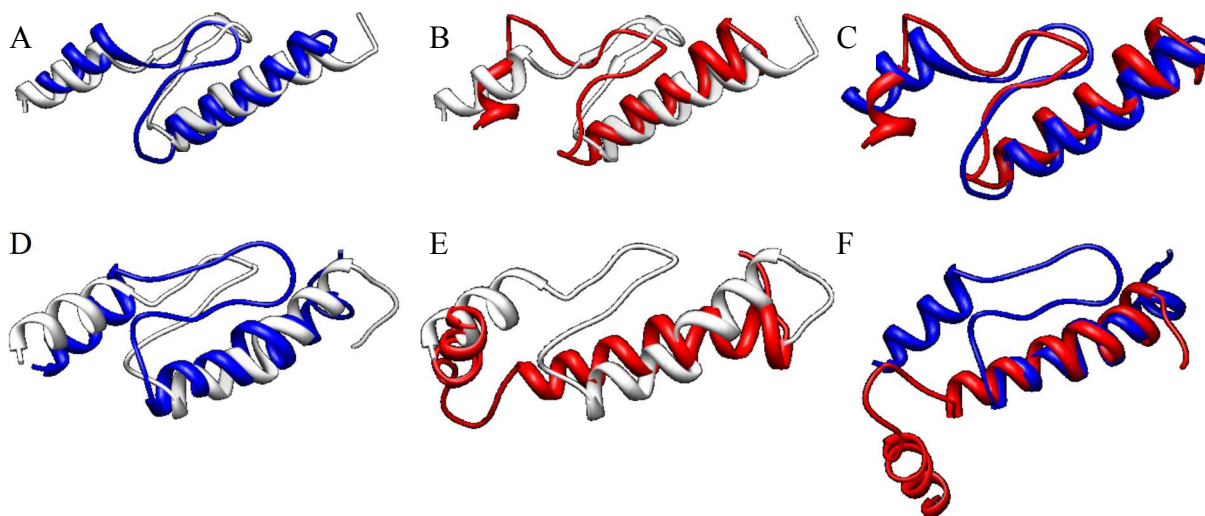
Figure 3-6: Representative ribbon structures from the last 5 ns of 30 ns of simulation.

The white ribbon is the starting PDB structure of the mobile domain of fsTnI. 1VDI (low $[Ca^{2+}]$ structure) is (**A-C**). 1VDJ (high $[Ca^{2+}]$ structure) is (**D-F**)

(**A**) WT *vs.* initial low $[Ca^{2+}]$ structure

(**B**) R174Q mutant *vs.* initial low $[Ca^{2+}]$ structure

(**C**) WT in blue *vs.* mutant in red low $[Ca^{2+}]$ final structures

(**D**) WT *vs.* initial high $[Ca^{2+}]$ structure

(**E**) R174Q mutant *vs.* initial high $[Ca^{2+}]$ structure

(**F**) WT in blue *vs.* mutant in red high $[Ca^{2+}]$ final structures

CHAPTER 4.   HUMAN FETAL SKELETAL MUSCLE

4.1 Items of Note

Parts of this section have been published[135] and are reproduced here with permission from John Wiley and Sons (see APPENDIX, Licenses for reprint, Racca *et. al.* 2013)

4.1.1 Aim: To observe the contractile and chemo mechanical properties of wild-type human fetal skeletal muscle.

Little is known about the contractile and chemo mechanical properties of embryonic myosin in human skeletal muscle. I have observed maximal force production and activation and relaxation kinetics from single isolated myofibrils from human skeletal muscle biopsies. I have also performed *in vitro* motility assay experiments to quantify the substrate sensitivity and ATPase rate of embryonic (*MYH3* gene) myosin.

4.1.2 Key points

1) Mutations in human fetal skeletal muscle sarcomere genes cause congenital contracture syndromes.

2) The contractile properties of human fetal skeletal muscle are unknown, but multiple forms of muscle disease present *in utero*.

3) Reductionist approaches such as isolated myofibril and isolated contractile protein biomechanical assays allow study of activation and relaxation properties of different skeletal muscle from different sources.

4) We have tested the contractile properties of human fetal skeletal muscle and compared them with human adult skeletal muscle and rabbit psoas muscle.

5) Human fetal skeletal myofibrils have much slower kinetics of activation and relaxation as compared to myofibrils from adult human or rabbit psoas skeletal muscle.

6) Investigations using altered substrate and product conditions using for both the *in vitro* motility assay and myofibril mechanics/kinetics indicate that fetal muscle acto-myosin

cross bridge cycle more slowly, but with similar rate-limiting steps, as the adult myosin isoforms.

4.1.3 Summary

Congenital contracture syndromes occur in 1 of 1000 live human births and can be caused by missense mutations in genes that encode prenatal specific skeletal myosin heavy chains. To understand how these mutations alter development of the contractile properties requires comparison with normal human fetal skeletal muscle, but these data are missing from the literature. Therefore, we characterized the contractile properties of developing human fetal skeletal muscle and compared them to adult human skeletal muscle and rabbit psoas muscle. Electron micrographs showed human fetal muscle sarcomeres are not fully formed but myofibril formation is visible. Isolated myofibril mechanical measurements revealed much lower specific force, and slower rates of isometric force development, slow phase relaxation, and fast phase relaxation. The duration of slow phase relaxation was also significantly longer compared to both adult groups, but was similarly affected by elevated ADP. F-actin sliding on human fetal skeletal myosin coated surfaces in *in vitro* motility assays was much slower compared with adult rabbit skeletal myosin, though the $K_{m(app)}$ of F-actin speed with ATP titration suggests a greater affinity of human fetal myosin for nucleotide binding. Replacing ATP with 2 deoxy-ATP (dATP) increased F-actin speeds for both groups by a similar amount. Titrations of ADP into IVM assays produced a similar inhibitory effect for both groups, suggesting ADP binding may be similar, at least under low load. Together, our results suggest slower but similar mechanisms of myosin chemo mechanical transduction for human fetal muscle that may also be limited by immature myofilament structure.

4.2 Introduction

Most of what is known about the contractile properties of developing mammalian muscle comes from experiments in model organisms. For example, contractility measurements of neonatal feline and rat skeletal muscle have found that the energetics and mechanical characteristics are similar to that of adult slow muscles[77–79]. Force production of cells significantly increases as development progresses, even after birth, but neither calcium sensitivity of force (pCa_{50}) nor cooperativity of thin filament activation (n_H) change significantly[77–80]. Increases in force may be

due to increased sarcomere alignment and myofibril density[80]. Additionally, a change in twitch contraction time between early and late gestation has been attributed to changes in myosin heavy chain isoform, with suppression of fast-twitch properties and elevation of slow-twitch properties[80].

To our knowledge, the contractility of human fetal and human adult skeletal muscle has not yet been described. Indeed, little is known about the chemo mechanical properties of the cross bridge cycle in developing animal muscle that control the kinetics of activation and relaxation, or whether rate limiting processes of contractility are similar or different from adult muscle. Knowledge of the chemo-mechanical properties of 'embryonic' fetal myosin could help identify potential avenues for early intervention into skeletal muscle diseases that develop *in utero*, such as DA. Additionally, recent evidence indicates the presence of small amounts of 'embryonic' skeletal myosin (*MYH3*) in adult skeletal muscle[157]. Thus mutations in this myosin isoform may affect contraction and relaxation of adult DA skeletal muscle tissue as well.

We characterized the structure and mechanical properties of human fetal distal skeletal muscle with a predominance of *MYH3*, using isolated myofibril preparations and purified actin and myosin (heavy meromyosin; HMM) in the *in vitro* motility assay (IVM). Myofibril preparations are small (<15 μm wide) and thus are not subject to diffusion limitations, allowing for accurate measurements of the rapid (millisecond timescale) kinetics of force development and relaxation [109,110,158]. *In vitro* motility assays can determine the hydrolytic properties of fetal myosin and its affinity for substrates and products. We report that human fetal myofibrils have less organized sarcomere structure and less myofibril alignment, lower force producing capabilities, and slower activation and relaxation kinetics. Unregulated F-actin filament sliding velocity (V_f) was much slower for fetal human *vs.* adult rabbit skeletal myosin, but was elevated to a similar extent with 2 deoxy-ATP (dATP), similar to data we have shown for adult fast skeletal (*MYH2*), α-cardiac (*MYH6*) and β-cardiac (*MYH7*) myosin [35,89,159,160]. Both the slow phase of myofibril relaxation and V_{MAX} of actin filaments were reduced to a similar extent by increasing ADP. Together, these data suggest ADP release may be the rate limiting process for fetal myosin ATPase activity, but other chemo-mechanical transitions may also contribute to slower fetal muscle contractile properties.

4.3   Results

4.3.1   Markers of human fetal muscle cell immaturity

Expression assays performed on the mRNA extracted from fetal skeletal muscle tissue showed that at the fetal age selected (~15 weeks gestation), *MYH3*, which codes for the embryonic myosin heavy chain protein, expression was 81% of the total *MYH* expression (Figure 4-1, left panel). Additionally, fetal immunohistochemistry showed positive staining for embryonic myosin heavy chain protein in all cells of cross-sections (Figure 4-2*A*).

Fetal muscle showed less structure and myofibril organization than adult skeletal muscle (Figure 4-2). The fetal histology H&E stains showed hallmarks of immaturity such as central nuclei in muscle cells (Figure 4-2*A*, top panel) and lacked of clear sarcomere structure such as well-defined A and I bands (Figure 4-2*B*, bottom two panels). This was consistent with animal models of gestational progress[80]. Acidic and basic pre-incubations traditionally used in ATPase assays to fiber-type adult muscle cells showed that most fetal muscle cells, unlike adult cells, stain under both conditions (Figure 4-2*A*). Fetal myosin likely has different pH sensitivity than adult myosin. Thus fiber typing by this method was inconclusive, as fetal myofibrils did not cleanly segregate into two (or three) categories. However, mRNA quantification showed that in fetal skeletal muscle, *TNNI2* for fast skeletal TnI constitutes >90% of the total amount of *TNNI* gene isoforms (*TNNI1, TNNI2*, and *TNNI3*) being expressed (Figure 4-1, right panel). This section of fetal skeletal muscle stained with Richardson stain also showed a paucity of sarcomere structure and embedded nuclei within the fetal skeletal muscle cells (Figure 4-2*B*, top panel).

4.3.2   Myofibrils activation and relaxation kinetics

Myofibrils were exposed to rapid solution switching (Myofibrils) for step increases and decreases in calcium, from pCa 9.0 to 4.0 and back to 9.0, to determine the magnitude and rate of tension generation and relaxation at 15°C. Figure 4-3 illustrates a representative fetal myofibril tension trace for this activation-relaxation protocol. The rate of tension rise (k_{ACT}, Figure 4-3*A*) represents the rate of process that includes calcium dependent thin filament activation, myosin cross bridge binding and force production. The data for fetal human myofibrils and comparative adult rabbit and human muscle myofibrils is summarized in Table 4-1. Fetal myofibrils produced significantly ($p < 0.05$) less force at a slower rate than either adult human gastrocnemius

myofibrils or adult rabbit psoas myofibrils, though the rate of force production was not significantly different between human adult and rabbit psoas myofibrils. Human fetal myofibril steady-state force (6 ± 1 mN•mm^{-2}) was an order of magnitude less compared to human adult myofibrils (84 ± 34 mN•mm^{-2}), which produced force values consistent with published human skinned muscle cell preparations[161,162]. Force was even greater for rabbit psoas myofibrils (220 ± 40 mN•mm^{-2}), as we have previously reported[111]. The k_{ACT} for fetal myofibrils (0.7 ± 0.1 s^{-1}) was ~3x slower than rates published for rabbit soleus muscle and more than 8x slower than values for rabbit psoas myofibrils in this study (5.7 ± 0.5 s^{-1}) and others[110,111,144,163]. The k_{ACT} for human gastrocnemius myofibrils was greater than for rabbit psoas fibers (7.5 ± 6.3 s^{-1}), but the large variability in rate suggests both fast and slow twitch myofibrils were sampled[144,164], but in general the human adult myofibrils activated at a faster rate than the human fetal myofibrils (Figure 4-3*B*). In contrast, human fetal myofibrils did not segregate into a bimodal distribution in any of measured parameters, indicating a single population of slow fibrils and not an aggregate of fast and slow fibrils[80,144]; mRNA expression results showed that *TNNI2*, the gene for fast skeletal troponin I, was >90% of the total *TNNI* expression in fetal distal leg of a similar age (Figure 4-1, right).

Fetal myofibril relaxation was significantly slower than for both adult muscle types for all parameters measured ($p < 0.05$). Tension relaxation in myofibrils is characterized by an initial slow ($k_{REL,slow}$, Figure 4-3*A*, inset) and secondary fast ($k_{REL,fast}$, Figure 4-3*A*) phase. $k_{REL,fast}$ is thought to reflect the phenomenon of sarcomere give and is independent of the calcium binding properties of Tn[114]. In contrast, $k_{REL,slow}$ is thought to be determined by the rate of cross bridge detachment during maximal calcium activation[144]. The duration of the slow phase of relaxation ($t_{REL,slow}$) may depend somewhat on the properties of thin filament regulatory proteins, as we have previously shown[111,150] and the level of calcium activation. $k_{REL,fast}$ was ~10-fold slower for fetal myofibrils (1.5 ± 0.2 s^{-1}) compared with adult human (11.8 ± 4.9 s^{-1}) or rabbit (20.8 ± 4.3 s^{-1}) myofibrils (Figure 4-3*C*).

This may be a result of less myofibril alignment resulting in less structural propagation of relaxation in fetal muscle[145]. The slow phase rate, $k_{REL,slow}$, was significantly less steep in fetal preparations (0.6 ± 0.2 s^{-1}) than in human adult myofibrils (2.9 ± 1.7 s^{-1}) and rabbit psoas

myofibrils (2.1 ± 0.4 s^{-1}), which matched to earlier studies[111,144] and suggest a slower rate of myosin (cross bridge) detachment (Figure 4-3*C* inset). Fetal myofibrils had a t$_{REL,slow}$ of 0.174 ± 0.013 s, while adult myofibrils, both human (0.071 ± 0.018 s) and rabbit (0.073 ± 0.014 s), were significantly shorter, though human adult and rabbit psoas were not significantly different from one another. Taken together, the differences in fetal and adult myofibrils in slow phase duration indicate there may be substantial differences in kinetics of myosin cross bridge chemo-mechanical and thin filament state transitions[111,150] of fetal myofibrils compared to adult human or rabbit myofibrils.

4.3.3 Fetal skeletal myosin sliding velocities

To further study the properties of fetal muscle myosin, we used the *in vitro* motility assay where myosin-actin interactions can be measured in the absence of regulatory proteins and it is easy to alter conditions of activation solution conditions, such as varying substrates and products of myosin cycling. The slow activation and relaxation kinetics of fetal myofibrils (compared with adult myofibrils) suggested much slower fetal myosin cross bridge cycling and ATPase activity. To investigate this we measured sliding velocity of F-actin (V_f) propelled by heavy meromyosin (HMM) prepared from either fetal human or adult rabbit muscle and determined the nucleotide dependence of V_f over a range of ATP concentrations ($0 - 2$ mM ATP)(Figure 4-4). Maximal sliding velocity (V_{MAX}) for fetal HMM was 2.64 ± 0.02 μm s^{-1} (30°C), almost 3-fold slower than V_{MAX} for adult HMM (6.72 ± 0.09 μm s^{-1}), and was consistent with slower k_{ACT}. This suggests that the fetal myosin has a reduced ATPase rate compared to adult myosin. The fitted value of K$_{m(app)}$ of V_f with varying ATP was found to be 3-fold less for fetal human *vs.* adult rabbit HMM (0.03 mM *vs.* 0.09 mM), indicating fetal myosin may have a greater affinity for ATP.

2-deoxy-ATP (dATP) is also an efficient energy substrate for skeletal muscle myosin, and we have shown that it enhances F-actin sliding speed in the *in vitro* motility assay, and the magnitude and rate of force production and relaxation in muscle fibers[119,159,160]. Chemo-mechanical analysis using protein solution biochemical, mechanical transients, and computational approaches suggest this occurs through faster attachment and detachment kinetics of cross bridges. To determine if dATP also enhances cross bridge cycling in fetal, we measured the F-actin sliding velocity with fetal HMM with increasing [dATP]. V_{MAX} was increased by

~50% with 2mM dATP (closed symbols) compared with ATP (open symbols) (Figure 4-4). Michaelis-Menten fits to the dATP data yielded a V_{MAX} of 3.25 ± 0.12 μm s^{-1} and a fitted $K_{m(app)}$ of 0.07 mM (rabbit $V_{MAX} = 9.51 \pm 0.03$ μm s^{-1}). This indicates somewhat lower affinity of dATP for fetal myosin, which is similar to what we reported for adult rabbit skeletal myosin at 10°C, but not 25°C[119,159,160]. As the fraction of smoothly moving F-actin filaments was high (> 0.8) and similar for fetal human and adult rabbit HMM, it is unlikely the results were influenced by a significant difference in the number of damaged or rigor HMM on the motility surface. These data, combined with the slower k_{ACT} in myofibrils suggest that fetal muscle has slower cross bridge cycling, not because of decreased myosin affinity for ATP but because of slower myosin attachment and/or detachment kinetics.

4.3.4   Effect of elevated ADP

The slower relaxation characteristics we observed for fetal myofibrils may also be associated with slower cross bridge cycling kinetics. If ATP binding affinity is equal or greater with fetal myosin, as indicated from ATP titration measurements in IVM assays, a likely candidate for differences is ADP release, which is thought to be rate-limiting for cross bridge detachment[2] and subsequent tension relaxation[144] in adult fast skeletal muscle. To examine this, we first measured the effects of ADP product inhibition on V_f of fetal and adult HMM over a range of $0 - 2$ mM. While V_f is significantly slower at all [ADP] for fetal HMM compared to adult HMM (Figure 4-5*A)*, these differences are eliminated when the data is normalized to V_{MAX} ([ADP] = 0) for each condition (Figure 4-5*B*). This suggests ADP affinity for myosin was not different for fetal and adult muscle and slower relaxation may not be exclusively attributed to cross bridge detachment rate. However, *in vitro* motility measurements are made under low load (strain) conditions; because some cross bridge transitions, like myosin-actin detachment and ADP release prior to ATP binding, are strain-sensitive, we also measured the effect of elevated ADP on myofibril relaxation.

For a separate group of myofibrils, following contraction in maximal activation solution (pCa 4.0) myofibrils were relaxed in pCa 9.0 solution containing a 2.5 mM ADP substitution for ATP. Relaxation of fetal and adult human skeletal muscle myofibrils were similarly affected by ADP, with the slow phase rate ($k_{REL,slow}$) not significantly affected, but the duration of the slow

phase ($t_{REL,slow}$) slightly prolonged (Table 4-2). Coupled with the similar effect of ADP on F-actin V_{MAX} in *in vitro* motility assays, these suggest that ADP release may be similar for fetal and adult human muscle. However the rate of ADP release is not the sole mechanism responsible for the slower contraction and relaxation kinetics of fetal muscle.
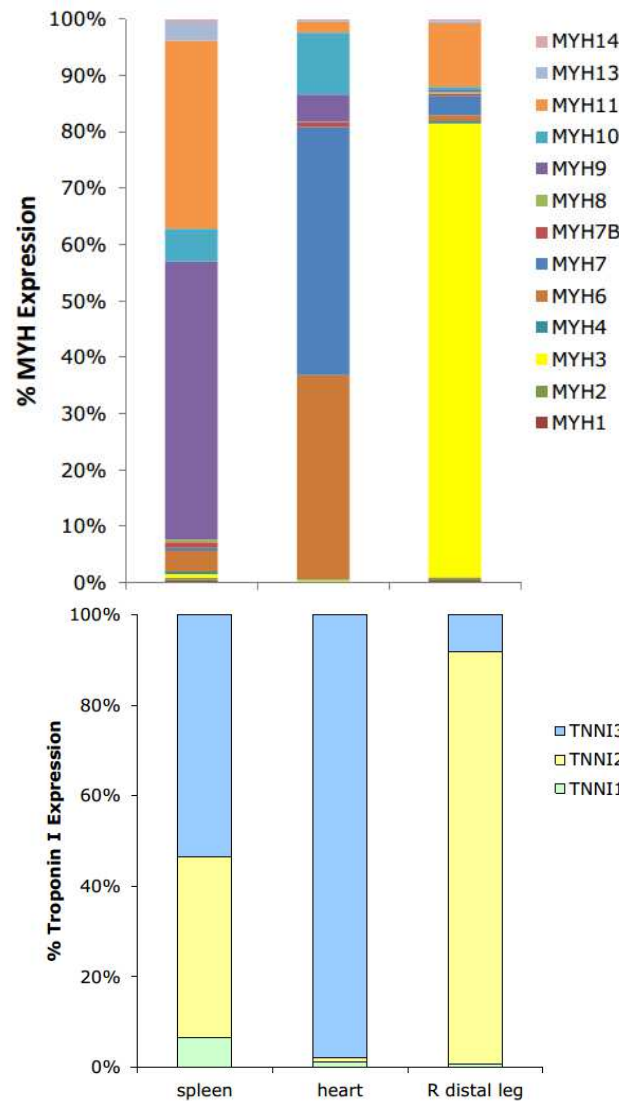
Figure 4-1: Percent mRNA expression levels for muscle, heart, and control (spleen) tissues in 14.7 weeks gestation fetus.

(**Top**) Myosin heavy chain isoforms. Note that embryonic myosin (yellow) constitutes the majority of myosin heavy chain isoform expression in 'distal leg'; whereas 'heart' expresses mostly cardiac isoforms and a negative control ('spleen') expresses mostly smooth muscle isoforms.

(**Bottom**) Troponin I isoforms. Note that the fast skeletal troponin I isoform (*TNNI2*) constitutes the majority of *TNNI* expression in distal leg, while cardiac troponin (*TNNI3*) constitutes the majority of *TNNI* expression in the heart. *TNNI2*, the slow skeletal troponin I, constitutes less than 5% of transcripts in either striated muscle group.
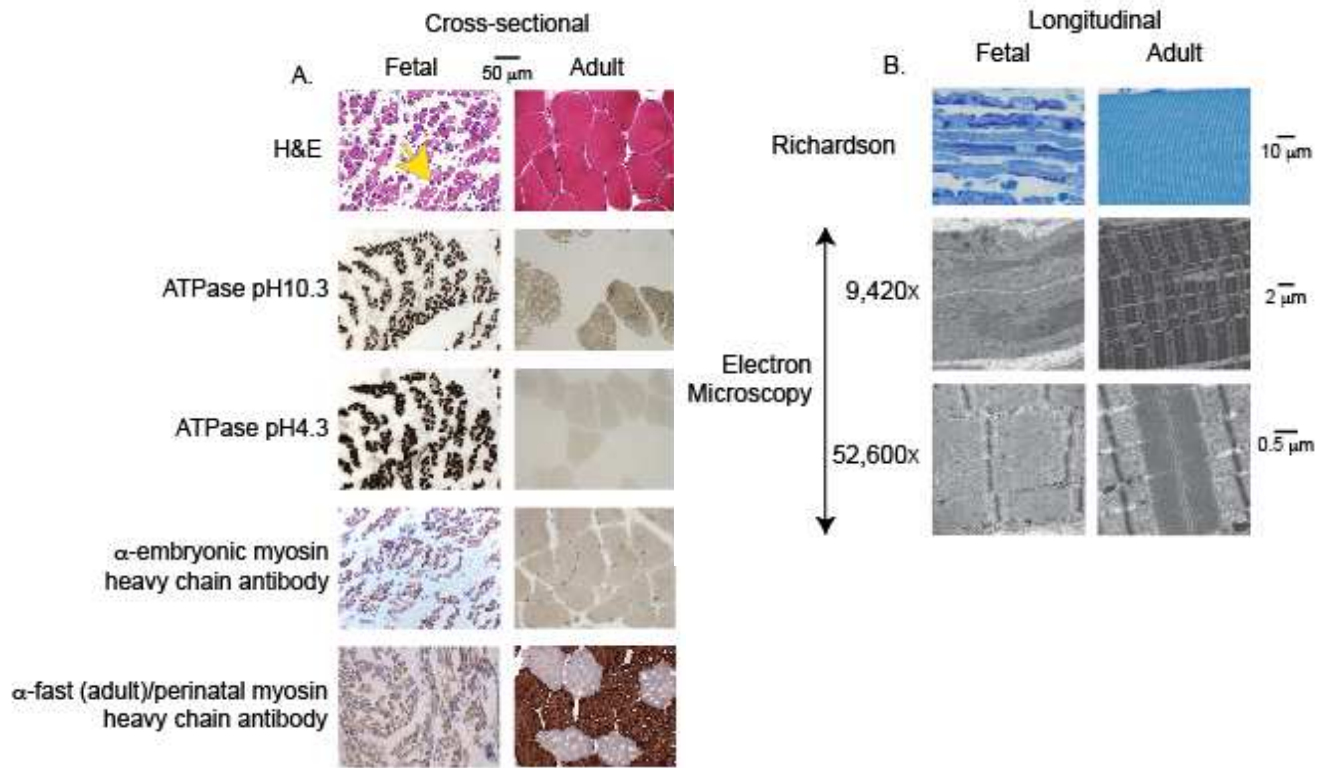
Figure 4-2: Structure of human fetal skeletal muscle of 12-15 weeks gestation with adult human skeletal muscle as a comparison.

(**A**) Cross-sectional images of tissue stained with H&E (the yellow arrow points to an example of a central nucleus), subjected to alkaline (Type II, fast-twitch are dark, pH 10.3) or acidic (Type I, slow-twitch are dark, pH 4.3) conditions in an ATPase assay, or hybridized with an anti-embryonic myosin heavy chain or an anti-adult fast/perinatal heavy chain antibody in an immunohistochemistry assay are shown.

(**B**) Longitudinal images stained with the Richardson stain or EM images at two magnifications demonstrating sarcomeric structure are shown.
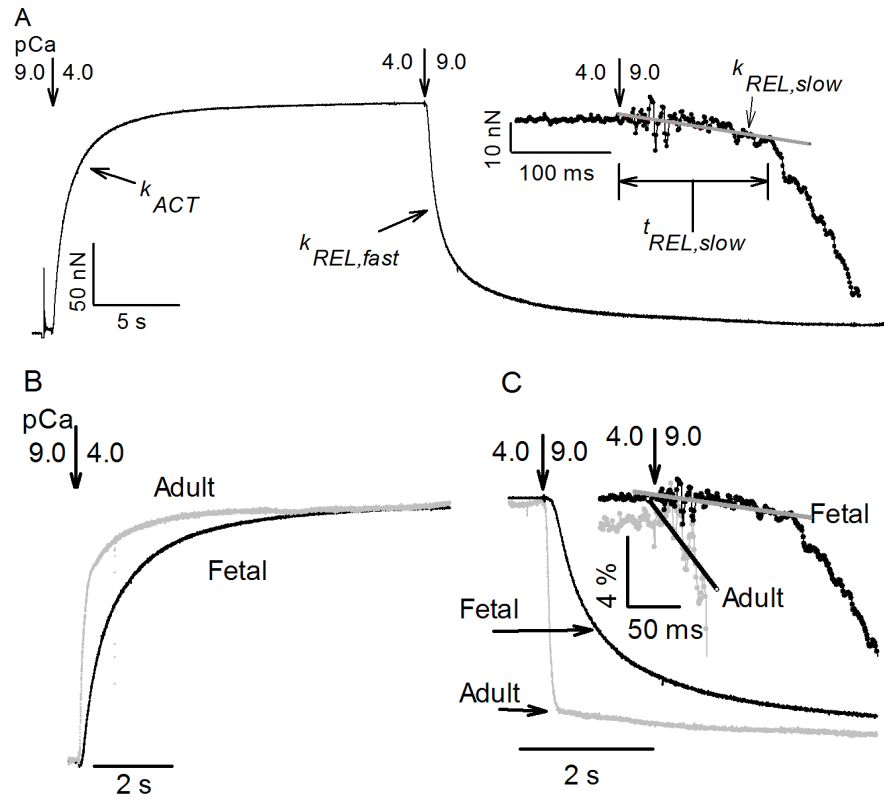
Figure 4-3: Human fetal and adult skeletal myofibril example traces.

(**A**) Full activation and relaxation trace of a single fetal skeletal myofibril. Shown in the inset is the relaxation slow phase on a smaller timescale.

(**B**) Human adult *vs.* human fetal activation kinetics.

(**C**) Human adult *vs.* human fetal relaxation kinetics, with an inset showing the slow phase of relaxation on a smaller timescale.
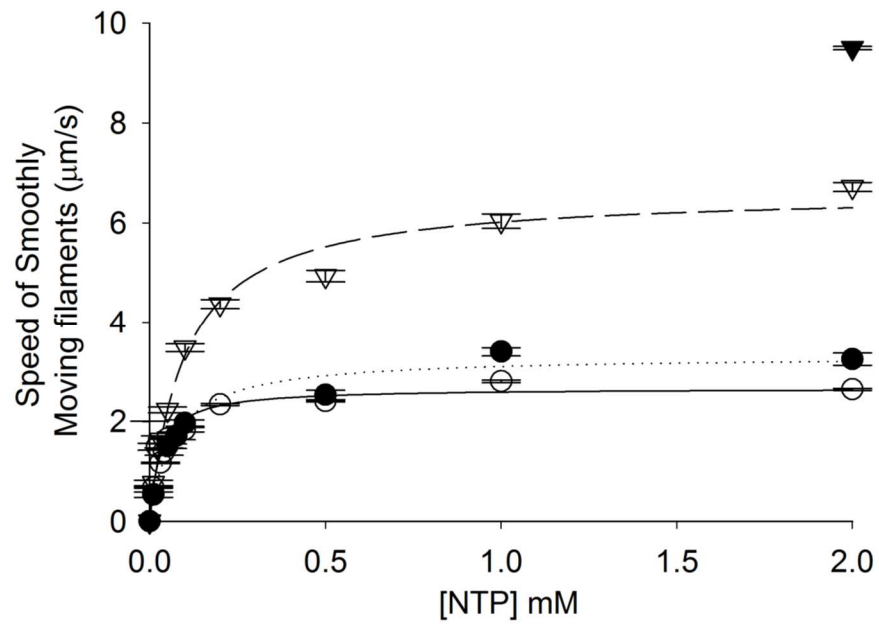
Figure 4-4: Unregulated filamented actin velocities in *in vitro* motility.

Human fetal skeletal (circle) and adult rabbit psoas (triangle) myosin with ATP (open) and dATP (closed).
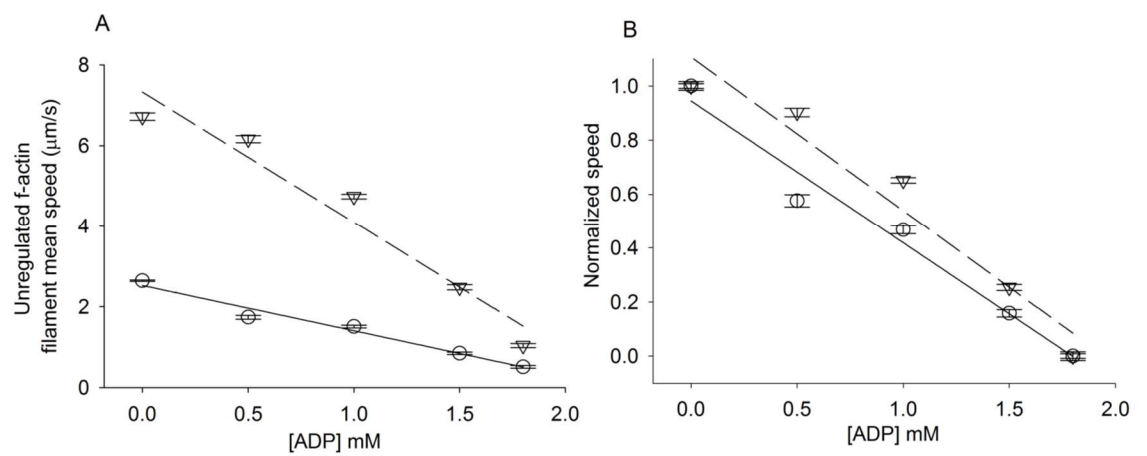
Figure 4-5: Unregulated filamented actin velocity in *in vitro* motility assay with product inhibition.

(**A**) Fetal skeletal (circle) and adult skeletal (triangle) velocities decrease as a function of increasing ADP.

(**B**) Decrease in velocities relative to maximum velocity for each myosin shows similar inhibitory affect.

Table 4-1: F_{MAX} and kinetic parameters for maximum $[Ca^{2+}]$ activation and relaxation of fetal myofibrils at 15°C.

[*] indicates p-value between group and fetal value of < 0.05. [x] indicates a p-value between group and adult human value of < 0.05.

| Parameter (units) | Activation | | Relaxation | | |
| | | | slow | | fast |
	F_{MAX} (mN•mm^{-2})	k_{ACT} (s^{-1})	$t_{REL,slow}$ (s)	$k_{REL,slow}$ (s^{-1})	$k_{REL,fast}$ (s^{-1})
Human Fetal	6 ± 1 (22)	0.7 ± 0.1 (22)	0.174 ± 0.013 (33)	0.6 ± 0.2 (11)	1.5 ± 0.2 (29)
Human Adult	84 ± 34 (6)*	7.5 ± 6.3 (5)*	0.071 ± 0.018 (6)*	2.9 ± 1.7 (11)*	11.8 ± 4.9 (5)*
Rabbit Psoas	220 ± 40 (6)*,x	5.7 ± 0.5 (6)*	0.073 ± 0.014 (5)*	2.1 ± 0.4 (5)*	20.8 ± 4.3 (5)*

Table 4-2: Effects of 2.5 mM MgADP substitution on relaxation of human Fetal and Adult myofibril kinetics at 15°C.

Parameter (units)	$t_{REL,slow}$ (s)	$k_{REL,slow}$ (s^{-1})	$k_{REL,fast}$ (s^{-1})
Fetal			
ATP	0.241 ± 0.017 (15)	0.5 ± 0.1 (15)	1.1 ± 0.1 (15)
ADP	0.256 ± 0.011 (15)	0.6 ± 0.1 (15)	0.8 ± 0.1 (15)
Adult			
ATP	0.181 ± 0.016 (8)	1.7 ± 0.5 (8)	2.1 ± 0.3 (7)
ADP	0.206 ± 0.028 (8)	2.6 ± 0.7 (7)	1.8 ± 0.2 (9)

4.4 Discussion

Understanding the functional characteristics of human fetal skeletal muscle is essential to understand how mutations in fetal myosin heavy chains *MYH3* might affect contractile performance. Additionally, knowing how fetal myosin chemo-mechanics respond to changes in nucleotide species and ATP hydrolysis products may identify important therapeutic avenues, in particular for potential *in utero* interventions or treatment of children and adults, in congenital skeletal muscle disease. To our knowledge, the contractile properties and contraction and relaxation kinetics of human fetal or human adult skeletal muscle have not been previously reported. In this study, we characterized critical aspects of the contractile behavior, making some comparisons with both human adult skeletal muscle and the much more extensively studied adult rabbit fast (psoas) muscle. The embryonic human fetal skeletal myosin heavy chain protein is expressed at a point in development during which ultrastructure is underdeveloped and less ordered. This can likely explain the much lower force production in fetal than adult muscle, while slower cross bridge cycling can explain the slower contraction and relaxation kinetics that appear to be closer to slow adult myosin than to fast adult myosin isoforms, even in muscle groups that are destined to become higher percentage fast twitch muscles. These subjects are discussed in more detail below.

4.4.1   Force Production:

The substantially lower force produced at maximum saturating calcium concentration (pCa 4.0) for fetal myofibrils may be attributed to the disarray in ultrastructure (particularly in the sarcomere) we observed in fetal samples. The fetal skeletal muscle sample we used for mechanical studies is from 108 days, or 39% of full gestation. At this point in development, several key structural aspects that are hallmarks of adult skeletal muscle are not yet present in our sample nor in animal models, such as strong I-banding and A-lines [80,165]. Our samples produced ~20-fold less force than values reported for adult human skeletal muscle fibers by others[161,162], and what we report here (Table 4-1). Our results from human fetal muscle myofibrils are consistent with previous studies in developing sheep[80] and mouse[165] muscle that attributed increased force to developmental changes such as increased acto-myosin density. At

66

this stage in development, human fetal skeletal muscle contains mostly 'embryonic' myosin, which is known from partial recombinant myosin studies to yield slower unregulated sliding velocities[164]. Additionally, while myofibrils from predominantly fast (psoas) and slow (soleus) muscle in adult rabbit[144] may produce different levels of force under the same conditions, our fetal myofibrils consistently produce less force at a slower rate than any type of adult myofibrils, and myofibril kinetics did not segregate into two distinct categories that would indicate distinct populations with different myosin isoform populations.

4.4.2 Kinetics of Activation and Relaxation:

Embryonic human fetal myosin (*MYH3)* is a slower myosin than adult human skeletal myosin or adult rabbit fast or slow skeletal myosin[144]. There are multiple transitions in the chemo-mechanical cross bridge cycle that could be slower for fetal myosin compared with adult myosin isoforms that would explain our results. The chemo-mechanical cycle of rabbit skeletal muscle acto-myosin interactions has been well-characterized (The function of thick filament protein, Figure 1-1)[1,159,160,166]. In brief 1) myosin hydrolyses ATP into ADP and Pi primarily in the detached state (M.ADP.Pi), 2) this M.ADP.Pi state has higher affinity for actin, increasing strong cross bridge attachment, 3) a isomerization of myosin occurs, resulting in a power stroke associated with force generation and/or shortening and the release of Pi, followed by ADP release, 4) a new ATP binds in the nucleotide pocket of myosin which lowers the affinity for actin, resulting in cross bridge detachment.

Differences in ATPase rates of adult myosin isoforms have primarily been ascribed to the rate of ADP release and cross bridge detachment following the power stroke[144,167]. It is also possible that cross bridge detachment rates could be affected by ATP binding kinetics that just precedes detachment. Unloaded shortening velocity of muscle fibers and V_{MAX} of F-actin in *in vitro* motility assays is thought to limited by cross bridge detachment rate and has been associated with the rate of ADP release from myosin[168,169]. The rate of the slow phase of myofibril relaxation ($k_{REL,slow}$) has also been associated with cross bridge detachment rate[144]. Both V_{MAX} of F-actin (Figure 4-4) and $k_{REL,slow}$ (Table 4-1) for preparations from fetal human skeletal muscle in this study suggest slower cross bridge detachment rates. These rates and $t_{REL,slow}$ (Table 4-2; Figure 4-5) were similarly affected by elevated ADP for fetal and adult

preparations. Thus, our data suggest that myosin affinity for ADP may be similar for fetal and adult human muscle, though this does not preclude a different ADP release rate from myosin. ADP is a product of cross bridge cycling and is closely linked to the rate of cross bridge cycling, in particular cross bridge detachment and the release of tension[167]. ADP, as a competitive inhibitor of cross bridge cycling by virtue of binding to the same site as ATP, has been shown to regulate the maximum speed of filaments in *in vitro* motility assays[124]. The slowing cross bridge detachment may lead to a net change in activation kinetics[170], and indeed, appears to slow down activation in fetal myofibrils dramatically, although cross bridge detachment is correlated with the slope[150], but not specifically the duration[111], of the slow phase of relaxation of myofibrils. ATP binding to myosin, following ADP release, is also required for cross bridge detachment. However, the lower $K_{m(app)}$ for V_{MAX} of F-actin with fetal HMM in *in vitro* motility assays (Figure 4-4) suggests ATP binding affinity was not responsible for slower fetal *vs.* adult myosins' cycling. We also found that fetal skeletal muscle myofibrils have a much slower rate of force development (k_{ACT}) than adult fast twitch skeletal muscle myofibrils, also indicating slower cross bridge cycling. This could result from a decrease in the rate of weak-to-strong acto-myosin binding and/or the force generating isomerization transition in the cross bridge cycle, rather than the ADP-dissociation or ATP-binding rate[36,171].

The fetal skeletal muscle myofibrils relax at rates between previously published rates for human adult myofibrils and rabbit adult skeletal muscle fast and slow twitch myofibrils [144], indicating an ADP release/ ATP binding rate that is between fast and slow twitch skeletal myosin. This evidence is re-enforced by *in vitro* motility data (Figure 4-4) where V_{MAX} was much slower for fetal skeletal muscle myosin compared with adult rabbit psoas myosin. The smaller V_{MAX} of 'embryonic' human fetal skeletal myosin isoforms has been reported for recombinant human fast adult skeletal and embryonic fetal skeletal isoforms of partial myosin protein [164].

4.4.3   Therapeutics and Future Directions:

Mutations in myosin heavy chain genes can cause several human congenital contracture syndromes. Specifically, mutations in the 'embryonic' myosin heavy chain gene (*MYH3*) are the cause of >90% of cases of Freeman-Sheldon syndrome and >10% of cases of Sheldon-Hall

syndrome, two of the congenital contracture syndromes included in distal arthrogryposis [15,38,62]. It is unknown whether these *MYH3* mutations change contractile properties of adult muscle; however, because the contractures are present at birth, we hypothesize that the *MYH3* mutations cause the dysfunction to develop *in utero* [15,172]. Here we have studied the contractility of human fetal skeletal muscle that is expressing predominantly embryonic myosin from the *MYH3* gene, and how it reacts to potential therapeutics such as dATP or modulations in ADP. Intervention during fetal development may improve quality of life or disease prognosis, especially in some forms of congenital contractures. The therapeutic potential of the acto-myosin modulator dATP is currently being investigated in animal models of the heart by our group [89]. Here we have demonstrated that dATP can also enhance the cross bridge cycling (ATPase) of 'embryonic' human fetal skeletal myosin, suggesting its potential as a future therapeutic to improve function of fetal myosin mutations that may affect force development or relaxation kinetics. Fetal myofibrils have reduced cross bridge attachment and detachment kinetics as compared to adult muscle, and DA is characterized by a mutation in this myosin that may further slow the essential kinetics of the fetal myosin. Thus our demonstration that fetal muscle contractile kinetics can be increased with dATP suggests further studies to determine its effectiveness as a therapeutic for DA.

4.5   Conclusions and Future Work

This project will be continued with younger and older fetal skeletal muscle tissues. Fetal skeletal tissues between the ages of 7.7 and 21.7 weeks gestation are available and further study into the changes in structure, force production, kinetics, and chemo mechanics could provide insight into the wild type physiology of human fetal skeletal muscle and its variation throughout the early stages of development. The continuation of this project would not be without challenges. Tissues from younger fetuses are not readily identifiable due to the state and/or size of the retrieved sample; therefore separating muscle tissue from non-muscular tissue may prove difficult. Additionally, these tissues may be more fragile at younger ages, and studies that require some retention in ultrastructure such as myofibril and muscle fiber studies may not be possible due to degradation of the developing sarcomere. Samples from the older fetal skeletal muscle will likely have more gene *MYH8* expression, but our Illumina data results have shown that *MYH3*

expression may continue into the 18th week of gestation, and results from fetuses between 18-22 weeks gestation may be convoluted by the presence of two myosin isoforms.

CHAPTER 5.   HUMAN FETAL CARDIAC MUSCLE

5.1   Items of Note

5.1.1   <u>Aim: To observe the contractile and chemo mechanical properties of wild-type human fetal cardiac muscle.</u>

Little is known about the contractile strength and myofilament kinetics of activation and relaxation of fetal human cardiac muscle.

I have observed maximal force production, activation kinetics, and relaxation kinetics from small bundles of myofibrils from fetal human cardiac muscle biopsies. I have also performed *in vitro* motility assay experiments to observe the maximum speed of filamented actin on fetal cardiac muscle myosin.

5.1.2   <u>Key points</u>

- The contractile properties of human fetal cardiac muscle are unknown.
- Reductionist approaches such as isolated myofibril and isolated contractile protein biomechanical assays allow study of activation and relaxation properties of cardiac muscle from different sources.
- I have tested the contractile properties of human fetal cardiac myofibrils and myosin across 52 days gestation to 134 days gestation.
- Human fetal cardiac myofibrils have slow kinetics of activation and relaxation that increase during this time period, but surprisingly these kinetics are related to both structural and protein isoform expression changes.

5.1.3   <u>Summary</u>

Little is known about the contraction and relaxation properties of human fetal cardiac muscle, and measurements thus far have been made with non-human mammalian muscle. There are no published reports on the kinetics or force production of human fetal cardiac myofibrils. Understanding the contractile properties of human fetal cardiac muscle would be valuable in understanding muscle development, as well as a variety of muscle diseases that are associated

with mutations in cardiac muscle sarcomere proteins. Therefore, we characterized the contractile properties of developing human fetal cardiac muscle and compared them across various states of gestation. Isolated myofibril mechanical measurements revealed low specific force and slow rates of isometric force development and of fast phase relaxation, though force and activation and relaxation rates appear to increase as the gestation progresses. The duration and slope of the slow phase relaxation changed throughout the 59 to 134 day gestation range, showing that the ventricle myofibrils change drastically in this period. F-actin sliding on human fetal skeletal myosin coated surfaces in *in vitro* motility (IVM) assays was slow, though it slowed significantly from 108 to 130 days gestation. Electron micrographs showed human fetal muscle myofibrils elongate and widen with age, but features such as the M-line and Z-band are apparent even as early as day 52. Together, our results suggest cardiac myofibrils' force production and kinetics of activation and relaxation increase with age and are strongly influenced by the structural maturation of the sarcomere.

5.1.4   Relevance to project

After initially looking at the human fetal skeletal muscle contractility to better understand the properties of the human embryonic myosin heavy chain, I realized that human fetal cardiac contractility and kinetics were also un-studied. Cardiomyopathy samples show a trend of increasing expression of some fetal isoforms of proteins, and better characterizing these isoforms in the native fetal heart will improve our understanding of the isoform function. Additionally, cardiomyocytes in culture, which are used to both study disease and test therapeutics, quickly revert to an immature morphology, making the study of immature cardiac muscle and its differences from adult cardiac muscle even more relevant to the study of disease.

5.2   Introduction

Most of what is known about the contractile properties of developing mammalian cardiac muscle comes from experiments in animal models. Studies in fetal mice report that the overall increase in myosin density is a key player in an age-correlated increase in force production. Fetal mice show a decrease in the Ca^{2+} sensitivity of contraction with age, related to a switch from slow skeletal TnI to cardiac TnI and a switch from cardiac TnT_1 (slow) and TnT_2 (fast) to cardiac TnT_3 and TnT_4 as the fetus ages[165]. However, these studies are limited in their applicability to

human cardiac development because human and mice predominantly express different myosin (and other) protein isoforms during development and as adults (mouse adult ventricle *MYH6*, human adult ventricle *MYH7*)[165]. Sheep, guinea pig, and mouse hearts have continuous increases in the proportion of cardiac troponin I to total troponin I, which is correlated with decreased Ca^{2+} sensitivity of contraction [165,173,174]. In sheep hearts, the dominant troponin T protein isoform expressed (and mRNA transcribed) appears to be the adult isoform from mid-gestation to birth. This is unlike the human, rabbit, or rat cardiac fetal TnT expression, which change isoforms during fetal and post-natal development [165,173–175]. Unlike humans, sheep, guinea pigs, and other precocial animals express adult isoforms before birth[176].

To our knowledge, the contractile properties of human fetal cardiac muscle have not yet been described and performance information has been primarily obtained via studies *in vivo* with echocardiography. As the human fetal heart ages, the longitudinal shortening (ratio of AV plane displacement to LV length) decreases [177] and the left-ventricle end diastolic volume increases [178,179]. While heart rate decreases with pre-birth age, the diastolic filling and atrial contraction durations, and the peak velocities of the septum, atrial contraction, ventricle ejection all increase[180]. However, conclusions from these studies are limited by a lack of *ex vivo* quantitative muscle contractile studies, and it is unknown if the changes in gross contraction of the heart are a property of protein isoform expression patterns, or structural developments.

Ex vivo studies on fetal human heart tissue report significant changes in morphology and ultrastructure as the human develops. The gross morphology of the heart undergoes considerable change through the first 112 days of development, including septation (separating the left and right halves between 35 and 53 days gestation), formation of the valve components between 49 and 56 days, and delamination of the leaflets into the tricuspid valve between 56 and 112 days [181]. At 119 days, myofibrils in the heart are scattered and few, very short, and with thick z-bands and loosely packed[182].

Ex vivo studies of protein isoforms in the human fetal heart report several key contractile proteins isoforms change in expression levels between 49 days and full term gestation. Human fetal heart ventricle shows a marked decrease in the small amount of α-myosin heavy chain (*MYH6*) between 47 and 110 days gestation[183], and slow skeletal troponin I is the predominate isoform (over cardiac troponin I) as early as 63 days gestation up to full term, and even at 12

weeks post-natal[184]. At 105 days gestation, the 'fast troponin T' isoform (TnT$_2$) is expressed more highly in human fetal left ventricle than the slow Troponin T (TnT$_1$) in comparison to failing adult heart and in sharp contrast to normal human adult heart, which expresses no detectable fast Troponin T[175]. This increase in TnT$_2$, combined with continued expression of slow skeletal troponin I, may lead to slower overall ATPase activity[175,185].

The contractile properties of the developing human fetal heart likely change over time due to this complex combination of protein isoform expression, as well as through structural maturation of sarcomeres. An in-depth study of the developing myocardium is needed to better understand the developmental process of the heart and create better informed hypotheses regarding the dysfunction that occurs in disease development from structural abnormalities or genetic mutations within the heart. Knowledge of the contractile properties of human fetal cardiac muscle could also help identify potential avenues for early intervention into cardiac muscle diseases that develop *in utero*.

Here we provide an initial report of the mechanical and structural properties of human fetal left ventricle cardiac muscle myofibrils (the contractile organelles of striated muscle cells) and isolated myosin, using isolated myofibril preparations and purified actin and myosin (heavy meromyosin; HMM) in the *in vitro* motility assay (IVM). In agreement with reports by others [183,184], throughout the age range studied (52 to 134 days gestation), the fetal cardiac muscle predominantly expresses the *MYH7* (β-myosin heavy chain) gene, and the ratio of cardiac troponin I to slow skeletal troponin I increases with age. We report that human fetal myofibrils produce more force, and have faster activation and relaxation kinetics as they develop, and this is correlated with maturation of sarcomere structure and myofibril alignment. Unregulated F-actin filament sliding velocity (V_f) on human fetal cardiac myosin decreases with age, and agrees with a decrease in cross-bridge detachment rate estimated from the early, slow phase of relaxation in myofibrils. The V_f of fetal cardiac myosin at 134 days is close to the speed on human adult left ventricle myosin [186]. Our study is an important step towards improved understanding of the development of the human fetal heart contractile properties and we conclude that the fetal left ventricle increases in force production magnitude and speed as it ages from 52 to 134 days gestation. Preliminary reports of this work were presented in abstract form [187].

5.3 Results

Overall 17 samples were acquired for this project, with the greatest number (N = 10) being between 101 and 116 days gestation. Samples outside of this age range were rare due to regulatory aspects (illegal at >24 weeks, 168 days gestation) and alternative procedures (Mifeprex for <9 weeks, 63 days gestation). 2 samples were acquired at 130 days gestation for use in myofibrils, one at 127 days gestation which was used for electron microscopy only, and one at 134 days gestation for use in myofibrils and in vitro motility. One fetal heart sample was collected from 52 day gestation fetus, which did not produce functional myofibrils but was used for electron microscopy imaging. The other two younger age fetal samples were at 59 days gestation and at 74 days gestation, and both were used for myofibril experiments only. These samples are typically small and fragile, especially samples less than 100 days gestation, and very few functional myofibrils were obtained from the younger ages.

5.3.1 Myofibrils activation and relaxation kinetics

Myofibrils were exposed to rapid solution switching (Methods) for step increases and decreases in Ca^{2+}, from pCa 9.0 to 4.0 and back to 9.0, to determine the magnitude and rate of tension generation and relaxation at 15°C. Representative fetal myofibril tension traces from 74 days and 130 days gestation tissue samples are shown in Figure 5-1 for activation (A) and relaxation (B). The data for all the fetal human myofibrils from tissue collected at multiple pre-natal ages is summarized in Figure 5-1 (C-G) and quantitative values are summarized in Table 5-1.

The magnitude of active force is derived from the displacement of the cantilever force probe (Figure 5-1A, inset), which is remarkably different between fetal samples <100 days gestation and those at 130 days gestation. Fetal myofibrils produced progressively more force as they aged. Steady-state force at 59 days (7.8 ± 3.0 (n = 3) mN•mm^{-2}) was one-third the force produced at 74 days (23.4 ± 8.3 (n = 5) mN•mm^{-2}) and 101 days gestation (25.2 ± 6.6 (n = 11)mN•mm^{-2}), slightly less than one-third the force produced at 105-107 days gestation (32.2 ± 7.1 (n = 22) mN•mm^{-2}) and 114-116 days gestation (28.2 ± 4.7 (n = 43) mN•mm^{-2}), and a fifth of what was produced at 130 days (49.9 ± 9.3 (n = 8) mN•mm^{-2}). Even at 130 days gestation, the

steady-state maximum force production was still considerably less than the reported values for human adult left ventricle ($\sim$ 110 mN•mm^{-2}) [188].

The rate of force production (k_{ACT}; Figure 5-1, A and D) is obtained from the time to reach 50% of final force (Figure 5-1, A and D) and represents the processes of Ca^{2+} dependent thin filament activation, myosin cross bridge binding, and force production. k_{ACT} for fetal myofibrils progressively increased in speed as myofibrils aged; compared to 59 days (0.27 $\pm$ 0.07 (n = 4) s^{-1}), k_{ACT} increased 60% by 74 -107 days gestation, and had tripled by 114-116 days (1.04 $\pm$ 0.08 (n = 41) s^{-1}) (p<0.05, ANOVA Tukey) gestation (Table 5-1). For the two 130 days gestation samples, k_{ACT} was still considerably higher (0.98 $\pm$ 0.21 (n = 8) s^{-1}), though with the low number of myofibrils, not of statistical significance. The 134 day sample was much slower to activate than both of the 130 day samples, but given that the single sample provided only 4 functional myofibrils, and these myofibrils also produced less force (36.0 $\pm$12.1 (n = 4) mN•mm^{-2}) than the myofibrils at 130 days gestation, we believe this sample was an outlier. The fetal heart samples produced force at a considerably slower rate than the reported values for human adult atrial tissue ($\sim$ 3.7 s^{-1}), but were faster at 114-116 days gestation and 130 days gestation than what has been reported for human adult ventricle tissue ($\sim$ 0.7 s^{-1}) [188].

Fetal cardiac myofibril relaxation increased in speed, described by both the time to 50% ($t_{REL,50}$)(59: 0.59 $\pm$ 0.06 (n = 2); 74: 0.7 $\pm$ 0.05 (n = 5); 101: 0.43 $\pm$ 0.04 (n = 13); 105-107: 0.61 $\pm$ 0.05 (n = 23); 110: 0.45 $\pm$ 0.05 (n = 12); 114-116: 0.46 $\pm$ 0.03 (n = 45); 130: 0.42 $\pm$ 0.06 (n = 7); 134: 0.4 $\pm$ 0.01 (n = 4)) and more pronounced in the time to 90% relaxation ($t_{REL,90}$) (59: 15.5 $\pm$ 2.0 (n = 3); 74: 14.4 $\pm$ 3.1 (n = 5); 101: 8.1 $\pm$ 2.0 (n = 10); 105-107: 10.0 $\pm$ 1.2 (n = 23); 110: 8.0 $\pm$ 1.5 (n = 12); 114-116: 5.4 $\pm$ 0.8 (n = 42); 130: 7.2 $\pm$ 2.3 (n= 7)). This difference in relaxation speed can be easily discerned in Figure 1B, which compares an example 74 day and 130 day gestation myofibril.

Tension relaxation in myofibrils is characterized by an initial slow ($k_{REL,slow}$, $t_{REL,slow}$; Figure 5-1B, inset) and secondary fast ($k_{REL,fast}$; Figure 5-1B) phase. $k_{REL,fast}$ is thought to reflect the phenomenon of sarcomere give[114], and may be independent of the Ca^{2+} sensitivity of the

76

myofilament[189]. Compared to 59 days (1.18 ± 0.13 (n = 2) s^{-1}) and 74 days (0.96 ± 0.05 (n = 5) s^{-1}), $k_{REL,fast}$ was ~50% higher by 101-116 days and nearly doubled in speed by 130 days (1.86 ± 0.24 (n = 7) s^{-1}); Table 1, Figure 5-1C). The fetal heart samples relaxed at a considerably slower rate than the reported values for human adult atrial (~ 16.0 s^{-1}) and human adult ventricle (~ 2.9 s^{-1}) tissue [188].

Early phase relaxation transients are the most difficult properties to pick up in the myofibril assay and may be heavily influenced by the acquisition procedure wait-time, in which samples are kept in a 4°C high-phosphate buffer solution. The slow phase rate of relaxation, $k_{REL,slow}$, is thought to be determined by the rate of cross bridge detachment during maximal Ca^{2+} activation [144]. In contrast to $k_{REL,fast}$, $k_{REL,slow}$ appeared to progressively increase between 59 days (0.14 ± 0.03 (n = 3) s^{-1}), 74 days (0.22 ± 0.05 (n = 5)), and 101 days (0.30 ± 0.07 (n = 12) s^{-1}). It appeared to decrease between 110 days (0.29 ± 0.07 (n = 12)), 114-116 days (0.22 ± 0.02 (n = 8)) and 130 days (0.11 ± 0.02 (n = 8) s^{-1}) (Figure 5-1E). The human adult ventricle slow k_{REL} is reported to be 0.15 s^{-1}, half of what we report at 101 days but close to what we report at 130 days; the human adult atria slow k_{REL} is reported as much faster at 0.52 s^{-1}[188].

We have previously reported that the slow phase duration ($t_{REL,slow}$) may depend on the properties of thin filament regulatory proteins[111,150] and the level of Ca^{2+} activation. The duration of the slow phase of relaxation, $t_{REL,slow}$, dropped as the fetal aged from 59 days (0.292 ± 0.035 s (n = 4)), 74 days (0.235 ± 0.015 s (n = 5), and 101 days (0.196 ± 0.012 s (n = 23)). Outside of the initial time point at 59 days, the other values we report for $t_{REL,slow}$ do not differ significantly from one another with respect to ages (Figure 5-1F). These values are close to the expected range for human adult ventricles (~0.226 s), and far faster than what is seen in human adult atria myofibrils (~0.126 s) [188].

In a subset of experiments for 114-116 days, myofibrils were stretched to different sarcomere lengths to examine whether the force - length dependence of human fetal cardiac myofibrils has been established at this time point. The pCa 4.0 force for these myofibrils was 22.5 ± 4.1 (n = 17) mN•mm^2 at a sarcomere length of 2.0 μm *vs.* 27.2 ± 8.5 (n = 12) mN•mm^2 at

a sarcomere length of 2.34 μm, suggesting a small gain in force with an increase in sarcomere length at this early stage of gestation. An increase in sarcomere length from 2.0 μm to 2.2 μm has previously been reported to increase the magnitude and Ca^{2+} sensitivity of force production in human adult ventricle cardiomyocytes by 30% and 0.02 pCa units, respectively[190], but a change in sarcomere length does not appear to affect the kinetics of activation or relaxation in zebrafish heart myofibrils [191].

In another subset of experiments myofibrils were activated at a submaximal concentration of calcium (pCa 5.8) to examine possible changes in calcium sensitivity. To avoid bias due to run-down of the myofibrils, half of the myofibrils were first activated in pCa 5.8, then following relaxation, activated in pCa 4.0. This order was reversed for the other half of the myofibrils. The force production at this submaximal calcium appeared to decrease with age. At 74 days, the force produced at pCa 5.8 was 82% of the force produced at maximum calcium concentration (pCa 4.0). At 114-166 days the percentage of maximum force produced at pCa 5.8 was down to 74% and by 134 days gestation active force at pCa 5.8 was only 62% of the force produced at pCa 4.0. This suggests a decrease (right shift) in calcium sensitivity as the fetal heart ages, similar to what has been reported in animal models[165,174,176].

5.3.2 Fetal cardiac myosin sliding velocities

To study the properties of the fetal cardiac myosin, we used the *in vitro* motility assay where myosin-actin interactions can be measured in the absence of regulatory proteins and at a temperature that is closer to physiological than can be used in myofibril mechanical assays. The slow activation and relaxation kinetics of fetal myofibrils (compared with adult myofibrils) suggested much slower fetal myosin cross bridge cycling and ATPase activity. To investigate this we measured sliding velocity of F-actin (V_f) propelled by heavy mero-myosin (HMM) prepared from fetal human left ventricle tissue at 108 to 134 days gestation and determined the nucleotide dependence of V_f over a range of ATP concentrations (0 – 2 mM ATP) (Figure 5-2). Maximal sliding velocity (V_{MAX}, 30°C) for fetal HMM at 108 days was 4.03 ± 0.62 μm s^{-1}, almost 2-fold faster than V_{MAX} f at 134 days (1.98 ± 0.76 μm s^{-1}). This was consistent with faster $k_{REL,slow}$ at 108 vs. 134 days, and suggests myosin cycling and crossbridge detachment may decrease over this time period.

5.3.3   Protein transcripts and expression

Total RNA isolated from human fetal tissues of a 103 days gestation male fetus was hybridized to an Illumina Human HT-12 whole transcriptome array. The fetal heart transcribed: *MYH7*: 44%; *MYH6*: 36% (Figure 5-3A). However, within fetal heart samples we found strong beta-myosin heavy chain expression (Figure 5-3D), with little to no expression of alpha-myosin heavy chain, which is consistent with reports by others [183], who reported very little average expression of alpha myosin heavy chain (~2-3 %) at 110 days gestation. While the TnI transcription indicates pure cardiac isoform (Figure 5-3B), the muscle itself contained both slow skeletal and fast skeletal Troponin I isoforms as confirmed by western blot (Figure 5-3, E and F) and in agreement with others[184]. Finally, we found that TnT transcription and western immunoblotting showed mostly cardiac TnT mRNA and protein (Figure 5-3, C and E).

5.3.4   Electron microscopy and ultrastructure of fetal left ventricle muscle

To elucidate the potential influence of structure on the functional changes in these fetal tissues, sections of left ventricle were imaged using electron microscopy (Figure 5-4). Within myofibrils at day 52, Z bands are of non-uniform thickness and darkness, and the width of the sarcomere is uneven. In all three samples, multiple myofibrils appear loosely packed (Figure 5-4A, bottom). Correlating with a doubling in force production (Figure 5-1C), by day 108 Z bands are straight and aligned across adjacent myofibrils (Figure 5-4B, bottom). Finally, at day 127, the myofibril density is larger and myofibrils appear wider (Figure 5-4C, bottom). In all of these SEM images, the H-zone, or thick filament region, is often not distinct., consistent with previous observations[182]; however, this may be the result of the delay between tissue death and fixation (2.1.3, Fetal Human Tissues).

5.4   Discussion

Herein, we report changes in human fetal cardiac muscle during 52 to 134 days gestation which, to our knowledge, is the first report on the contractile properties and kinetics of contraction and relaxation of human fetal cardiac muscle. In this study, we characterized critical aspects of the contractile behavior, making some comparisons with human adult cardiac muscle. Myofibril preparations are small (3-15 μm wide) and thus are not subject to diffusion limitations, allowing for accurate measurements of the rapid (ms timescale) kinetics of force development and

relaxation[109,110,158]. We have found several changes to the subcellular kinetics of contraction and relaxation, and we have found compelling evidence to relate these changes in kinetics to underlying changes in protein expression and sarcomere development.

While our study was limited by the use of biopsies from a limited population, the broad range of ages studied and considerable differences seen between them makes the data robust.

We have previously reported that human fetal skeletal muscle ultrastructure is underdeveloped at 108 days gestation [135]; in this study, we see cardiac muscle ultrastructure lacks order. The lack of order in the structure of the muscle can explain the low force production and some of the changes in kinetics of activation and relaxation. However, the slower crossbridge cycling as the fetus ages may be a combination of a reduction in the faster alpha-cardiac myosin as the ventricle develops as well as the increased ultrastructural order, allowing for more cross-bridges to be under less strain. These topics are discussed in more detail below.

5.4.1   Force Production

The gains in force production from 59 to 134 days gestation have at least two potential explanations. 1) During this period of gestation, the ultrastructure of the fetal heart myofibrils, in particular the sarcomeres, Z-bands, and thick filaments, undergoes significant modelling and growth, allowing for more force to be translated along the sarcomeres and the myofibril. 2) During this period of gestation, the myosin density increases in the sarcomere, increasing the number of cross-bridges binding and force production.

The fetal cardiac muscle samples we used for mechanical studies are from 59 days, or 21% of full gestation, up to 134 days, or 48%. The ultrastructure hypothesis is supported by electron microscopy data from animal studies from similar time periods within gestation showing increasing myofibril density of cells, elongation and alignment of neighboring myofibrils, and increased thick filament (myosin) density [165,192,193]. A study looking at later term human fetal hearts (17 weeks (119 days) gestation forward) found myofibrils at 119 days gestation to be short, loosely packed, and lacking consistently definitive Z-bands [182]. These results agree with

80

our findings that the myofibrils are short and narrow at 52 days gestation, but lengthen and widen by 128 days gestation.

Our data are consistent with both of these explanations; however, detailed myosin density measurements and repeated electron microscopy imaging were beyond the scope of this study. The increasing force during development is likely due to increased acto-myosin interaction (with sarcomere maturation) and changes in myosin protein density.

5.4.2 Myosin and structure

The chemo-mechanical cycles of the faster alpha myosin heavy chain and slower beta myosin heavy chain have been well characterized [35,89,159,160].

In vitro motility measurements of the maximum velocity of unregulated actin filaments and myofibril $k_{REL,slow}$ measurements indicate a decrease in cross-bridge cycling or cross-bridge detachment, respectively, between approximately 100 and 130 days gestation. The unregulated F-actin filament sliding velocity (V_f) on myosin from the younger fetal heart was much slower than data we have shown for adult fast skeletal (gene *MYH2*) and alpha (α)-cardiac (gene *MYH6*), but faster than the speeds reported for beta (β)-cardiac (gene *MYH7*) myosin [35,159,160,186].

SDS-PAGE electrophoretic gels show very little, if any, alpha myosin heavy chain is present at any age, indicating that changes to the activation and cross-bridge cycling would be the result of a small amount of alpha myosin in a primarily beta myosin heavy chain heart. A small amount of the faster alpha myosin isoform known to increase the kinetics of cardiac muscle containing primarily beta myosin[3,149,194]; conversely, a small amount of beta myosin isoform is known from partial recombinant myosin studies to yield slower unregulated sliding velocities than a pure alpha myosin isoform [164].

However, the cross-bridge detachment rate increases between 59 and ~100 days gestation, as does the myofibril activation and fast phase relaxation rates. Due to limitations in tissue size, we were unable to isolate sufficient myosin from samples younger than 100 days gestation for *in vitro* motility testing; however, previous work shows that the percent of alpha myosin heavy chain in human fetal left ventricle tissue decreases with gestational age from ~8% at 47 days gestation to ~2% at 110 days gestation [183]. Thus, we can presume that the alpha

myosin content is not increasing between 59 and ~100 days gestation, and that there is another mechanism behind the increasing cross-bridge detachment rate.

One likely mechanism for the increase in cross-bridge detachment rate and activation and relaxation kinetics is that the ultrastructure development between 59 and ~100 days gestation allows for better z-band and sarcomere alignment, which may decrease compliance and cause strain to translate across the myofibril more efficiently, and more tightly bundled thick and think filaments, which would increase interaction of myosin and actin[143,148]. This increase in ultrastructural order could be responsible for both the increase in cross-bridge detachment and decrease, as the overall myosin density may be increasing during this period, reaching a critical density at which the myosin and actin can better interact.

5.4.3   Thin filament regulation

Increases activation kinetics as a function of gestational age could also be influenced by changes to the thin filament regulation. Both mouse [165] and sheep [174] show decreases in calcium sensitivity as the fetus ages. A decrease in calcium sensitivity caused by a change in TnC may cause a decrease in the rate of activation [150]. However, in the developing heart, the change in calcium sensitivity stems from a change in TnI and/or TnT isoforms, and the resulting decrease in calcium sensitivity is instead accompanied by an increase in the rate of activation. The duration of the slow phase is an indication of the thin filament "on" period and shortens between 59 days gestation and ~100 days gestation. A shorter thin filament "on" period may be consistent with less calcium sensitivity[150]. We hypothesize that this shorter filament "on" period is the result of either 1) decreased thin filament compliance, caused by more tightly bound thick and thin filaments, resulting in better translation of one troponin subunit turning "off" affecting its neighbor, 2) a change in TnI isoform, switching to the adult cardiac TnI isoform over the fetal cardiac/ slow skeletal TnI isoform, or 3) better thin filament regulation of acto-myosin binding, caused by a higher density of TnC, resulting in less cross-bridge binding in the absence of calcium.

Table 5-1: F_{MAX} and kinetic parameters for maximum $[Ca^{2+}]$ activation and relaxation of fetal myofibrils at 15°C, listed as mean ± SEM (# of myofibrils).

Significance testing was done with a one way ANOVA, using Tukey post-hoc analysis. * indicates p-value between groups of < 0.05. x indicates a p-value between groups of < 0.01. Pairs are indicated with shared letters. N indicates the number of separate fetal samples at a particular age or age range.

| Parameter (units) | Activation | | Relaxation | | |
| | | | slow | | fast |
	F_{MAX} (mN mm^{-2})	k_{ACT} (s^{-1})	$t_{REL,slow}$ (s)	$k_{REL,slow}$ (s^{-1})	$k_{REL,fast}$ (s^{-1})
59d (N=1)	7.8 ± 3.0 (3)	0.27 ± 0.07 (4)[*a]	0.292 ± 0.035 (4)[*a, xb]	0.14 ± 0.03 (3)	1.18 ± 0.13 (2)
74d (N=1)	23.1 ± 8.3 (5)	0.43 ± 0.12 (5)[*b]	0.235 ± 0.015 (5)	0.22 ± 0.05 (5)	0.96 ± 0.05 (5)
101d (N=1)	25.2 ± 6.6 (11)	0.45 ± 0.05 (11)[xc]	0.196 ± 0.012 (12)	0.30 ± 0.07 (12)	1.76 ± 0.15 (13)
105-107d (N=2)	32.2 ± 7.1 (22)	0.53 ± 0.08 (22)[xd]	0.197 ± 0.013 (23)[a]	0.18 ± 0.03 (21)	1.34 ± 0.13 (23)
110d (N=2)	19.9 ± 5.6 (12)	0.43 ± 0.05 (12)[xe]	0.200 ± 0.017 (12)	0.29 ± 0.07 (12)	1.75± 0.20 (12)
114-116d (N=3)	28.2 ± 4.7 (43)	1.04 ± 0.08 (41)[a-e]	0.180 ± 0.007 (44)[b]	0.22 ± 0.02 (44)	1.71± 0.08 (45)
130d (N=2)	49.9 ± 9.3 (8)	0.98 ± 0.21 (8)	0.210 ± 0.032 (8)	0.11 ± 0.02 (8)	1.64± 0.30 (8)
134d (N=1)	36.0 ± 12.1 (4)	0.55 ± 0.04 (4)	0.189 ± 0.013 (4)	0.13 ± 0.02 (4)	1.71± 0.04 (4)
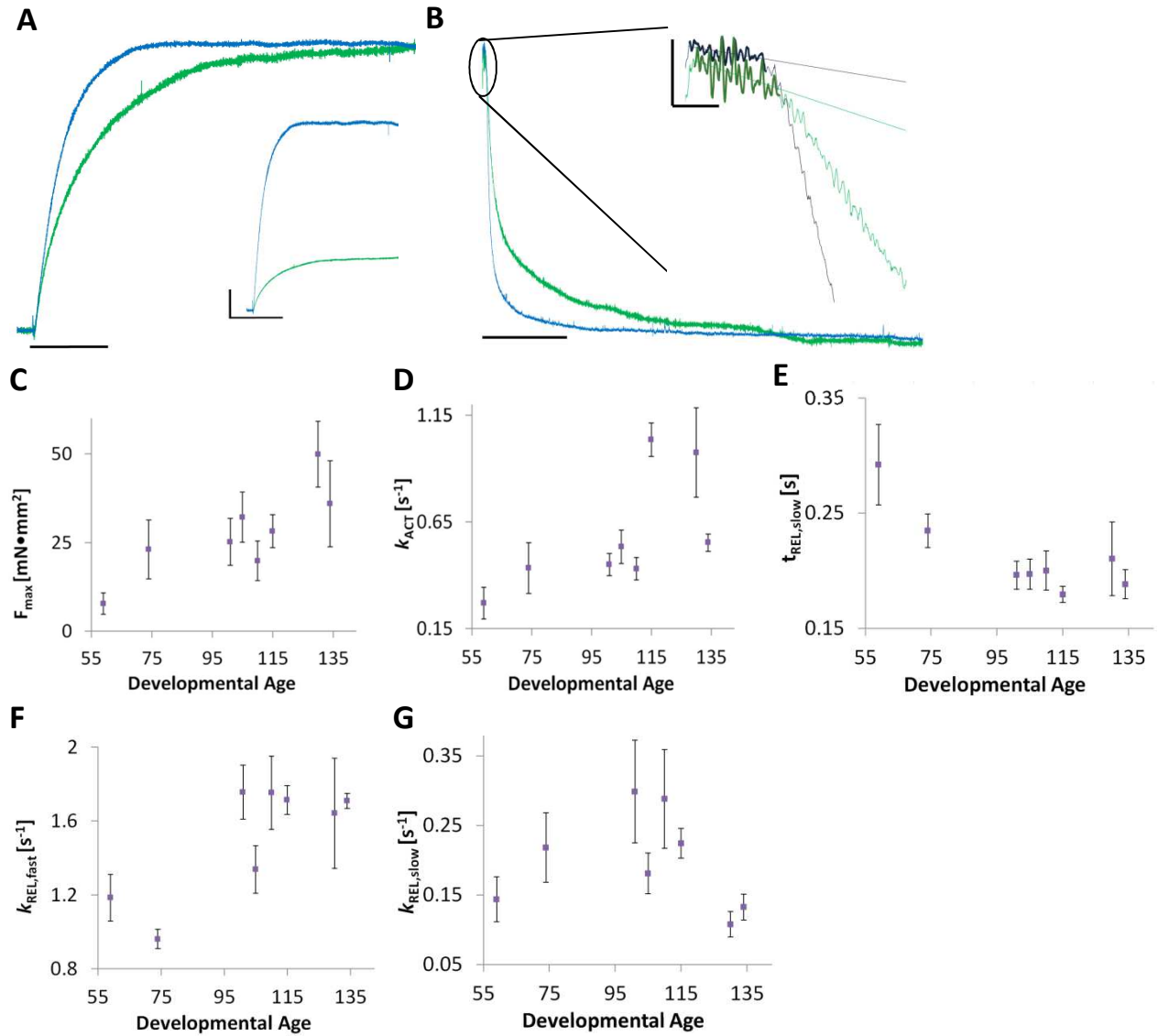
Figure 5-1: Representative traces of human fetal cardiac myofibril kinetics.

(**A-B**) Typical myofibril force traces for a human fetal cardiac myofibrils at 74 days gestation (green) and 130 days gestation (blue). (**A**) Activation traces showing activation kinetics differences between human fetal myofibrils at different ages; y-axis is force normalized to each myofibril's F_{MAX}; bar shows 5 seconds. (**A, inset**) Activation trace showing magnitude of activation; vertical bar shows 10 mN•mm^{-2}; horizontal bar shows 5 seconds. (**B**) Relaxation traces showing relaxation kinetics differences between human fetal myofibrils at different ages; y-axis is force normalized to each myofibril's F_{MAX}; bar shows 5 seconds. (**B, inset**) Close-up of the slow phase of relaxation of the fetal myofibrils (bold lines), in response to a change from maximum $[Ca^{2+}]$ (*p*Ca 4.0) to minimum $[Ca^{2+}]$ (*p*Ca 9.0), features slow phase kinetics; vertical bar shows 10% F_{max}; horizontal bar shows 100 milliseconds. Straight lines indicate the slow phase fit ($k_{REL,slow}$); bold lines indicate data considered part of the slow phase; thin lines indicate the total normalized relaxation data.

(**C-G**) Charts illustrating changes in kinetics across fetal samples grouped by age.

84
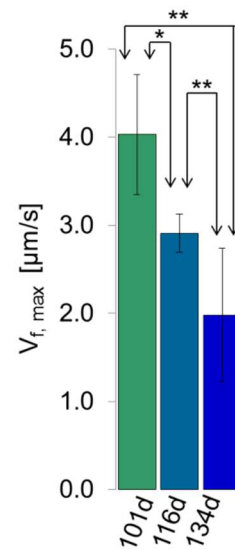
Figure 5-2: *In vitro* motility unregulated F-actin speeds for human fetal hearts.

Maximum filamented actin velocity for human fetal heart myosins from three different ages. * indicates $p < 0.05$, ** indicates $p < 0.01$; statistical analysis with ANOVA, post-hoc Tukey testing.
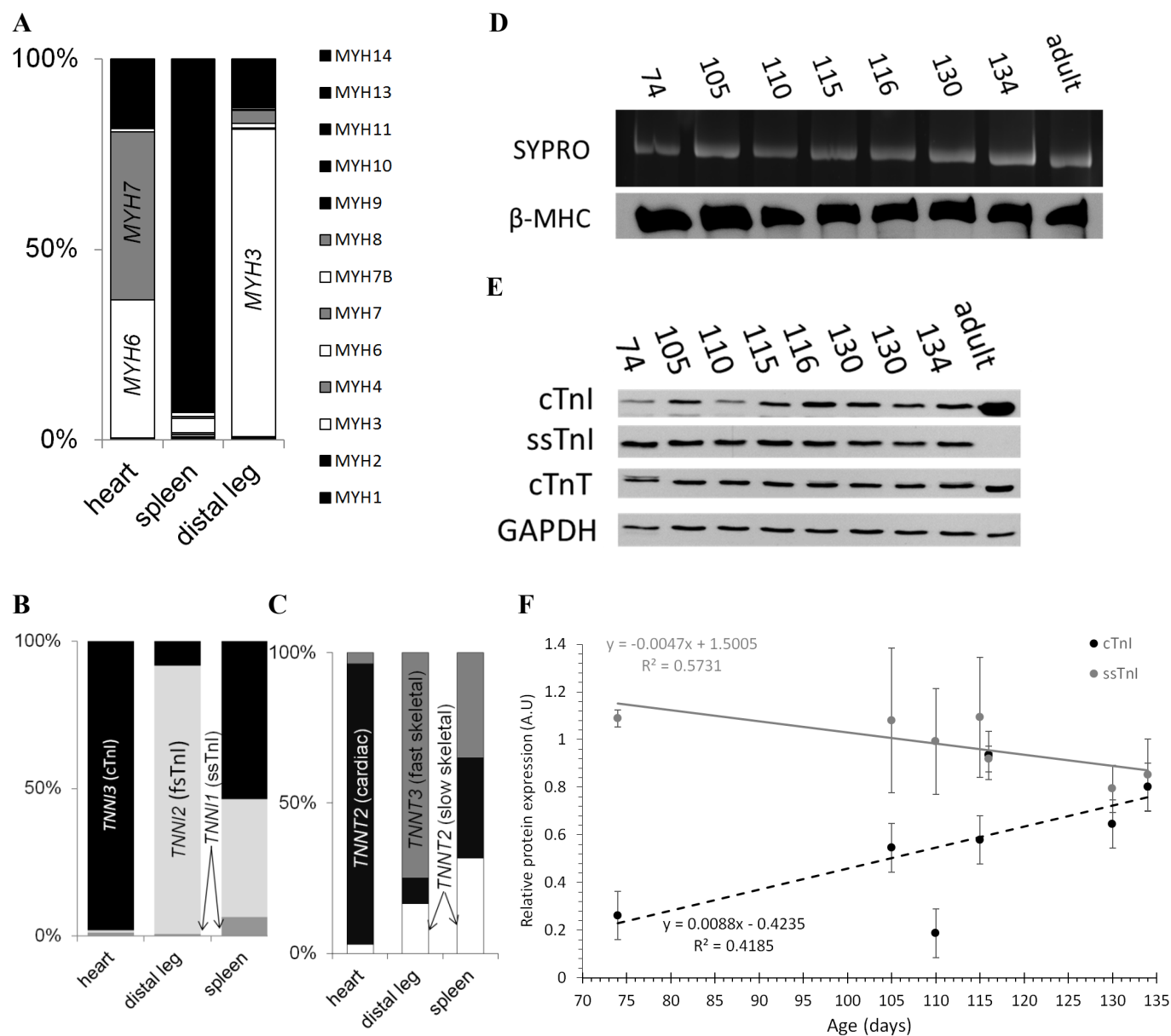
Figure 5-3: Myosin and Troponin expression in human fetal hearts.

(**A**) mRNA transcripts of fetal myosin isoform from Illumina human HT-12 whole transcriptome assay from 103 days gestation fetal whole heart. (**B**) mRNA transcripts of troponin I expression from Illumina human HT-12 whole transciptome assay from 103 days gestation fetal whole heart. (**C**) mRNA transcripts of troponin T expression from Illumina human HT-12 whole transciptome assay from 103 days weeks gestation fetal whole heart. (**D**) Sypro stain and western immunoblott showing beta myosin heavy chain expression in fetal heart ventricle samples across the 74 to 130 days gestation range. (**E**) Western immunoblott showing increasing ratio of cTnI to ssTnI as the fetal heart ages from 74 to 130 days gestation. Also shown are cTnT western immunoblot and a loading control. (**F**) Densiometric analysis showing increasing ratio of cTnI to ssTnI as the fetal heart ages from 74 to 134 days gestation.

86
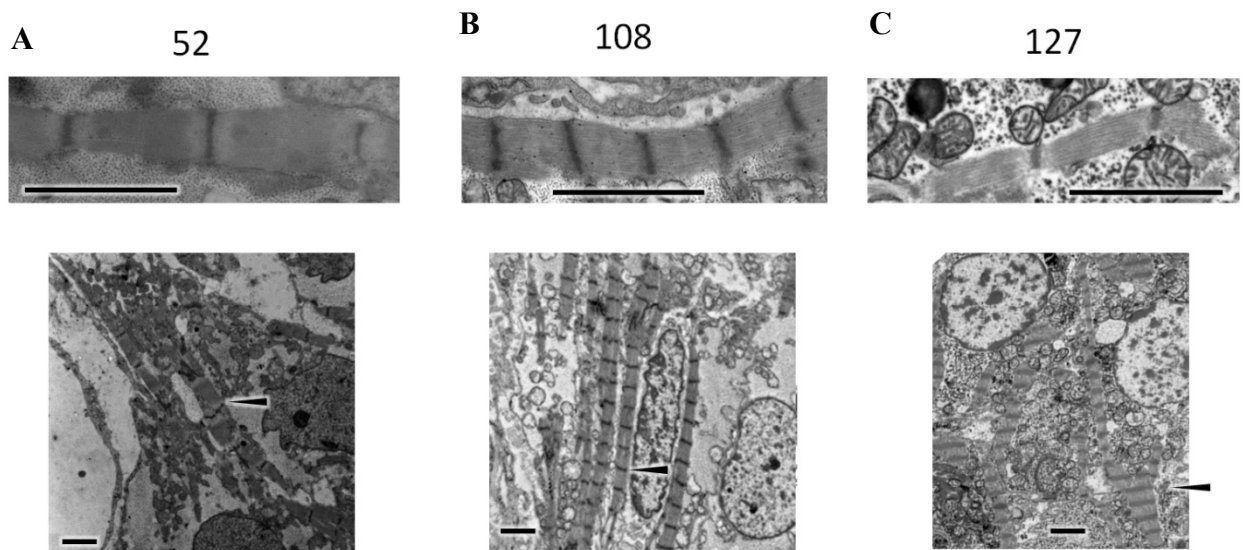
Figure 5-4: Ultrastructural assessments in human fetal heart left ventricle. Scanning electron microscopy images of left ventricle sections from fetal hearts aged 52-127 days gestation. All scale bars are 2 μm.

(**A, top**) 52 day left ventricle shows thick filament presence and thin myofibrils.

(**A, bottom**) 52 day left ventricle shows poor z-disk alignment between myofibrils, wavy z-disks within myofibrils (arrow), and low myofibril density.10,000x magnification of 128d left ventricle.

(**B, top**) 108 day left ventricle shows definitive m-line within sarcomeres.

(**B, bottom**) 108 day left ventricle shows medium myofibril density and z-disk alignment between adjacent myofibril (arrow).

(**D, top**) 127 day left ventricle shows definitive m-line within sarcomeres.

(**D, bottom**) 127 day left ventricle shows high myofibril density and z-disk alignment between adjacent myofibril (arrow), as well as larger myofibril widths overall.

5.5   Continuing and Future Work

Further work on the fetal cardiac myofibrils should include increasing the number of fetal hearts at the lower (<100 days gestation) and upper (between 116 and 130 days gestation) ranges, to increase the robustness of the data set shown here and confidence in these findings. Additionally, these studies have been limited to the left ventricle; however, the atria are known to carry far more α-myosin heavy chain, which is implicated in several forms of genetic-based congenital heart defects, and would be an important part of the fetal heart to study in the future.

Other future work to continue this project would be to compare human – induced – pluripotent – stem- cell –derived cardiomyocytes (hiPSC-CM) to human fetal cardiac samples from both atria and ventricle tissues. This is a project which the lab has already started, with the fetal ventricle samples shown in this chapter, and it is apparent the hiPSC-CM myofibrils, grown by J. Manuel Pioner (2.2, Human Stem Cells) and tested by myself and Mr. Pioner, contract with a strength and speed more similar to fetal heart myofibrils (Figure 5-5) than those values reported in the literature for human adult ventricle or atria tissue, though the crossbridge detachment rate ($k_{REl,slow}$) is similar to human atria and the thin filament "off" time ($t_{REL,slow}$) is similar to human ventricle[188]. The hiPSC-CM cells appear to have less Z-band alignment, but more distinguishable thick filaments (presumably more myosin content) than fetal myofibrils in electron microscopy (Figure 5-6)
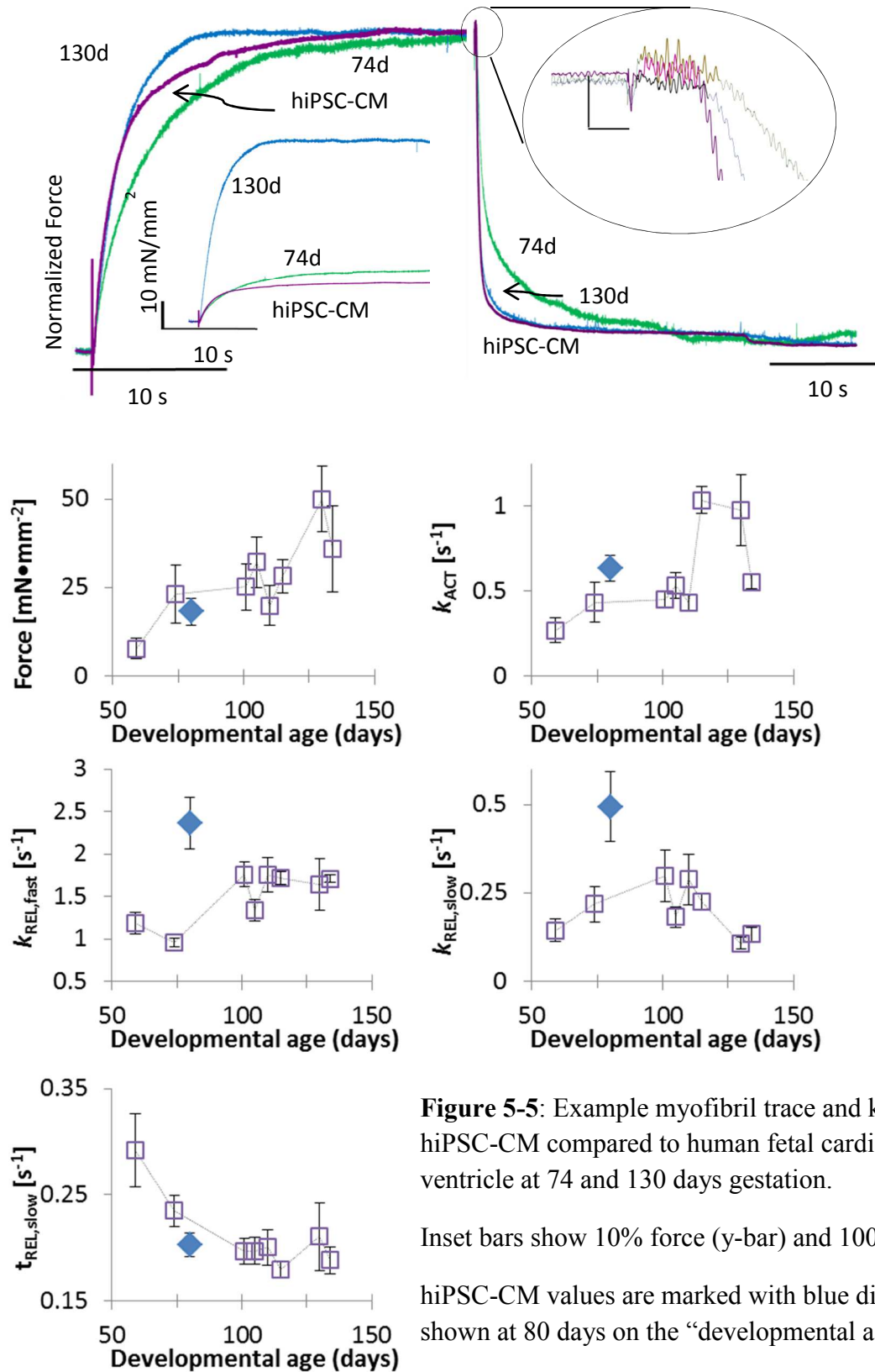
Figure 5-5: Example myofibril trace and kinetics from hiPSC-CM compared to human fetal cardiac left ventricle at 74 and 130 days gestation.

Inset bars show 10% force (y-bar) and 100 ms (x-bar).

hiPSC-CM values are marked with blue diamonds, shown at 80 days on the "developmental age" x-axis.
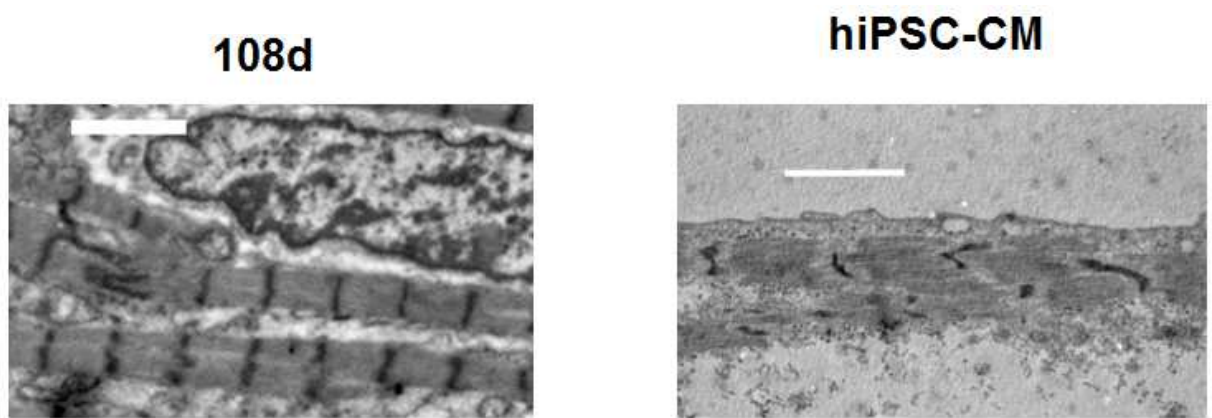
Figure 5-6: Transmission Electron Microscopy images of fetal heart and hiPSC-CMs.

White bar indicates 2 μm.

CHAPTER 6.   CARDIAC MUSCLE in HEART DISEASE

6.1   Items of Note

Parts of this section have been previously published[186] and are reproduced here with permission from Elsevier (see APPENDIX, Moussavi-Harami *et. al*).

6.1.1   <u>Aim – To observe the effects of multiple forms of heart disease on myofibril kinetics and address changes through the use of potential therapeutics</u>**.**

6.1.2   <u>Key Points</u>

- Contraction in human heart failure sample was measured in presences of ATP or dATP
- dATP increases isometric force in myofibril samples
- dATP increases rate of force development in myofibril samples
- dATP does not alter myofibril relaxation kinetics

6.1.3   <u>Summary</u>

We are developing a novel treatment for heart failure by increasing myocardial 2 deoxy-ATP (dATP). Our studies in rodent models have shown that substitution of dATP for adenosine triphosphate (ATP) as the energy substrate *in vitro* or elevation of dATP *in vivo* increases myocardial contraction and that small increases in the native dATP pool of heart muscle are sufficient to improve cardiac function. Here we report, for the first time, the effect of dATP on human adult cardiac muscle contraction. The rate of contractile activation (k_{ACT}) in isolated myofibrils was increased with the use of dATP, indicating increased cross-bridge binding and cycling compared with ATP in failing human myocardium. These data suggest dATP could increase dP/dT and end systolic pressure in failing human myocardium. Importantly, even though the magnitude and rate of force development was increased, there was no increase in the time to 50% and 90% myofibril relaxation. These data, along with our previous studies in rodent models shows the promise of elevating myocardial dATP to enhance contraction and restore cardiac pump function. These data also support further pre-clinical evaluation of this new approach for treating heart failure.

6.2 Introduction

Heart failure is a growing epidemic in developed countries, with the incidence and prevalence rising each year [81]. Despite advancements in treatment, the five year mortality approaches fifty percent [195]. At least half of the patients suffering from heart failure have low systolic function[196]. However, currently available inotropic agents which increase contractility via altering intracellular calcium do not improve survival in patients with heart failure[197,198]. Some of the reasons for failure of inotropic agents include tachyarrhythmias, increased myocardial oxygen consumption, decreased coronary perfusion and alteration of intracellular calcium[198]. Hence, there is an urgent need for development of novel agents that improve contractility and systolic function. One way to avoid unwanted side effects may be to directly target myofilaments to alter contractility at level of the sarcomere and motor proteins.

In previous animal studies we found that use of 2-deoxy adenosine triphosphate (dATP) instead of adenosine triphosphate (ATP) as the energy source improves contractility in striated muscle by enhancing crossbridge binding and cycling kinetics and improving allosteric activation[35,36,159,160]. In fact, increasing the dATP level from the typical $\leq$0.1% of the adenosine nucleotide pool to 1% is enough to significantly increase contraction[89]. We have developed a novel approach to elevate dATP *in vivo* by increasing the expression of the enzyme ribonucleotide reductase (R1R2), the rate-limiting step in de novo dNTP biosynthesis. This results in increased levels of 2-deoxy ATP (dATP). We have shown that increasing dATP in intact cardiomyocytes via adenovirus mediated transfection increased contractile magnitude and kinetics[89]. In addition, transgenic mice that overexpress R1R2 have increased left ventricular systolic function compared to control animals[156]. Based on these results, overexpression of R1R2 and increased cardiomyocytes dATP constitutes an exciting and novel therapy with potential to treat heart failure. However, before clinical studies in humans are convened, a critical step is to test the efficacy of elevated dATP levels on human cardiac myocardium to ensure that effect of dATP is consistent across species.

Here we report for the first time that dATP improves contraction in myocardial samples isolated from human subjects with end-stage heart failure. We show that for isolated myofibrils there is an increase in activated force and rate of activation without alteration of relaxation. This study represents an important next logical step in the progression toward using dATP therapy in a

clinical setting. We conclude that elevation of myocardial dATP has merit as an approach worth further investigation for the treatment of heart failure and in particular patients with low systolic function.

6.3   Results

6.3.1   Patient Characteristics

Sixteen samples were collected from fifteen patients that were enrolled in the study. For one patient, there was sample collected both at time of left ventricular assist device (LVAD) and transplant and used for different assays at the two time points. Thirteen out of fifteen patients (87%) were males and the average age of the cohort was 49±13 years old (26-67 years). Twelve of the sixteen samples were collected from patients undergoing LVAD implantation and four samples were collected at the time of cardiac transplantation. Samples used for isometric contraction were exclusively from patients undergoing LVAD implantation. For the myofibril measurements, NTPase and *in vitro motility* assays, there was a mixture of samples at time of LVAD surgery and transplantation. The etiology of heart failure in 87% (13 out of 15) of the patients was non-ischemic and 13% (2 out of 15) was ischemic.

6.3.2   NTPase and In vitro motility assays

The V_{max} (actin activated) of isolated human myosin at 23°C calculated by NTPase assay was increased by sixty percent from 1.00 ± 0.20 s^{-1}/head to 1.60 ± 0.32 s^{-1}/head (N=5, p=0.042) when dATP was substituted for ATP (Figure 6-1A). Our *in vitro motility* measurements were performed at 30°C, which is closer to the physiologic temperature, and these measurements also provide an indication of NTPase. Maximum sliding velocity (V_f) for isolated human cardiac HMM was increased by 47%, from 1.78 ± 0.53 μm/s to 2.62 ± 0.79 μm/s (N=3), when dATP was substituted for ATP (Figure 6-1B). This suggests a higher NTPase rate when dATP is used by failing human adult myosin.

6.3.3   Myofibrillar contraction measurements

Small myofibril bundles were used to assess the kinetics of activation and relaxation. To control for the effects of repeated activations, separate myofibril bundles from each patient were activated and relaxed at pCa 5.6 in the presence of 2 mM ATP and 2 mM dATP. Figure 6-2A

shows an example of activation and relaxation of 2 myofibril bundles, one in presence of 2 mM ATP and the other in the presence of 2 mM dATP. The force for both traces is normalized to highlight the rates of activation and relaxation. This example demonstrates the increase in the rate of activation in the presence of dATP. The data for all measurements is summarized in Figure 6-2B. The relaxation trace shows that the time course of relaxation to baseline was similar. dATP significantly increased both force production (76.1 ± 1.0 *vs*. 85.9 ± 6.9 mN/mm^2, p= 0.039, n = 27, N = 7) and rate of activation (0.64 ± 0.01 *vs*. 0.92 ± 0.08 s^{-1}, p = 0.003, n = 27, N = 7) at pCa=5.6. Myofibril relaxation measurements did not show a decrease in time to 50% (0.38 ± 0.03 vs. 0.47 ± 0.05 s, p = 0.064, n = 16, N = 7) or 90% (4.44 ± 0.75 *vs*.5.11 ± 1.01 s, p = 0.31, n = 16, N = 7) relaxation. Myofibril tension relaxation consists of an initial slow ($k_{REL,slow}$) phase, associated with crossbridge detachment rates, and a secondary, large amplitude fast ($k_{REL,fast}$) phase that dominates overall relaxation time[114]. Neither the duration (0.182 ± 0.002 s (ATP) *vs*. 0.194 ± 0.009 s (dATP), p = 0.17, n = 25, N = 7), nor rate of the slow phase of relaxation ($k_{REL,slow}$) (0.273 ± 0.009 *vs*. 0.310 ± 0.05 s^{-1}, p = 0.32, n = 25, N = 7) are significantly increased when dATP was substituted for ATP. Similarly, there was no significant increase in the rate of the fast phase of relaxation ($k_{REL,fast}$) (1.81 ± 0.03 *vs*. 1.70 ± 0.11 s^{-1}, p = 0.29, n = 27, N = 7).
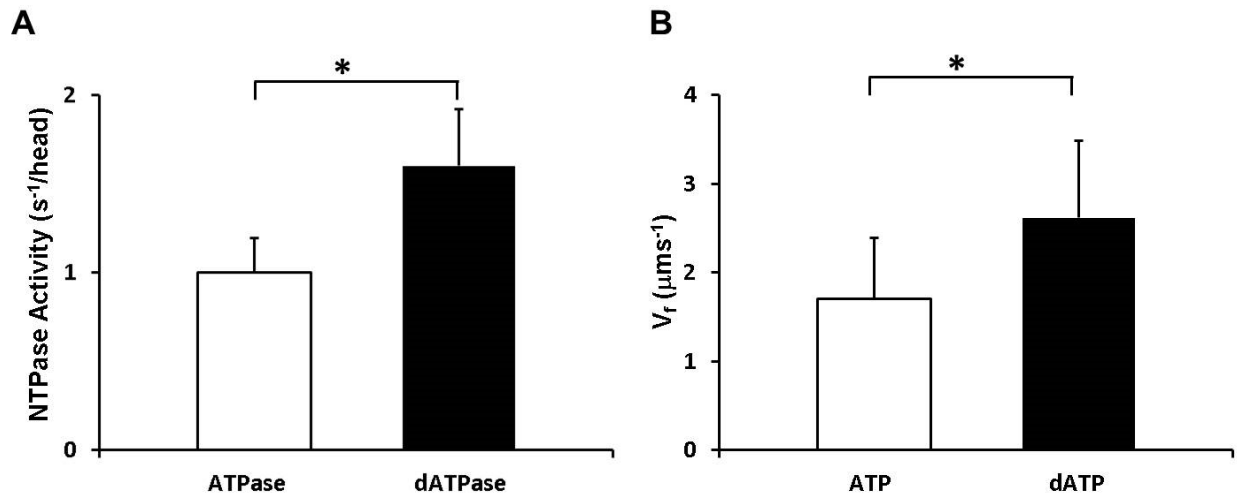
Figure 6-1. ATP increases NTPase activity.

(**A**) NTPase activity of myosin from failing human myocardium in presence of actin and 1 mM ATP or dATP (N = 5). Data are reported as mean with standard error of the mean. *p <0.05 by paired student's t-test. Data courtesy of F. Moussavi-Harami.

(**B**) Speed of smoothly moving actin filaments (V_f) over failing human cardiac heavy meromyosin in presence of 2 mM ATP (n = 576 filaments) or dATP (n = 1493 filaments). Data are reported as weighted mean with standard deviation (N = 3) * p< 0.05 by non-paired student's t-test.
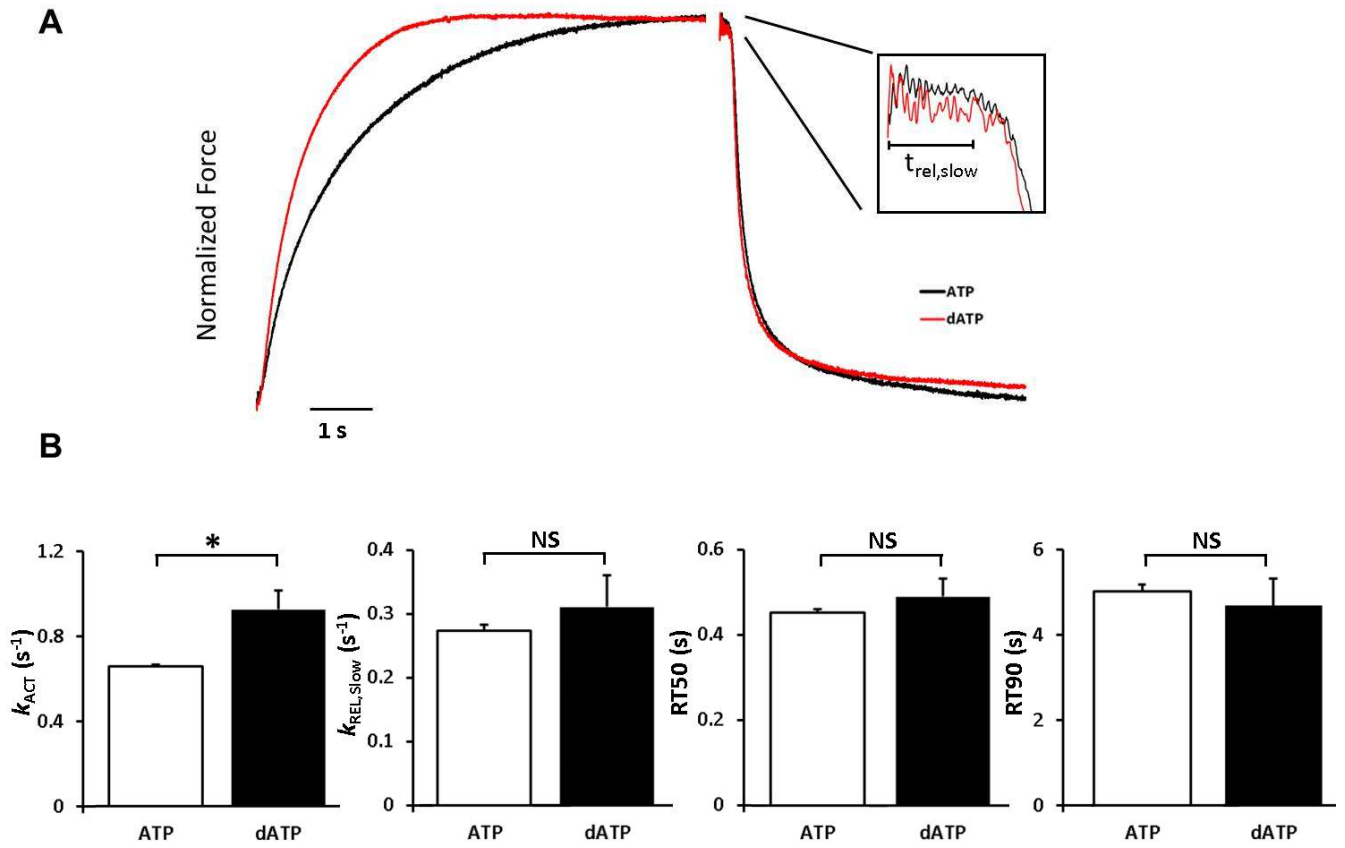
Figure 6-2. dATP increases myofibril activation rate without altering relaxation.

(**A**) Typical normalized myofibril force trace from a patient with end-stage congestive heart failure in presence of ATP (Black) or dATP (Red). The left trace is the activation trace at pCa=5.6 and the right trace is relaxation when switched to pCa=9.0 solution. The inset is close up of the slow phase of relaxation.

(**B**) Rate of activation (k_{ac}), rate of the slow phase of relaxation ($k_{REL,slow}$), time to 50% (RT50) and 90% (RT90) relaxation of human myofibrils in presence of 2 mM ATP (white) and dATP (black). Data are reported as mean±SE (n = 25-27, N = 7). * P<0.05 compared to ATP by non-paired student's t-test

6.4   Discussion

Here we have reported the first observations of the effect of dATP on the contractile properties of cardiac muscle from human heart failure patients. This cohort of patients has severe systolic function, indicating severe contractile dysfunction in the cardiac muscle. The main findings from our studies are that dATP 1) increases human cardiac myosin binding (to actin) and cycling kinetics and 2) the magnitude and rate of contraction at a near physiological (pCa 5.6) calcium concentration of activation. Importantly, this occurs without altering the relaxation properties of cardiac muscle, which can occur with other cardiac inotropes (discussed below). Our pCa_{50} values (5.44 to 5.87 for ATP group[186]) are within the range reported in the literature (5.6-5.8 in non-failing hearts and 5.8-6.0 in failing heart)[199,200]. These previous studies were performed on skinned isolated cells rather than multicellular preparations, as in our study.

Our previous studies in rodent models demonstrated that the magnitude and rate of force development was increased at all calcium activation levels in cardiac muscle preparations when dATP is substituted for ATP[35,155,156,160]. However, there are known differences between contractile proteins in humans and rodents. The predominant myosin subtype in human is β-MHC, compared to the faster α-MHC subtype that is predominant in rodents[201]. While the two isoforms show significant homology, β-MHC exhibits a slower ATPase rate, slower sliding velocity and maximal shortening velocity, and significantly lower power generation capabilities [3]. At the same time, β -MHC is more energy efficient and produces the same amount of force per crossbridge[202].

On the molecular level, differences between the two cardiac myosin isoforms are thought to be primarily in loop 1 and loop 2 of the myosin head[203]. Our molecular dynamic simulations predict that dATP changes the charge exposure on loop 2[204], so it was possible that the effect of dATP could be MHC dependent. We have reported that dATP increases force and the rate of force development at all levels of calcium activation in demembranated cardiac preparations from normal and PTU treated rats, the latter of which express primarily β-MHC respectively[36]. In a report by Schoffstall et al., porcine cardiac preparations had a similar dATP-induced increase in maximal force production and at sub-maximal calcium levels > pCa 5.5, but did not show change in calcium sensitivity of force, a result that was attributed to troponin and tropomyosin

isoform differences by the authors[205]. It may also be that phosphorylation of myofilament proteins was significantly different in their cardiac muscle preparations, as phosphorylation of proteins such as troponin I, troponin T, myosin binding protein C and titin are known to affect the calcium sensitivity of force and affect the myosin dependence of thin filament activation and force development. They did report a 47% increase in unregulated (no troponin or tropomyosin) actin filament sliding velocity over immobilized myosin heads via the *in vitro* motility assay, which is the same magnitude increase we report for actin motility on surface covered with myosin from failing human hearts (Figure 6-1B), supporting a myosin specific effect of dATP.

The interspecies difference in ATPase rates and actin sliding velocity within α and β MHC[201] and reported alterations in myosin subtype expression in human failing hearts[183,206,207] warranted an assessment of the effect of dATP on failing human myocardium. To our knowledge, this is the first study to evaluate the effect of dATP on the contraction of human samples from end-stage heart failure patients. Our data demonstrate that, in addition to augmenting cardiac muscle contraction, dATP increases crossbridge cycling in purified human cardiac myosin and HMM. Coupled with our previous studies, this suggests that dATP enhances crossbridge activity independent of myosin isoform and calcium levels present in cardiac muscle cells. Our isometric force measurements from isolated myofibrils demonstrate an increase in the magnitude and the rate of force development (Figure 6-2) at physiological and maximum levels of calcium activation with dATP. Our current human data confirms the previous mechanism that has been shown in rodents, where we demonstrated an increase in myosin binding to actin with dATP, which leads to increased thin filament activation at all levels of calcium activation, and that the level of thin filament activation is an important determinant in the rate that force develops[35,36]. Our data can be interpreted using the 2-state model of crossbridge to understand how dATP improves contraction in human cardiac samples. In the 2-state crossbridge model, the rate constants for crossbridge attachment and force generation are summed together as f_{app} and rate of crossbridge detachment is g_{app}. Our current data in human samples shows that dATP increases rate of force redevelopment ($k_{tr} = f_{app} + g_{app}$), F_{max} ($\sim f_{app} / (f_{app} + g_{app})$) and V_f, indicating an increase in $f_{app} + g_{app}$ and f_{app} / g_{app}. This is also consistent with recent modeling results from our group showing dADP stabilizes myosin in a conformation that favors binding to actin. Thus dATP elevates contractile activation via increased myosin binding to actin, without extending the

time of myosin-actin interaction, such that it should increase the amount and rate of force development, but not retard the rate of myosin detachment and muscle relaxation.

The increase in both magnitude and rate of force development at the sub-cellular and tissue levels correlates (respectively) to systolic ventricular function, particularly the isovolumic phase of pressure development (+dP/dT). Indeed, we have reported that +dP/dT is significantly increased in transgenic mice with elevated [dATP][156], in normal and infarcted mice[208,209] and infarcted pigs treated with a viral vector to overexpress R1R2 and elevate dATP in the heart (unpublished data, Regnier lab). As such, it suggests that +dP/dT could be increased by elevating myocardial dATP in failing human hearts. An aspect that may be unique to elevated dATP as a treatment for heart failure may be that, in addition to improving systolic pressure development, myocardial relaxation and the rate of ventricular pressure decline (-dP/dT) at beginning of diastole is not prolonged and may even be improved. This may be related to faster nucleotide hydrolysis product release by myosin with dATP as the substrate[160].

One of the limitations of our study is that it was skewed towards non-ischemic cardiomyopathy. We would expect similar increase in contractility in other forms of systolic heart failure. We also need to evaluate our approach in isolated cardiomyocytes treated with R1R2 overexpression viral vector to ensure the effect is present event with the elevated diastolic calcium levels seen in end-stage heart failure. ATP is an indispensable biological molecule and in our novel therapeutic approach, we anticipate replacing less than 10% of the ATP content by dATP. It is noted that dATP can be used instead of ATP by enzymes such as hexokinase, polynucleotide kinase, T4 DNA ligase, T4 RNA ligase and sarcoplasmic reticulum calcium dependent ATPase (SERCA)[210,211]. It has been shown that ATP and dATP are hydrolyzed at similar rate by SERCA[210]. Whether these ATPases would have enhanced activity with a dATP pool that is less than 10% of ATP, as is the case for myofilament contractility, is unclear.

We have previously shown that overexpression of the enzyme ribonucleotide reductase in rodents, using transgene or gene therapy, can improve contraction via increased dATP[155,156]. Now we show that dATP can increase contraction in failing human myocardial tissue. Our novel approach to treat heart failure focuses at the myofilament where the primary contractile deficit occurs. Levosimendan and Omecamtiv mercarbil are two medications in investigational trials

that also focus on treating heart failure at the level of the myofilament. Levosimendan is a calcium sensitizer[212] that binds to calcium-saturated cTnC. Levosimendan does have off-target effects, such as interaction with the vascular smooth muscle K^+ channel, and has shown favorable hemodynamic effects without any clear clinical benefit[213]. Omecamtiv mercarbil enhances the ATPase activity of myosin[214], and also improves cardiac function in both healthy volunteers and those with stable heart failure. However, this medication increases the duration of cardiomyocyte twitches, increases systolic ejection time, and decreases time in diastole. Furthermore, there is concern that Omecamtiv marcarbil decreases coronary perfusion and coronary filling[215,216]. Our approach to treating heart failure is myofilament specific, and we have previously shown the nucleotide dATP can transfer from one cell to another via gap junctions[217] so elevation of ribonucleotide reductase need not be accomplished throughout the myocardium. Additionally, cardiomyocyte contractions are stronger and faster, but not prolonged, and both +dP/dT and –dP/dT are increased with a resulting increase in ejection fraction[155,156].

6.5   Conclusions and Future Work

We have demonstrated for the first time that dATP can increase contraction and the rate of crossbridge cycling in cardiac muscle from patients with end-stage heart failure, without retarding relaxation. We have used isolated protein and myofibril assays to show this occurs at the level of the contractile apparatus of the heart. Coupled with our previous and ongoing work in animal models, these data support a novel myofilament approach for treating heart failure that warrants further pre-clinical evaluation.

Ex vivo mechanical and kinetic studies of subcellular contractile units is an effective assay for testing the therapeutic potential of dATP and possibly other therapeutics that directly target the myofilament proteins such as EMD7055.

Here we've shown that dATP enhances the force production and rate, without affecting relaxation, results which concur with animal models of infarcted hearts and which support the hypothesis that dATP enhances systole without slowing diastole.

A next step in studying the effects on kinetics of activation and relaxation in heart disease would be to use this therapeutic on hiPSC-CM models of heart disease. hiPSC-CM myofibrils show significant contractile deficits as a result of genetic mutations in both sarcomere proteins (Figure 6-2, Top) and non-sarcomere proteins (Figure 6-2, bottom). Because the precursors to the stem cells are obtained in a minimally invasive manner, it would be possible to obtain a wider or more selective cohort to test therapeutics on. Future work in using this potential therapeutic would involve working by modelling heart disease with hiPSC-CMs, which would allow greater control over the cause of the cardiomyopathy, and in turn, allow for full picture of which types of cardiomyopathy this potential therapeutic is most effective against.
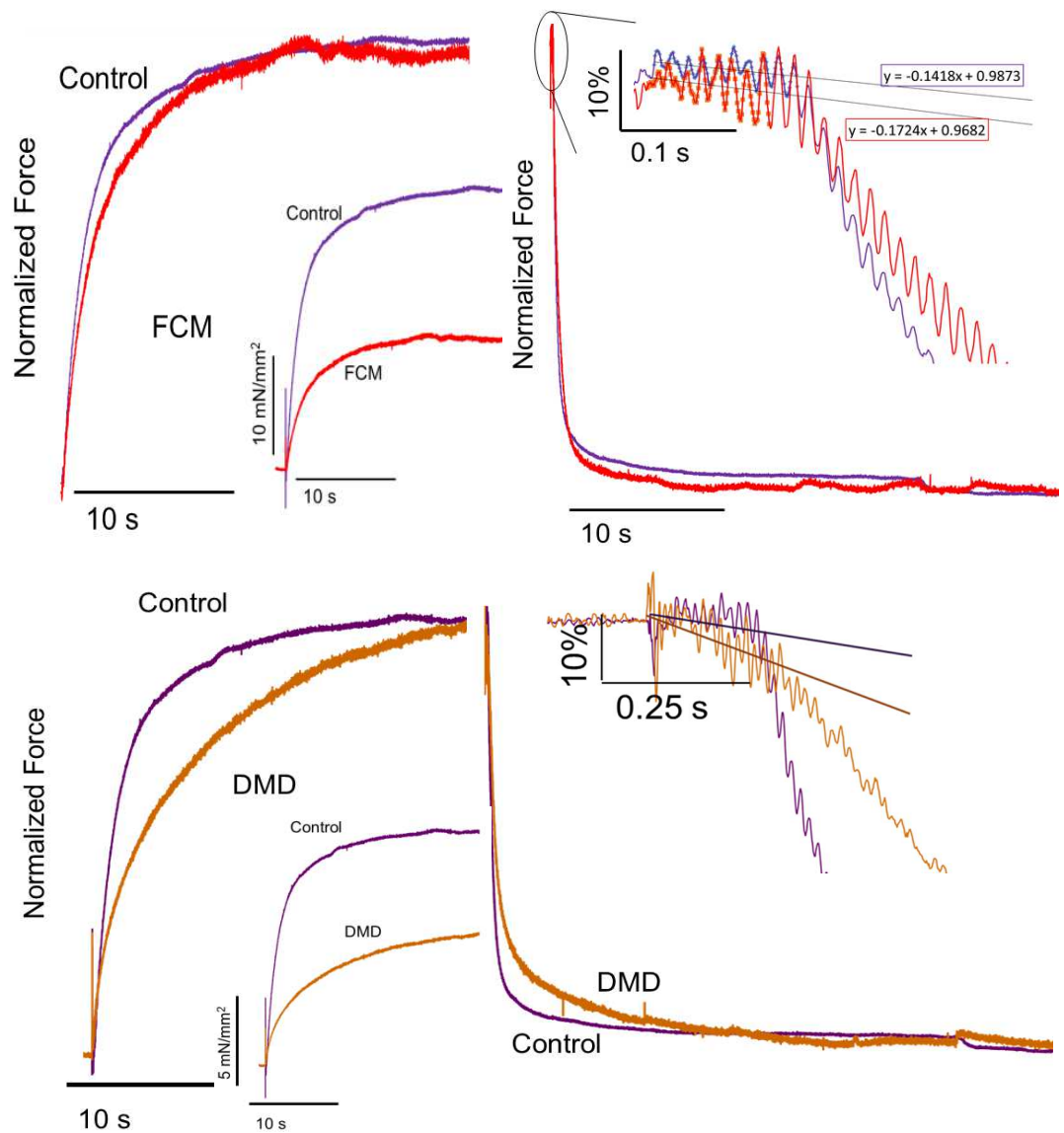
Figure 6-3: hiPSC-CM myofibrils show contractile deficits in sarcomere and non-sarcomere protein mutation – related cardiomyopathy.

(Top) Familial Cardiomyopathy (β-myosin heavy chain E848G) hiPSC-CM myofibrils show reduced force compared to control hiPSC-CM myofibrils.

(**Bottom**) DMD (Dystrophin exon 50 deletion) hiPSC-CM myofibrils show reduced force, slower total relaxation, and longer early phase relaxation than control hiPSC-CM myofibrils.

CHAPTER 7.   FUTURE DIRECTIONS

The ultimate goal of this research is to increase knowledge of human fetal heart and skeletal muscle contractility during development, as a gateway to improving overall understanding of disease development. Following this initial characterization of contractility and kinetics of human fetal skeletal (CHAPTER 4), additional contractility experiments at other age points would increase our understanding of how the contraction changes within development and upon the addition of neonatal (gene *MYH8*) myosin. Similarly, I have studied human fetal cardiac (CHAPTER 5) muscle in great detail, but additional work on sarcomere protein isoform switches, and other key muscle cell components, such as the development of the sarcoplasmic reticulum, metabolomics, and the formation and effect of the t-tubules and excitation-contraction coupling complex, are important studies for the future. Finally, mRNA was extracted from several fetal tissues of multiple ages in addition to samples of tissue that were flash-frozen and stored at -80°C; this "gene transcription" and tissue library is a fantastic resource which will allow for a matching between gene transcription and protein expression within fetal tissues of many types, including striated muscle, and will be useful in further studies in developing muscle physiology.

The studies on human fetal skeletal muscle have informed my initial work on distal arthrogryposis type 2A (CHAPTER 3), and set a foundation for understanding how the different subtypes of distal arthrogryposis form *in utero*. The next step in studying distal arthrogryposis will be to exchange distal arthrogryposis-causing mutant troponin subunits into fetal skeletal and adult skeletal myofibrils, to study the contraction and relaxation changes in distal arthrogryposis caused by thin filament mutations. By studying the mutations' effect in both fetal and adult muscle, we can better understand how the disease develops contractures *in utero* and continues to have an effect post-natal. Then, we can progress to studying potential therapeutic treatments for distal arthrogryposis, tailored to the individual deficits in contraction and kinetics caused by the mutations.

Human fetal heart studies have greatly informed other work in the Regnier lab in modeling heart disease. With the timeline of the human fetal heart contractility and kinetics, we have been able to confirm that the human induced pluripotent stem cell myofibrils produce force and relax with similar magnitude and kinetics as the human fetal heart left ventricle myofibrils. Studies in contraction and kinetics of adult heart failure samples (CHAPTER 6) in comparison the human induced-pluripotent stem-cell-derived cardiomyocyte samples are better understood with the knowledge that the latter samples are less mature and thus may demonstrate early onset changes to contraction and kinetics, setting the stage for developing potential therapeutics.

The human adult heart failure muscle studies have demonstrated the ability of dATP to enhance contraction force and speed without affecting relaxation and highlight dATP's potential use as a therapeutic for distal arthrogryposis 2A muscle, in which activation is severally affected and force production per cross-sectional area of the cell is lower. Finally, the investigation of multiple forms of heart disease, in human cardiomyocytes in muscular dystrophy or familial cardiomyopathy or in biopsies of human stage IV heart failure, has created groundwork for understanding the different manifestations of contractile kinetics changes in cardiomyopathy and may help in determining which therapeutics would more effective. Future studies will include comparing troponin mutant exchanges, EMD50733, and the nucleotide dATP, as well as other therapeutics, to elucidate a model for how kinetics of contraction and relaxation can be modulated with therapeutics and which therapeutics are most effective in correcting specific malfunctions.

REFERENCES

1.   Gordon AM, Regnier M, Homsher E. Skeletal and cardiac muscle contractile activation: tropomyosin "rocks and rolls." *News in Physiological Sciences: An International Journal of Physiology Produced Jointly by the International Union of Physiological Sciences and the American Physiological Society*. 2001;16:49-55.

2.   Siemankowski RF, Wiseman MO, White HD. ADP dissociation from actomyosin subfragment 1 is sufficiently slow to limit the unloaded shortening velocity in vertebrate muscle. *Proceedings of the National Academy of Sciences of the United States of America*. 1985;82(3):658-662.

3.   Herron TJ, Korte FS, McDonald KS. Loaded shortening and power output in cardiac myocytes are dependent on myosin heavy chain isoform expression. *Am J Physiol - Heart C*. 2001;281(3):H1217-H1222.

4.   Toydemir RM, Chen H, Proud VK, et al. Trismus-pseudocamptodactyly syndrome is caused by recurrent mutation of MYH8. *Am J Med Genet*. 2006;140(22):2387-2393. doi:10.1002/ajmg.a.31495.

5.   Kühner S, Fischer S. Structural mechanism of the ATP-induced dissociation of rigor myosin from actin. *Proc Natl Acad Sci USA*. 2011;108(19):7793-7798. doi:10.1073/pnas.1018420108.

6.   Goodno CC. Inhibition of myosin ATPase by vanadate ion. *Proc Natl Acad Sci USA*. 1979;76(6):2620-2624.

7.   Goodno CC, Taylor EW. Inhibition of actomyosin ATPase by vanadate. *Proc Natl Acad Sci USA*. 1982;79(1):21-25.

8.   Phan B, Reisler E. Inhibition of myosin ATPase by beryllium fluoride. *Biochemistry - US*. 1992;31(20):4787-4793.

9.   Smith CA, Rayment I. X-ray structure of the magnesium(II)-pyrophosphate complex of the truncated head of Dictyostelium discoideum myosin to 2.7 A resolution. *Biochemistry - US*. 1995;34(28):8973-8981.

10.   Fisher AJ, Smith CA, Thoden JB, et al. X-ray structures of the myosin motor domain of Dictyostelium discoideum complexed with MgADP.BeFx and MgADP.AlF4-. *Biochemistry - US*. 1995;34(28):8960-8972.

11.   Gulick AM, Bauer CB, Thoden JB, Rayment I. X-ray structures of the MgADP, MgATPgammaS, and MgAMPPNP complexes of the Dictyostelium discoideum myosin motor domain. *Biochemistry - US*. 1997;36(39):11619-11628. doi:10.1021/bi9712596.

12.   Bauer CB, Holden HM, Thoden JB, Smith R, Rayment I. X-ray structures of the apo and MgATP-bound states of Dictyostelium discoideum myosin motor domain. *J Biol Chem*. 2000;275(49):38494-38499. doi:10.1074/jbc.M005585200.

13.   Warrick HM, De Lozanne A, Leinwand LA, Spudich JA. Conserved protein domains in a myosin heavy chain gene from Dictyostelium discoideum. *Proc Natl Acad Sci USA*. 1986;83(24):9433-9437.

14.   Toydemir RM, Rutherford A, Whitby FG, Jorde LB, Carey JC, Bamshad MJ. Mutations in embryonic myosin heavy chain (MYH3) cause Freeman-Sheldon syndrome and Sheldon-Hall syndrome. *Nat Genet*. 2006;38(5):561-565. doi:10.1038/ng1775.

15.   Toydemir RM, Rutherford A, Whitby FG, Jorde LB, Carey JC, Bamshad MJ. Mutations in embryonic myosin heavy chain (MYH3) cause Freeman-Sheldon syndrome and Sheldon-Hall syndrome. *Nature Genetics*. 2006;38(5):561-565. doi:10.1038/ng1775.

16.   Köhler J, Chen Y, Brenner B, et al. Familial hypertrophic cardiomyopathy mutations in troponin I (K183D, G203S, K206Q) enhance filament sliding. *Physiol Genomics*. 2003;14(2):117-128. doi:10.1152/physiolgenomics.00101.2002.

17.   Posch MG, Waldmuller S, Muller M, et al. Cardiac Alpha-Myosin (MYH6) Is the Predominant Sarcomeric Disease Gene for Familial Atrial Septal Defects. *PLoS ONE*. 2011;6(12). doi:10.1371/journal.pone.0028872.

18.   Bonne G, Carrier L, Richard P, Hainque B, Schwartz K. Familial Hypertrophic Cardiomyopathy From Mutations to Functional Defects. *Circ Res*. 1998;83(6):580-593. doi:10.1161/01.RES.83.6.580.

19.   Richard P, Charron P, Carrier L, et al. Hypertrophic cardiomyopathy: distribution of disease genes, spectrum of mutations, and implications for a molecular diagnosis strategy. *Circulation*. 2003;107(17):2227-2232. doi:10.1161/01.CIR.0000066323.15244.54.

20.   Tyska MJ, Hayes E, Giewat M, Seidman CE, Seidman JG, Warshaw DM. Single-molecule mechanics of R403Q cardiac myosin isolated from the mouse model of familial hypertrophic cardiomyopathy. *Circ Res*. 2000;86(7):737-744.

21.   Palmiter KA, Tyska MJ, Haeberle JR, Alpert NR, Fananapazir L, Warshaw DM. R403Q and L908V mutant beta-cardiac myosin from patients with familial hypertrophic cardiomyopathy exhibit enhanced mechanical performance at the single molecule level. *J Muscle Res Cell Motil*. 2000;21(7):609-620.

22.   Lowey S, Lesko LM, Rovner AS, et al. Functional effects of the hypertrophic cardiomyopathy R403Q mutation are different in an alpha- or beta-myosin heavy chain backbone. *J Biol Chem*. 2008;283(29):20579-20589. doi:10.1074/jbc.M800554200.

23.   Belus A, Piroddi N, Scellini B, et al. The familial hypertrophic cardiomyopathy-associated myosin mutation R403Q accelerates tension generation and relaxation of human

cardiac myofibrils. *J Physiol (Lond)*. 2008;586(Pt 15):3639-3644. doi:10.1113/jphysiol.2008.155952.

24.   Kraft T, Witjas-Paalberends ER, Boontje NM, et al. Familial hypertrophic cardiomyopathy: Functional effects of myosin mutation R723G in cardiomyocytes. *J Mol Cell Cardiol*. 2013;57:13-22. doi:10.1016/j.yjmcc.2013.01.001.

25.   Brenner B, Seebohm B, Tripathi S, Montag J, Kraft T. Familial hypertrophic cardiomyopathy: functional variance among individual cardiomyocytes as a trigger of FHC-phenotype development. *Front Physiol*. 2014;5:392. doi:10.3389/fphys.2014.00392.

26.   Lindqvist J, Iwamoto H, Blanco G, Ochala J. The formation of strongly bound cross-bridges is favored in mice carrying the myopathy-linked myosin heavy chain mutation, MYH4L342Q. *Dis Mode Mech*. 2013. doi:10.1242/dmm.011155.

27.   Lodish H, Berk A, Zipursky SL, Matsudaira P, Baltimore D, Darnell J. Muscle: A Specialized Contractile Machine. 2000. http://www.ncbi.nlm.nih.gov/books/NBK21670/. Accessed February 8, 2015.

28.   Gordon AM, Homsher E, Regnier M. Regulation of contraction in striated muscle. *Physiol Rev*. 2000;80(2):853-924.

29.   Katrukha IA. Human cardiac troponin complex. Structure and functions. *Biochemistry Mosc*. 2013;78(13):1447-1465. doi:10.1134/S0006297913130063.

30.   Murakami K, Yumoto F, Ohki S, Yasunaga T, Tanokura M, Wakabayashi T. Structural Basis for Ca2+-regulated Muscle Relaxation at Interaction Sites of Troponin with Actin and Tropomyosin. *J Mol Biol*. 2005;352(1):178-201. doi:10.1016/j.jmb.2005.06.067.

31.   Galińska-Rakoczy A, Engel P, Xu C, et al. Structural Basis for the Regulation of Muscle Contraction by Troponin and Tropomyosin. *J Mol Biol*. 2008;379(5):929-935. doi:10.1016/j.jmb.2008.04.062.

32.   Streng AS, de Boer D, van der Velden J, van Dieijen-Visser MP, Wodzig WKWH. Posttranslational modifications of cardiac troponin T: an overview. *J Mol Cell Cardiol*. 2013;63:47-56. doi:10.1016/j.yjmcc.2013.07.004.

33.   Regnier M, Rivera AJ, Wang C-K, Bates MA, Chase PB, Gordon AM. Thin filament near-neighbour regulatory unit interactions affect rabbit skeletal muscle steady-state force-Ca(2+) relations. *J Physiol (Lond)*. 2002;540(Pt 2):485-497.

34.   Fitzsimons DP, Moss RL. Cooperativity in the regulation of force and the kinetics of force development in heart and skeletal muscles: cross-bridge activation of force. *Adv Exp Med Biol*. 2007;592:177-189. doi:10.1007/978-4-431-38453-3_16.

35.   Regnier M, Rivera AJ, Chen Y, Chase PB. 2-deoxy-ATP enhances contractility of rat cardiac muscle. *Circulation Research*. 2000;86(12):1211-1217.

36. Regnier M, Martin H, Barsotti RJ, Rivera AJ, Martyn DA, Clemmens E. Cross-bridge versus thin filament contributions to the level and rate of force development in cardiac muscle. *Biophysical Journal*. 2004;87(3):1815-1824. doi:10.1529/biophysj.103.039123.

37. Hall JG, Reed SD, Greene G. The distal arthrogryposes: delineation of new entities--review and nosologic discussion. *Am J Med Genet*. 1982;11(2):185-239. doi:10.1002/ajmg.1320110208.

38. Bamshad M, Jorde LB, Carey JC. A revised and extended classification of the distal arthrogryposes. *Am J Med Genet*. 1996;65(4):277-281. doi:10.1002/(SICI)1096-8628(19961111)65:4<277::AID-AJMG6>3.0.CO;2-M.

39. Kee AJ, Hardeman EC. Tropomyosins in skeletal muscle diseases. *Adv Exp Med Biol*. 2008;644:143-157.

40. Clarke NF. Skeletal muscle disease due to mutations in tropomyosin, troponin and cofilin. *Adv Exp Med Biol*. 2008;642:40-54.

41. Ochala J. Thin filament proteins mutations associated with skeletal myopathies: defective regulation of muscle contraction. *J Mol Med*. 2008;86(11):1197-1204. doi:10.1007/s00109-008-0380-9.

42. Shyy W, Wang K, Sheffield VC, Morcuende JA. Evaluation of embryonic and perinatal myosin gene mutations and the etiology of congenital idiopathic clubfoot. *J Pediatr Orthop*. 2010;30(3):231-234. doi:10.1097/BPO.0b013e3181d35e3f.

43. Judith R. Bale, Barbara J. Stoll, Adetokunbo O. Lucas, Editors, Committee on Improving Birth Outcomes. *Reducing Birth Defects: Meeting the Challenge in the Developing World*. Washington, D.C.: The National Academies Press; 2003.

44. Lochmiller C, Johnston D, Scott A, Risman M, Hecht JT. Genetic epidemiology study of idiopathic talipes equinovarus. *Am J Med Genet*. 1998;79(2):90-96.

45. Chapman C, Stott NS, Port RV, Nicol RO. Genetics of club foot in Maori and Pacific people. *J Med Genet*. 2000;37(9):680-683.

46. De Andrade M, Barnholtz JS, Amos CI, et al. Segregation analysis of idiopathic talipes equinovarus in a Texan population. *Am J Med Genet*. 1998;79(2):97-102.

47. Rebbeck TR, Dietz FR, Murray JC, Buetow KH. A single-gene explanation for the probability of having idiopathic talipes equinovarus. *Am J Hum Genet*. 1993;53(5):1051-1063.

48. Wang JH, Palmer RM, Chung CS. The role of major gene in clubfoot. *Am J Hum Genet*. 1988;42(5):772-776.

49. Dietz F. The genetics of idiopathic clubfoot. *Clin Orthop Relat R*. 2002;(401):39-48.

50.   Yang HY, Chung CS, Nemechek RW. A genetic analysis of clubfoot in Hawaii. *Genet Epidemiol*. 1987;4(4):299-306. doi:10.1002/gepi.1370040408.

51.   Honein MA, Paulozzi LJ, Moore CA. Family history, maternal smoking, and clubfoot: an indication of a gene-environment interaction. *Am J Epidemiol*. 2000;152(7):658-665.

52.   Sung SS, Brassington A-ME, Grannatt K, et al. Mutations in genes encoding fast-twitch contractile proteins cause distal arthrogryposis syndromes. *Am J Hum Genet*. 2003;72(3):681-690. doi:10.1086/368294.

53.   Sung SS, Brassington A-ME, Krakowiak PA, Carey JC, Jorde LB, Bamshad M. Mutations in TNNT3 cause multiple congenital contractures: a second locus for distal arthrogryposis type 2B. *Am J Hum Genet*. 2003;73(1):212-214. doi:10.1086/376418.

54.   Shrimpton AE, Hoo JJ. A TNNI2 mutation in a family with distal arthrogryposis type 2B. *Eur J Med Genet*. 2006;49(2):201-206. doi:10.1016/j.ejmg.2005.06.003.

55.   Jiang M, Zhao X, Han W, et al. A novel deletion in TNNI2 causes distal arthrogryposis in a large Chinese family with marked variability of expression. *Hum Genet*. 2006;120(2):238-242. doi:10.1007/s00439-006-0183-4.

56.   Kimber E, Tajsharghi H, Kroksmark A-K, Oldfors A, Tulinius M. A mutation in the fast skeletal muscle troponin I gene causes myopathy and distal arthrogryposis. *Neurology*. 2006;67(4):597-601. doi:10.1212/01.wnl.0000230168.05328.f4.

57.   Tajsharghi H, Kimber E, Holmgren D, Tulinius M, Oldfors A. Distal arthrogryposis and muscle weakness associated with a beta-tropomyosin mutation. *Neurology*. 2007;68(10):772-775. doi:10.1212/01.wnl.0000256339.40667.fb.

58.   Tajsharghi H, Kimber E, Kroksmark A-K, Jerre R, Tulinius M, Oldfors A. Embryonic myosin heavy-chain mutations cause distal arthrogryposis and developmental myosin myopathy that persists postnatally. *Arch Neurol - Chicago*. 2008;65(8):1083-1090. doi:10.1001/archneur.65.8.1083.

59.   Veugelers M, Bressan M, McDermott DA, et al. Mutation of perinatal myosin heavy chain associated with a Carney complex variant. *N Engl J Med*. 2004;351(5):460-469. doi:10.1056/NEJMoa040584.

60.   Gurnett CA, Desruisseau DM, McCall K, et al. Myosin binding protein C1: a novel gene for autosomal dominant distal arthrogryposis type 1. *Hum Mol Genet*. 2010;19(7):1165-1173. doi:10.1093/hmg/ddp587.

61.   Bamshad M, Watkins WS, Zenger RK, et al. A gene for distal arthrogryposis type I maps to the pericentromeric region of chromosome 9. *Am J Hum Genet*. 1994;55(6):1153-1158.

62.   Beck AE, McMillin MJ, Gildersleeve HIS, et al. Spectrum of mutations that cause distal arthrogryposis types 1 and 2B. *Am J Med Genet A*. 2013;161A(3):550-555. doi:10.1002/ajmg.a.35809.

63.   Robinson P, Lipscomb S, Preston LC, et al. Mutations in fast skeletal troponin I, troponin T, and beta-tropomyosin that cause distal arthrogryposis all increase contractile function. *FASEB J*. 2007;21(3):896-905. doi:10.1096/fj.06-6899com.

64.   Ochala J, Li M, Tajsharghi H, et al. Effects of a R133W beta-tropomyosin mutation on regulation of muscle contraction in single human muscle fibres. *J Physiol (Lond)*. 2007;581(Pt 3):1283-1292. doi:10.1113/jphysiol.2007.129759.

65.   Ochala J, Li M, Ohlsson M, Oldfors A, Larsson L. Defective regulation of contractile function in muscle fibres carrying an E41K beta-tropomyosin mutation. *J Physiol (Lond)*. 2008;586(Pt 12):2993-3004. doi:10.1113/jphysiol.2008.153650.

66.   Ochala J, Iwamoto H, Larsson L, Yagi N. A myopathy-linked tropomyosin mutation severely alters thin filament conformational changes during activation. *Proc Natl Acad Sci USA*. 2010;107(21):9807-9812. doi:10.1073/pnas.1001733107.

67.   Racca AW, Beck AE, McMillin MJ, Korte FS, Bamshad MJ, Regnier M. The embryonic myosin R672C mutation that underlies Freeman-Sheldon syndrome impairs crossbridge detachment and cycling in adult muscle. *Hum Mol Genet*. 2015. doi:10.1093/hmg/ddv084.

68.   Blumenschein TMA, Stone DB, Fletterick RJ, Mendelson RA, Sykes BD. Dynamics of the C-terminal region of TnI in the troponin complex in solution. *Biophys J*. 2006;90(7):2436-2444. doi:10.1529/biophysj.105.076216.

69.   Zhang Z, Akhter S, Mottl S, Jin J-P. Calcium-regulated conformational change in the C-terminal end segment of troponin I and its binding to tropomyosin. *FEBS J*. 2011;278(18):3348-3359. doi:10.1111/j.1742-4658.2011.08250.x.

70.   Watkins H, McKenna WJ, Thierfelder L, et al. Mutations in the genes for cardiac troponin T and alpha-tropomyosin in hypertrophic cardiomyopathy. *N Engl J Med*. 1995;332(16):1058-1064. doi:10.1056/NEJM199504203321603.

71.   Murphy AM. Another new kinase targets troponin I. *Circ Res*. 2004;95(11):1043-1045. doi:10.1161/01.RES.0000150051.81155.88.

72.   Deng Y, Schmidtmann A, Kruse S, et al. Phosphorylation of human cardiac troponin I G203S and K206Q linked to familial hypertrophic cardiomyopathy affects actomyosin interaction in different ways. *J Mol Cell Cardiol*. 2003;35(11):1365-1374.

73.   Jin J-P, Chong SM. Localization of the two tropomyosin-binding sites of troponin T. *Arch Biochem Biophys*. 2010;500(2):144-150. doi:10.1016/j.abb.2010.06.001.

74.   Stefancsik R, Randall JD, Mao C, Sarkar S. Structure and sequence of the human fast skeletal troponin T (TNNT3) gene: insight into the evolution of the gene and the origin of the developmentally regulated isoforms. *Comp Funct Genom*. 2003;4(6):609-625. doi:10.1002/cfg.343.

75.   Li D, Czernuszewicz GZ, Gonzalez O, et al. Novel Cardiac Troponin T Mutation as a Cause of Familial Dilated Cardiomyopathy. *Circulation*. 2001;104(18):2188-2193. doi:10.1161/hc4301.098285.

76.   Montgomery DE, Tardiff JC, Chandra M. Cardiac troponin T mutations: correlation between the type of mutation and the nature of myofilament dysfunction in transgenic mice. *J Physiol (Lond)*. 2001;536(Pt 2):583-592.

77.   Buller AJ, Eccles JC, Eccles RM. Differentiation of fast and slow muscles in the cat hind limb. *The Journal of Physiology*. 1960;150(2):399-416.

78.   Close R. Dynamic properties of fast and slow skeletal muscles of the rat during development. *The Journal of Physiology*. 1964;173(1):74-95.

79.   Buller AJ, Lewis DM. Further observations on the differentiation of skeletal muscles in the kitten hind limb. *The Journal of Physiology*. 1965;176(3):355-370.

80.   West JM, Barclay CJ, Luff AR, Walker DW. Developmental changes in the activation properties and ultrastructure of fast- and slow-twitch muscles from fetal sheep. *Journal of Muscle Research and Cell Motility*. 1999;20(3):249-264.

81.   Mozaffarian D, Benjamin EJ, Go AS, et al. Heart disease and stroke statistics-2015 update: a report from the american heart association. *Circulation*. 2015;131(4):e29-e322. doi:10.1161/CIR.0000000000000152.

82.   Negishi J, Ohuchi H, Yasuda K, Miyazaki A, Norifumi N, Yamada O. Unscheduled hospitalization in adults with congenital heart disease. *Korean Circ J*. 2015;45(1):59-66. doi:10.4070/kcj.2015.45.1.59.

83.   Angelini C. Prevention of cardiomyopathy in Duchenne muscular dystrophy. *The Lancet Neurology*. 2015;14(2):127-128. doi:10.1016/S1474-4422(14)70326-6.

84.   James S, Barton D, O'Connell E, et al. Life expectancy for community-based patients with heart failure from time of diagnosis. *Int J Cardiol*. 2015;178:268-274. doi:10.1016/j.ijcard.2014.09.131.

85.   O'Meara E, Thibodeau-Jarry N, Ducharme A, Rouleau JL. The epidemic of heart failure: a lucid approach to stemming the rising tide. *Can J Cardiol*. 2014;30(12 Suppl):S442-S454. doi:10.1016/j.cjca.2014.09.032.

86.   Regnier M, Homsher E. The effect of ATP analogs on posthydrolytic and force development steps in skinned skeletal muscle fibers. *Biophys J*. 1998;74(6):3059-3071. doi:10.1016/S0006-3495(98)78013-0.

87.   Regnier M, Lee DM, Homsher E. ATP analogs and muscle contraction: mechanics and kinetics of nucleoside triphosphate binding and hydrolysis. *Biophys J*. 1998;74(6):3044-3058. doi:10.1016/S0006-3495(98)78012-9.

88.   Regnier M, Martyn DA, Chase PB. Calcium regulation of tension redevelopment kinetics with 2-deoxy-ATP or low [ATP] in rabbit skeletal muscle. *Biophys J*. 1998;74(4):2005-2015. doi:10.1016/S0006-3495(98)77907-X.

89.   Korte FS, Dai J, Buckley K, et al. Upregulation of cardiomyocyte ribonucleotide reductase increases intracellular 2 deoxy-ATP, contractility, and relaxation. *Journal of Molecular and Cellular Cardiology*. 2011;51(6):894-901. doi:10.1016/j.yjmcc.2011.08.026.

90.   Adhikari BB, Regnier M, Rivera AJ, Kreutziger KL, Martyn DA. Cardiac length dependence of force and force redevelopment kinetics with altered cross-bridge cycling. *Biophys J*. 2004;87(3):1784-1794. doi:10.1529/biophysj.103.039131.

91.   Moreno-Gonzalez A, Gillis TE, Rivera AJ, Chase PB, Martyn DA, Regnier M. Thin-filament regulation of force redevelopment kinetics in rabbit skeletal muscle fibres. *J Physiol (Lond)*. 2007;579(Pt 2):313-326. doi:10.1113/jphysiol.2006.124164.

92.   Ottenheijm CAC, Hooijman P, DeChene ET, Stienen GJ, Beggs AH, Granzier H. Altered myofilament function depresses force generation in patients with nebulin-based nemaline myopathy (NEM2). *J Struct Biol*. 2010;170(2):334-343. doi:10.1016/j.jsb.2009.11.013.

93.   Ottenheijm CAC, Lawlor MW, Stienen GJM, Granzier H, Beggs AH. Changes in cross-bridge cycling underlie muscle weakness in patients with tropomyosin 3-based myopathy. *Hum Mol Genet*. 2011;20(10):2015-2025. doi:10.1093/hmg/ddr084.

94.   Laflamme MA, Chen KY, Naumova AV, et al. Cardiomyocytes derived from human embryonic stem cells in pro-survival factors enhance function of infarcted rat hearts. *Nat Biotechnol*. 2007;25(9):1015-1024. doi:10.1038/nbt1327.

95.   Brandt PW, Colomo F, Piroddi N, Poggesi C, Tesi C. Force regulation by Ca2+ in skinned single cardiac myocytes of frog. *Biophysical journal*. 1998;74(4):1994-2004. doi:10.1016/S0006-3495(98)77906-8.

96.   Regnier M, Morris C, Homsher E. Regulation of the cross-bridge transition from a weakly to strongly bound state in skinned rabbit muscle fibers. *Am J Physiol*. 1995;269(6 Pt 1):C1532-C1539.

97.   Ostap EM. 2,3-Butanedione monoxime (BDM) as a myosin inhibitor. *J Muscle Res Cell Motil*. 2002;23(4):305-308.

98.   Regnier M, Martyn DA, Chase PB. Calmidazolium alters Ca2+ regulation of tension redevelopment rate in skinned skeletal muscle. *Biophys J*. 1996;71(5):2786-2794. doi:10.1016/S0006-3495(96)79471-7.

99.   Ottenheijm CAC, Witt CC, Stienen GJ, Labeit S, Beggs AH, Granzier H. Thin filament length dysregulation contributes to muscle weakness in nemaline myopathy patients with nebulin deficiency. *Hum Mol Genet*. 2009;18(13):2359-2369. doi:10.1093/hmg/ddp168.

100.   Matsubara I, Umazume Y, Yagi N. Lateral filamentary spacing in chemically skinned murine muscles during contraction. *J Physiol (Lond)*. 1985;360:135-148.

101.   Martyn DA, Gordon AM. Length and myofilament spacing-dependent changes in calcium sensitivity of skeletal fibres: effects of pH and ionic strength. *J Muscle Res Cell Motil*. 1988;9(5):428-445.

102.   Brenner B. Technique for stabilizing the striation pattern in maximally calcium-activated skinned rabbit psoas fibers. *Biophys J*. 1983;41(1):99-102. doi:10.1016/S0006-3495(83)84411-7.

103.   Ward AW, Beck AE, Bamshad MJ, Regnier M. Congenital contracture syndrome caused by mutation in embryonic myosin heavy chain characterized by significant changes in adult muscle contractility. 2010.

104.   Beck AE, Ward AW, McMillin MJ, Korte FS, Regnier M, Bamshad MJ. Defects of embryonic myosin in Freeman-Sheldon syndrome reduce force and prolong relaxation of skeletal myofibers. 2010.

105.   Beck AE, McMillin MJ, Korte FS, Ward AW, Regnier M, Bamshad MJ. Contractility of individual myofibers is altered in individuals with myosin mutations that cause Freeman-Sheldon syndrome. 2008.

106.   Racca AW, Beck AE, McMillin MJ, Korte FS, Regnier M, Bamshad M. Defects of embryonic myosin in Freeman-Sheldon syndrome cause reduced force and prolonged relaxation of skeletal myofibers. *In Revision*. 2012.

107.   Brenner B, Eisenberg E. Rate of force generation in muscle: correlation with actomyosin ATPase activity in solution. *Proceedings of the National Academy of Sciences of the United States of America*. 1986;83(10):3542-3546.

108.   Colomo F, Piroddi N, Poggesi C, te Kronnie G, Tesi C. Active and passive forces of isolated myofibrils from cardiac and fast skeletal muscle of the frog. *The Journal of physiology*. 1997;500 (Pt 2:535-548.

109.   Colomo F, Nencini S, Piroddi N, Poggesi C, Tesi C. Calcium dependence of the apparent rate of force generation in single striated muscle myofibrils activated by rapid solution changes. *Advances in Experimental Medicine and Biology*. 1998;453:373-382.

110. Tesi C, Colomo F, Nencini S, Piroddi N, Poggesi C. The effect of inorganic phosphate on force generation in single myofibrils from rabbit skeletal muscle. *Biophysical Journal*. 2000;78(6).

111. Kreutziger KL, Piroddi N, Scellini B, Tesi C, Poggesi C, Regnier M. Thin filament Ca2+ binding properties and regulatory unit interactions alter kinetics of tension development and relaxation in rabbit skeletal muscle. *The Journal of Physiology*. 2008;586(Pt 15):3683-3700. doi:10.1113/jphysiol.2008.152181.

112. Kreutziger KL, Piroddi N, Scellini B, Tesi C, Poggesi C, Regnier M. Thin filament Ca2+ binding properties and regulatory unit interactions alter kinetics of tension development and relaxation in rabbit skeletal muscle. *J Physiol (Lond)*. 2008;586(Pt 15):3683-3700. doi:10.1113/jphysiol.2008.152181.

113. Tesi C, Piroddi N, Colomo F, Poggesi C. Relaxation kinetics following sudden Ca(2+) reduction in single myofibrils from skeletal muscle. *Biophys J*. 2002;83(4):2142-2151. doi:10.1016/S0006-3495(02)73974-X.

114. Poggesi C, Tesi C, Stehle R. Sarcomeric determinants of striated muscle relaxation kinetics. *Pflugers Arch*. 2005;449(6):505-517. doi:10.1007/s00424-004-1363-5.

115. Margossian SS, Lowey S. Preparation of myosin and its subfragments from rabbit skeletal muscle. *Methods in Enzymology*. 1982;85 Pt B:55-71.

116. Kron SJ, Toyoshima YY, Uyeda TQ, Spudich JA. Assays for actin sliding movement over myosin-coated surfaces. *Methods in Enzymology*. 1991;196:399-416.

117. Kron SJ, Uyeda TQ, Warrick HM, Spudich JA. An approach to reconstituting motility of single myosin molecules. *Journal of Cell Science Supplement*. 1991;14:129-133.

118. Clemmens EW, Entezari M, Martyn DA, Regnier M. Different effects of cardiac versus skeletal muscle regulatory proteins on in vitro measures of actin filament speed and force. *The Journal of Physiology*. 2005;566(Pt 3):737-746. doi:10.1113/jphysiol.2005.084194.

119. Clemmens EW, Regnier M. Skeletal regulatory proteins enhance thin filament sliding speed and force by skeletal HMM. *Journal of Muscle Research and Cell Motility*. 2004;25(7):515-525. doi:10.1007/s10974-004-3787-0.

120. Pardee JD, Spudich JA. Purification of muscle actin. *Methods in Enzymology*. 1982;85 Pt B:164-181.

121. Spudich JA, Pardee JD, Simpson PA, Yamamoto K, Kuczmarski ER, Stryer L. Actin and myosin: control of filament assembly. *Philosophical Transactions of the Royal Society of London Series B, Biological Sciences*. 1982;299(1095):247-261.

122. Gordon AM, LaMadrid MA, Chen Y, Luo Z, Chase PB. Calcium regulation of skeletal muscle thin filament motility in vitro. *Biophysical Journal*. 1997;72(3):1295-1307.

123. Razumova M V, Shaffer JF, Tu A-Y, Flint G V, Regnier M, Harris SP. Effects of the N-terminal domains of myosin binding protein-C in an in vitro motility assay: Evidence for long-lived cross-bridges. *The Journal of Biological Chemistry*. 2006;281(47):35846-35854. doi:10.1074/jbc.M606949200.

124. Yamashita H, Sata M, Sugiura S, Momomura S, Serizawa T, Iizuka M. ADP inhibits the sliding velocity of fluorescent actin filaments on cardiac and skeletal myosins. *Circulation Research*. 1994;74(6):1027-1033.

125. Homsher E, Wang F, Sellers JR. Factors affecting movement of F-actin filaments propelled by skeletal muscle heavy meromyosin. *The American Journal of Physiology*. 1992;262(3 Pt 1):C714-C723.

126. Dubowitz V, Sewry CA. *Muscle Biopsy: A Practical Approach*. 3rd ed. Elsevier Health Sciences; 2007.

127. Webster C, Silberstein L, Hays A, Blau H. Fast Muscle Fibers Are Preferentially Affected in Duchenne Muscular Dystrophy. 1988;52:503-513.

128. Butler-Browne GS, Whalen RG. Myosin isozyme transitions occurring during the postnatal development of the rat soleus muscle. *Dev Biol*. 1984;102(2):324-334.

129. Clemmens EW, Regnier M. Skeletal regulatory proteins enhance thin filament sliding speed and force by skeletal HMM. *J Muscle Res Cell Motil*. 2004;25(7):515-525. doi:10.1007/s10974-004-3787-0.

130. Clemmens EW, Entezari M, Martyn DA, Regnier M. Different effects of cardiac versus skeletal muscle regulatory proteins on in vitro measures of actin filament speed and force. *J Physiol (Lond)*. 2005;566(Pt 3):737-746. doi:10.1113/jphysiol.2005.084194.

131. Razumova MV, Shaffer JF, Tu A-Y, Flint GV, Regnier M, Harris SP. Effects of the N-terminal domains of myosin binding protein-C in an in vitro motility assay: Evidence for long-lived cross-bridges. *J Biol Chem*. 2006;281(47):35846-35854. doi:10.1074/jbc.M606949200.

132. Kreutziger KL, Piroddi N, McMichael JT, Tesi C, Poggesi C, Regnier M. Calcium binding kinetics of troponin C strongly modulate cooperative activation and tension kinetics in cardiac muscle. *J Mol Cell Cardiol*. 2011;50(1):165-174. doi:10.1016/j.yjmcc.2010.10.025.

133. Kreutziger KL, Gillis TE, Davis JP, Tikunova SB, Regnier M. Influence of enhanced troponin C Ca2+-binding affinity on cooperative thin filament activation in rabbit skeletal muscle. *J Physiol (Lond)*. 2007;583(Pt 1):337-350. doi:10.1113/jphysiol.2007.135426.

134. Tesi C, Colomo F, Nencini S, Piroddi N, Poggesi C. The effect of inorganic phosphate on force generation in single myofibrils from rabbit skeletal muscle. *Biophys J*. 2000;78(6):3081-3092. doi:10.1016/S0006-3495(00)76845-7.

135.   Racca AW, Beck AE, Rao VS, et al. Contractility and kinetics of human fetal and human adult skeletal muscle. *J Physiol (Lond)*. 2013;591(Pt 12):3049-3061. doi:10.1113/jphysiol.2013.252650.

136.   Hall J. Arthrogryposis. In: *Principles and Practice of Medical Genetics*. 2nd ed. Edinburgh: Churchill Livingstone; 1992:989-1035.

137.   Ackermann MA, Patel PD, Valenti J, et al. Loss of actomyosin regulation in distal arthrogryposis myopathy due to mutant myosin binding protein-C slow. *FASEB J*. 2013;27(8):3217-3228. doi:10.1096/fj.13-228882.

138.   Silberstein L, Webster SG, Travis M, Blau HM. Developmental progression of myosin gene expression in cultured muscle cells. *Cell*. 1986;46(7):1075-1081.

139.   Webster C, Silberstein L, Hays AP, Blau HM. Fast muscle fibers are preferentially affected in Duchenne muscular dystrophy. *Cell*. 1988;52(4):503-513.

140.   Gambke B, Rubinstein NA. A monoclonal antibody to the embryonic myosin heavy chain of rat skeletal muscle. *J Biol Chem*. 1984;259(19):12092-12100.

141.   Resnicow DI, Deacon JC, Warrick HM, Spudich JA, Leinwand LA. Functional diversity among a family of human skeletal muscle myosin motors. *Proc Natl Acad Sci USA*. 2010;107(3):1053-1058. doi:10.1073/pnas.0913527107.

142.   Brenner B, Yu LC. Characterization of radial force and radial stiffness in Ca(2+)-activated skinned fibres of the rabbit psoas muscle. *J Physiol (Lond)*. 1991;441:703-718.

143.   Williams CD, Regnier M, Daniel TL. Axial and Radial Forces of Cross-Bridges Depend on Lattice Spacing. *PLoS Comput Biol*. 2010;6(12):e1001018. doi:10.1371/journal.pcbi.1001018.

144.   Tesi C, Piroddi N, Colomo F, Poggesi C. Relaxation kinetics following sudden Ca(2+) reduction in single myofibrils from skeletal muscle. *Biophysical Journal*. 2002;83(4):2142-2151. doi:10.1016/S0006-3495(02)73974-X.

145.   Stehle R, Krüger M, Pfitzer G. Force kinetics and individual sarcomere dynamics in cardiac myofibrils after rapid ca(2+) changes. *Biophys J*. 2002;83(4):2152-2161.

146.   Morgan DL, Proske U. Sarcomere popping requires stretch over a range where total tension decreases with length. *J Physiol (Lond)*. 2006;574(Pt 2):627-628. doi:10.1113/jphysiol.2006.574201.

147.   Brenner B. Effect of Ca2+ on cross-bridge turnover kinetics in skinned single rabbit psoas fibers: implications for regulation of muscle contraction. *Proc Natl Acad Sci USA*. 1988;85(9):3265-3269.

148.   Williams CD, Salcedo MK, Irving TC, Regnier M, Daniel TL. The length–tension curve in muscle depends on lattice spacing. *Proc R Soc Lond, B, Biol Sci*. 2013;280(1766):20130697. doi:10.1098/rspb.2013.0697.

149.   Cuda G, Pate E, Cooke R, Sellers JR. In vitro actin filament sliding velocities produced by mixtures of different types of myosin. *Biophys J*. 1997;72(4):1767-1779. doi:10.1016/S0006-3495(97)78823-4.

150.   Kreutziger KL, Piroddi N, McMichael JT, Tesi C, Poggesi C, Regnier M. Calcium binding kinetics of troponin C strongly modulate cooperative activation and tension kinetics in cardiac muscle. *Journal of Molecular and Cellular Cardiology*. 2011;50(1):165-174. doi:10.1016/j.yjmcc.2010.10.025.

151.   Fyrberg E, Fyrberg CC, Beall C, Saville DL. Drosophila melanogaster troponin-T mutations engender three distinct syndromes of myofibrillar abnormalities. *J Mol Biol*. 1990;216(3):657-675. doi:10.1016/0022-2836(90)90390-8.

152.   Moreno-Gonzalez A, Korte FS, Dai J, et al. Cell therapy enhances function of remote non-infarcted myocardium. *J Mol Cell Cardiol*. 2009;47(5):603-613. doi:10.1016/j.yjmcc.2009.07.030.

153.   Regnier M, Rivera AJ, Chase PB, Smillie LB, Sorenson MM. Regulation of skeletal muscle tension redevelopment by troponin C constructs with different Ca2+ affinities. *Biophys J*. 1999;76(5):2664-2672. doi:10.1016/S0006-3495(99)77418-7.

154.   Feest ER, Steven Korte F, Tu A-Y, et al. Thin filament incorporation of an engineered cardiac troponin C variant (L48Q) enhances contractility in intact cardiomyocytes from healthy and infarcted hearts. *J Mol Cell Cardiol*. 2014;72:219-227. doi:10.1016/j.yjmcc.2014.03.015.

155.   Korte FS, Dai J, Buckley K, et al. Upregulation of cardiomyocyte ribonucleotide reductase increases intracellular 2 deoxy-ATP, contractility, and relaxation. *J Mol Cell Cardiol*. 2011;51(6):894-901. doi:10.1016/j.yjmcc.2011.08.026.

156.   Nowakowski SG, Kolwicz SC, Korte FS, et al. Transgenic overexpression of ribonucleotide reductase improves cardiac performance. *Proc Natl Acad Sci USA*. 2013;110(15):6187-6192. doi:10.1073/pnas.1220693110.

157.   Beck AE, Ward AW, McMillin MJ, Korte FS, Regnier M, Bamshad MJ, eds. Defects of embryonic myosin in Freeman-Sheldon syndrome reduce force and prolong relaxation of skeletal myofibers. *60th Annual Meeting of the American Society of Human Genetics*. 2010.

158.   Tesi C, Colomo F, Nencini S, Piroddi N, Poggesi C. Modulation by substrate concentration of maximal shortening velocity and isometric force in single myofibrils from frog and rabbit fast skeletal muscle. *The Journal of Physiology*. 1999;516 (Pt 3:847-853.

159.   Regnier M, Homsher E. The effect of ATP analogs on posthydrolytic and force development steps in skinned skeletal muscle fibers. *Biophysical Journal*. 1998;74(6):3059-3071. doi:10.1016/S0006-3495(98)78013-0.

160.   Regnier M, Lee DM, Homsher E. ATP analogs and muscle contraction: mechanics and kinetics of nucleoside triphosphate binding and hydrolysis. *Biophysical Journal*. 1998;74(6):3044-3058. doi:10.1016/S0006-3495(98)78012-9.

161.   Szentesi P, Bekedam MA, van Beek-Harmsen BJ, et al. Depression of force production and ATPase activity in different types of human skeletal muscle fibers from patients with chronic heart failure. *Journal of Applied Physiology (Bethesda, Md: 1985)*. 2005;99(6):2189-2195. doi:10.1152/japplphysiol.00542.2005.

162.   Ottenheijm CAC, Lawlor MW, Stienen GJM, Granzier H, Beggs AH. Changes in cross-bridge cycling underlie muscle weakness in patients with tropomyosin 3-based myopathy. *Human Molecular Genetics*. 2011;20(10):2015-2025. doi:10.1093/hmg/ddr084.

163.   Kreutziger KL, Gillis TE, Davis JP, Tikunova SB, Regnier M. Influence of enhanced troponin C Ca2+-binding affinity on cooperative thin filament activation in rabbit skeletal muscle. *The Journal of Physiology*. 2007;583(Pt 1):337-350. doi:10.1113/jphysiol.2007.135426.

164.   Resnicow DI, Deacon JC, Warrick HM, Spudich JA, Leinwand LA. Functional diversity among a family of human skeletal muscle myosin motors. *Proceedings of the National Academy of Sciences of the United States of America*. 2010;107(3):1053-1058. doi:10.1073/pnas.0913527107.

165.   Siedner S, Krüger M, Schroeter M, et al. Developmental changes in contractility and sarcomeric proteins from the early embryonic to the adult stage in the mouse heart. *The Journal of Physiology*. 2003;548(Pt 2):493-505. doi:10.1113/jphysiol.2002.036509.

166.   Pate E, Cooke R. A model of crossbridge action: the effects of ATP, ADP and Pi. *Journal of Muscle Research and Cell Motility*. 1989;10(3):181-196.

167.   Wang Y, Tanner BCW, Lombardo AT, et al. Cardiac myosin isoforms exhibit differential rates of MgADP release and MgATP binding detected by myocardial viscoelasticity. *Journal of molecular and cellular cardiology*. 2012. doi:10.1016/j.yjmcc.2012.10.010.

168.   Regnier M, Chase PB, Martyn DA. Contractile properties of rabbit psoas muscle fibres inhibited by beryllium fluoride. *Journal of Muscle Research and Cell Motility*. 1999;20(4):425-432.

169.   Morris CA, Tobacman LS, Homsher E. Thin filament activation and unloaded shortening velocity of rabbit skinned muscle fibres. *The Journal of physiology*. 2003;550(Pt 1):205-215. doi:10.1113/jphysiol.2003.040899.

170.   Lu Z, Moss RL, Walker JW. Tension transients initiated by photogeneration of MgADP in skinned skeletal muscle fibers. *The Journal of General Physiology*. 1993;101(6):867-888.

171.   Stehle R, Solzin J, Iorga B, Poggesi C. Insights into the kinetics of Ca2+-regulated contraction and relaxation from myofibril studies. *Pflügers Archiv: European Journal of Physiology*. 2009;458(2):337-357. doi:10.1007/s00424-008-0630-2.

172.   Hall JG, Reed SD, Greene G. The distal arthrogryposes: delineation of new entities--review and nosologic discussion. *American Journal of Medical Genetics*. 1982;11(2):185-239. doi:10.1002/ajmg.1320110208.

173.   McAuliffe JJ, Robbins J. Troponin T expression in normal and pressure-loaded fetal sheep heart. *Pediatr Res*. 1991;29(6):580-585. doi:10.1203/00006450-199106010-00012.

174.   Posterino GS, Dunn SL, Botting KJ, Wang W, Gentili S, Morrison JL. Changes in cardiac troponins with gestational age explain changes in cardiac muscle contractility in the sheep fetus. *J Appl Physiol*. 2011;111(1):236-243. doi:10.1152/japplphysiol.00067.2011.

175.   Anderson PA, Malouf NN, Oakeley AE, Pagani ED, Allen PD. Troponin T isoform expression in humans. A comparison among normal and failing adult heart, fetal heart, and adult and fetal skeletal muscle. *Circ Res*. 1991;69(5):1226-1233.

176.   Krüger M, Kohl T, Linke WA. Developmental changes in passive stiffness and myofilament Ca2+ sensitivity due to titin and troponin-I isoform switching are not critically triggered by birth. *Am J Physiol Heart Circ Physiol*. 2006;291(2):H496-H506. doi:10.1152/ajpheart.00114.2006.

177.   Elmstedt N, Ferm-Widlund K, Lind B, Brodin L-Å, Westgren M. Fetal cardiac muscle contractility decreases with gestational age: a color-coded tissue velocity imaging study. *Cardiovasc Ultrasound*. 2012;10:19. doi:10.1186/1476-7120-10-19.

178.   Luewan S, Tongprasert F, Srisupundit K, Traisrisilp K, Tongsong T. Reference ranges of myocardial performance index from 12 to 40 weeks of gestation. *Arch Gynecol Obstet*. 2014. doi:10.1007/s00404-014-3288-3.

179.   Brooks PA, Khoo NS, Hornberger LK. Systolic and diastolic function of the fetal single left ventricle. *J Am Soc Echocardiogr*. 2014;27(9):972-977. doi:10.1016/j.echo.2014.06.012.

180.   Elmstedt NN, Johnson JJ, Lind BB, et al. Reference values for fetal tissue velocity imaging and a new approach to evaluate fetal myocardial function. *Cardiovasc Ultrasound*. 2013;11:29. doi:10.1186/1476-7120-11-29.

181.   Lamers WH, Virágh S, Wessels A, Moorman AF, Anderson RH. Formation of the tricuspid valve in the human heart. *Circulation*. 1995;91(1):111-121.

182.   Kim HD, Kim DJ, Lee IJ, Rah BJ, Sawa Y, Schaper J. Human fetal heart development after mid-term: morphometry and ultrastructural study. *J Mol Cell Cardiol*. 1992;24(9):949-965.

183.   Reiser PJ, Portman MA, Ning XH, Schomisch Moravec C. Human cardiac myosin heavy chain isoforms in fetal and failing adult atria and ventricles. *Am J Physiol - Heart Circ Ph*. 2001;280(4):H1814-H1820.

184.   Sasse S, Brand NJ, Kyprianou P, et al. Troponin I gene expression during human cardiac development and in end-stage heart failure. *Circ Res*. 1993;72(5):932-938.

185.   Purcell IF, Bing W, Marston SB. Functional analysis of human cardiac troponin by the in vitro motility assay: comparison of adult, foetal and failing hearts. *Cardiovasc Res*. 1999;43(4):884-891.

186.   Moussavi-Harami F, Razumova MV, Racca AW, Cheng Y, Stempien-Otero A, Regnier M. 2-Deoxy adenosine triphosphate improves contraction in human end-stage heart failure. *J Mol Cell Cardiol*. 2015;79:256-263. doi:10.1016/j.yjmcc.2014.12.002.

187.   Racca AW, Beck AE, Bamshad MJ, Regnier M. Differences in Activation and Relaxation Kinetics of Human Fetal Skeletal and Cardiac Myofibrils. *Biophysical Journal*. 2014;106(2):562a. doi:10.1016/j.bpj.2013.11.3121.

188.   Piroddi N, Belus A, Scellini B, et al. Tension generation and relaxation in single myofibrils from human atrial and ventricular myocardium. *Pflugers Arch*. 2007;454(1):63-73. doi:10.1007/s00424-006-0181-3.

189.   De Tombe PP, Belus A, Piroddi N, et al. Myofilament calcium sensitivity does not affect cross-bridge activation-relaxation kinetics. *Am J Physiol Regul Integr Comp Physiol*. 2007;292(3):R1129-R1136. doi:10.1152/ajpregu.00630.2006.

190.   Van der Velden J, de Jong JW, Owen VJ, Burton PB, Stienen GJ. Effect of protein kinase A on calcium sensitivity of force and its sarcomere length dependence in human cardiomyocytes. *Cardiovasc Res*. 2000;46(3):487-495.

191.   Dvornikov AV, Dewan S, Alekhina OV, Pickett FB, de Tombe PP. Novel approaches to determine contractile function of the isolated adult zebrafish ventricular cardiac myocyte. *J Physiol (Lond)*. 2014;592(Pt 9):1949-1956. doi:10.1113/jphysiol.2014.270678.

192.   Sheldon CA, Friedman WF, Sybers HD. Scanning electron microscopy of fetal and neonatal lamb cardiac cells. *J Mol Cell Cardiol*. 1976;8(11):853-862.

193.   Rolph TP, Jones CT, Parry D. Ultrastructural and enzymatic development of fetal guinea pig heart. *Am J Physiol*. 1982;243(1):H87-H93.

194.   Herron TJ, McDonald KS. Small amounts of alpha-myosin heavy chain isoform expression significantly increase power output of rat cardiac myocyte fragments. *Circ Res*. 2002;90(11):1150-1152.

195.   Roger VL, Weston SA, Redfield MM, et al. Trends in heart failure incidence and survival in a community-based population. *JAMA*. 2004;292(3):344-350. doi:10.1001/jama.292.3.344.

196. McMurray JJV. Clinical practice. Systolic heart failure. *N Engl J Med*. 2010;362(3):228-238. doi:10.1056/NEJMcp0909392.

197. Abraham WT, Adams KF, Fonarow GC, et al. In-hospital mortality in patients with acute decompensated heart failure requiring intravenous vasoactive medications: an analysis from the Acute Decompensated Heart Failure National Registry (ADHERE). *J Am Coll Cardiol*. 2005;46(1):57-64. doi:10.1016/j.jacc.2005.03.051.

198. Teerlink JR, Metra M, Zacà V, et al. Agents with inotropic properties for the management of acute heart failure syndromes. Traditional agents and beyond. *Heart Fail Rev*. 2009;14(4):243-253. doi:10.1007/s10741-009-9153-y.

199. Van der Velden J, Boontje NM, Papp Z, et al. Calcium sensitivity of force in human ventricular cardiomyocytes from donor and failing hearts. *Basic Res Cardiol*. 2002;97 Suppl 1:I118-I126.

200. Ambardekar AV, Walker JS, Walker LA, Cleveland JC, Lowes BD, Buttrick PM. Incomplete recovery of myocyte contractile function despite improvement of myocardial architecture with left ventricular assist device support. *Circ Heart Fail*. 2011;4(4):425-432. doi:10.1161/CIRCHEARTFAILURE.111.961326.

201. Malmqvist UP, Aronshtam A, Lowey S. Cardiac myosin isoforms from different species have unique enzymatic and mechanical properties. *Biochemistry*. 2004;43(47):15058-15065. doi:10.1021/bi0495329.

202. Sugiura S, Kobayakawa N, Fujita H, et al. Comparison of unitary displacements and forces between 2 cardiac myosin isoforms by the optical trap technique: molecular basis for cardiac adaptation. *Circ Res*. 1998;82(10):1029-1034.

203. Krenz M, Sanbe A, Bouyer-Dalloz F, et al. Analysis of myosin heavy chain functionality in the heart. *J Biol Chem*. 2003;278(19):17466-17474. doi:10.1074/jbc.M210804200.

204. Nowakowski SG, Adamek N, Geeves MA, et al. 2-deoxy-ATP Alters Myosin Structure to Enhance Cross-Bridge Cycling and Improve Cardiac Function. *Biophysical Journal*. 2013;104(2):17a. doi:10.1016/j.bpj.2012.11.125.

205. Schoffstall B, Clark A, Chase PB. Positive inotropic effects of low dATP/ATP ratios on mechanics and kinetics of porcine cardiac muscle. *Biophys J*. 2006;91(6):2216-2226. doi:10.1529/biophysj.105.079061.

206. Miyata S, Minobe W, Bristow MR, Leinwand LA. Myosin heavy chain isoform expression in the failing and nonfailing human heart. *Circ Res*. 2000;86(4):386-390.

207. Noguchi T, Camp P, Alix SL, et al. Myosin from failing and non-failing human ventricles exhibit similar contractile properties. *J Mol Cell Cardiol*. 2003;35(1):91-97.

208.   Gay E, Nowakowski SG, Kolwicz SC, et al. AAV6-Mediated Overexpression of Ribonucleotide Reductase (R1R2) Enhances 2-Deoxy-ATP Concentration in Vivo and Improves Cardiac Function. *Biophysical Journal*. 2014;106(2):345a. doi:10.1016/j.bpj.2013.11.1970.

209.   Korte FS, Odom GL, Dai J, et al. Broad Transgenic, and Cardiac-Specific Viral Mediated, Over-Expression of Ribonucleotide Reductase Increases In Vivo Cardiac Contractility. *Biophysical Journal*. 2012;102(3):615a. doi:10.1016/j.bpj.2011.11.3351.

210.   Trumble WR, Sutko JL, Reeves JP. Cardiac sarcolemmal and sarcoplasmic reticulum membrane vesicles exhibit distinctive (Ca-Mg)-ATPase substrate specificities. *J Biol Chem*. 1981;256(14):7101-7104.

211.   Kinoshita Y, Nishigaki K. Unexpectedly general replaceability of ATP in ATP-requiring enzymes. *J Biochem*. 1997;122(1):205-211.

212.   Papp Z, Édes I, Fruhwald S, et al. Levosimendan: molecular mechanisms and clinical implications: consensus of experts on the mechanisms of action of levosimendan. *Int J Cardiol*. 2012;159(2):82-87. doi:10.1016/j.ijcard.2011.07.022.

213.   Packer M, Colucci W, Fisher L, et al. Effect of levosimendan on the short-term clinical course of patients with acutely decompensated heart failure. *JACC Heart Fail*. 2013;1(2):103-111. doi:10.1016/j.jchf.2012.12.004.

214.   Meijs MFL, Asselbergs FW, Doevendans PA. Omecamtiv mecarbil: a promising new drug in systolic heart failure. *Eur J Heart Fail*. 2012;14(3):232-233. doi:10.1093/eurjhf/hfr178.

215.   Cleland JGF, Teerlink JR, Senior R, et al. The effects of the cardiac myosin activator, omecamtiv mecarbil, on cardiac function in systolic heart failure: a double-blind, placebo-controlled, crossover, dose-ranging phase 2 trial. *Lancet*. 2011;378(9792):676-683. doi:10.1016/S0140-6736(11)61126-4.

216.   Teerlink JR, Clarke CP, Saikali KG, et al. Dose-dependent augmentation of cardiac systolic function with the selective cardiac myosin activator, omecamtiv mecarbil: a first-in-man study. *Lancet*. 2011;378(9792):667-675. doi:10.1016/S0140-6736(11)61219-1.

217.   Lundy SD, Murphy SA, Dupras SK, et al. Cell-based delivery of dATP via gap junctions enhances cardiac contractility. *J Mol Cell Cardiol*. 2014;72:350-359. doi:10.1016/j.yjmcc.2014.04.010.

Web Resources

The URLs referred to herein are as follows:

Developmental Studies Hybridoma Bank at the University of Iowa

http://dshb.biology.uiowa.edu/

Online Mendelian Inheritance in Man (OMIM)

http://www.ncbi.nlm.nih.gov/omim/

APPENDIX

Visual Basic Programming Code for Myofibril Analysis

From data file of the Myofibril Acquisition program (LabVIEW)

Load file into excel, and then run in the following order:

Module5: Norm102213()

Now that file is sorted, make any necessary adjustments (such as if KTR was used, edits to remove this from activation trace are required), then run

Module4: findvalues()

Module4: SlowPhase40to150()

Module4: Fmax()

To ease copying data into a summary spreadsheet, run

```
Module2:MakeEasyCoPy()
Attribute VB_Name = "Module5"

Sub Norm102213()
Attribute Norm102213.VB_ProcData.VB_Invoke_Func = "n\n14"
'
' NormNorm102213 Macro
'

'
    Dim activationEnd As Long
    Dim actEnd As String
    Dim actAll As String
    Dim actRange As Range

' normalized activation end, eventually in ms, which is the number of data points in activation
    Dim NAE As Long
' normalized activation range (eventually used as local variable for ranges) and axis ranges for graph
    Dim NAR As String
    Dim NArangeX As String
    Dim NArangeY As String

    Dim freq As Integer
```

```vba
    Dim relaxationStart As Long
    Dim relaxationEnd As Long
    Dim relStart As String
    Dim relEnd As String
    Dim relAll As String
    Dim relRange As Range

' normalized relaxation end, eventually in ms, which is the number of data points in relaxation
    Dim NRE As Long
' normalized relaxation range and axis ranges for graph
    Dim NRR As String
    Dim NRrangeX As String
    Dim NRrangeY As String


' create a copy and move information section over
    ActiveSheet.Select
    ActiveSheet.Copy Before:=Sheets(1)
    Range("A1:F39").Select
    Selection.Cut
    Range("G1").Select
    ActiveSheet.Paste
    Range("A1:C39").Select
    Selection.Delete Shift:=xlUp

' Find the activation time length in spreadsheet after it has been modified to move setup information
    Range("I33").Select

' Normalized Activation End (NAE) is the time the pipette is on pCa 4.0
' activationEnd (long) is the trace time for the end of the activation
' (26 seconds = 25 seconds of pCa 4.0 + 1 second of baseline
' relaxation starts (relaxationStart, Long) when activation ends (activationEnd, Long)
    NAE = Selection.Value
    activationEnd = NAE + 1
    relaxationStart = activationEnd

' Normalized Relaxation End (NRE, long) is the time the pipette is on pCa 9.0
' relaxationEnd (Long) is the total time length of the trace
    Range("H33").Select
    relaxationEnd = Selection.Value
    Range("I33").Select
    relaxationEnd = Selection.Value + relaxationEnd
    Range("J33").Select
    relaxationEnd = Selection.Value + relaxationEnd
    NRE = Selection.Value

' Find the sampling frequency in spreadsheet after it has been modified to move setup information
' freq is the sampling frequency used
' NAE, NRE and activationEnd are modified to be in data point values, or ms, instead of s
' NRE includes slop of 1000 ms
    Range("H19").Select
    freq = Selection.Value
    activationEnd = activationEnd * freq
```

```vba
    NAE = NAE * freq
    NRE = NRE * freq + (1 * freq)
' relaxationStart is modified to be in data point values (ms) and add 1 ms to start at 26 s
    relaxationStart = relaxationStart * freq + 1
' relaxationEnd is mofified to be in data point values (ms) and add 1*freq = 1000 ms of slop at end
    relaxationEnd = (relaxationEnd * freq) + (1 * freq)

' start creating the string (actAll) which will contain the range containing the activation raw data
' this assumes the start of the activation is at A1001, following 1 s (1000 ms) of baseline and FIS
' this uses activationEnd (set earlier to the be the length of time pCa 4.0 is on times the frequency
' of the data acquisition) to be the last cell inclueded
    actEnd = "C"
    actEnd = actEnd & activationEnd
    actAll = "A1001" & ":" & actEnd

' start creating the string (relAll) which will contain the range of relaxation raw data
' this assumes the start of the relaxation is at relStart, 1 ms after activationEnd
' this uses relaxationEnd (set earlier to the be the length time of the of trace times the frequency
' of the data acquisition, plus 1000 ms of slop) to be the last cell included
    relStart = "A"
    relEnd = "C"
    relStart = relStart & relaxationStart
    relEnd = relEnd & relaxationEnd
    relAll = relStart & ":" & relEnd

' select the activation range in the raw data (actRange, also actAll) and paste into columns N through P
    Set actRange = Range(actAll)
    actRange.Select
    Selection.Copy
    Range("N1").Select
    ActiveSheet.Paste
    Application.CutCopyMode = False
    Selection.End(xlUp).Select
    Range(Selection, Selection.End(xlDown)).Select
    NAE = Selection.Rows.Count

' select the relaxation range in the raw data (relRange, also relAll which includes slop) and paste
' into columns AA through AC
    Set relRange = Range(relAll)
    relRange.Select
    Selection.Copy
    Range("AA1").Select
    ActiveSheet.Paste
    Application.CutCopyMode = False
' select the actual range of raw data
    Selection.End(xlUp).Select
    Range(Selection, Selection.End(xlDown)).Select
    NRE = Selection.Rows.Count

' activation math stuff - setup the max, min, normalization functions,
' binary 50% and binary 90%, index match estimates
    Range("Q1").Select
    Application.CutCopyMode = False
    ActiveCell.FormulaR1C1 = "=MAX(C[-1])"
```

```vba
    Range("Q2").Select
    ActiveCell.FormulaR1C1 = "=MIN(C[-1])"

' normalization function, if the cell is blank, do not paste a value
    Range("R1").Select
    ActiveCell.FormulaR1C1 = "=if(RC[-2]="""","""",(RC[-2]-R2C[-1])/(R1C[-1]-R2C[-1]))"
    Range("R1").Select
' NAR becomes a roamining, changing range for autofill destinations based on the length of the activation
' NArangeY (the range for the activation graph y-axis) is set to be the current selected autofill values
    NAR = "R1:R" & NAE
    Range("R1").Select
    Selection.AutoFill Destination:=Range(NAR)
    NArangeY = NAR

' time is t - 1
    Range("S1").Select
    ActiveCell.FormulaR1C1 = "=if(RC[-5]="""","""",RC[-5]-1)"
    NAR = "S1:S" & NAE
    Range("S1").Select
    Selection.AutoFill Destination:=Range(NAR)
    NArangeX = NAR

' find >= 50% values and label them with 1, else label 0
    Range("T1").Select
    ActiveCell.FormulaR1C1 = "=IF(RC[-2]="""","""",if(RC[-2]>0.5,1,0))"
    NAR = "T1:T" & NAE
    Range("T1").Select
    Selection.AutoFill Destination:=Range(NAR)

' find >= 90% values and label them with 1, else label 0
    Range("U1").Select
    ActiveCell.FormulaR1C1 = "=if(RC[-3]="""","""",IF(RC[-3]>0.9,1,0))"
    NAR = "U1:U" & NAE
    Range("U1").Select
    Selection.AutoFill Destination:=Range(NAR)

' Index and match function as a checkpoint/rough estimate
    Range("V1").Select
    ActiveCell.FormulaR1C1 = "=INDEX(C[-3],MATCH(0.5,C[-4]))"
    Range("V2").Select
    ActiveCell.FormulaR1C1 = "=INDEX(C[-3],MATCH(0.9,C[-4]))"
    Range("W1").Select
    ActiveCell.FormulaR1C1 = "50%"
    Range("W2").Select
    ActiveCell.FormulaR1C1 = "90%"

' insert graph of activation
    Range("W5").Select
    ActiveSheet.Shapes.AddChart.Select
    ActiveChart.ChartType = xlXYScatterSmoothNoMarkers
    ActiveChart.SeriesCollection.NewSeries
    ActiveChart.SeriesCollection(1).XValues = Range(NArangeX)
    ActiveChart.SeriesCollection(1).Values = Range(NArangeY)
```

```
'   find max and min
    Range("AD1").Select
    ActiveCell.FormulaR1C1 = "=MAX(C[-1])"
    Range("AD2").Select
    ActiveCell.FormulaR1C1 = "=MIN(C[-1])"


' normalize
    NRR = "AE1:AE" & NRE
    Range("AE1").Select
    ActiveCell.FormulaR1C1 = "=if(RC[-2]="""","""",(RC[-2]-R2C[-1])/(R1C[-1]-R2C[-1]))"
    Selection.AutoFill Destination:=Range(NRR)
    NRrangeY = NRR

' fix time t-26 (can I replace this with a cell value?)
    NRR = "AG1:AG" & NRE
    Range("AG1").Select
    ActiveCell.FormulaR1C1 = "=IF(RC[-6]="""","""",RC[-6]-" & (NAE / freq) + 1 & ")"
    Range("AG1").Select
    Selection.AutoFill Destination:=Range(NRR)
    NRrangeX = NRR

' put in binary for 50% and 90%
    NRR = "AH1:AH" & NRE
    Range("AH1").Select
    ActiveCell.FormulaR1C1 = "=IF(RC[-3]="""","""",IF(RC[-3]<0.5,0,1))"
    Range("AH1").Select
    Selection.AutoFill Destination:=Range(NRR)

    NRR = "AI1:AI" & NRE
    Range("AI1").Select
    ActiveCell.FormulaR1C1 = "=IF(RC[-4]="""","""",IF(RC[-4]<0.1,0,1))"
    Range("AI1").Select
    Selection.AutoFill Destination:=Range(NRR)

'create reverse relaxation trace
    NRR = "AF1:AF" & NRE
    Range("AF1").Select
    ActiveCell.FormulaR1C1 = "=IF(RC[-1]="""","""",1-RC[-1])"
    Range("AF1").Select
    Selection.AutoFill Destination:=Range(NRR)

' index and match for rough 50% and 90% values
    Range("AJ1").Select
    ActiveCell.FormulaR1C1 = "=INDEX(C[-3],MATCH(0.5,C[-4]))"
    Range("AJ2").Select
    ActiveCell.FormulaR1C1 = "=INDEX(C[-3],MATCH(0.9,C[-4]))"

    Range("AK1").Select
    ActiveCell.FormulaR1C1 = "50%"
    Range("AK2").Select
    ActiveCell.FormulaR1C1 = "90%"

' insert graph of relaxation
```

```
    Range("Al5").Select
    ActiveSheet.Shapes.AddChart.Select
    ActiveChart.ChartType = xlXYScatterSmoothNoMarkers
    ActiveChart.SeriesCollection.NewSeries
    ActiveChart.SeriesCollection(1).XValues = Range(NRrangeX)
    ActiveChart.SeriesCollection(1).Values = Range(NRrangeY)

' chart cleanup, such as deleting legends, gridlines, and changing shapes
    ActiveSheet.ChartObjects("Chart 1").Activate
    ActiveChart.Axes(xlValue).MajorGridlines.Select
    Selection.Delete
    ActiveSheet.ChartObjects("Chart 1").Activate
    ActiveChart.Legend.Select
    Selection.Delete
    ActiveSheet.ChartObjects("Chart 1").Activate
    ActiveChart.SeriesCollection(1).Select
    With Selection.Format.Line
        .Visible = msoTrue
        .Weight = 0.1
    End With
    ActiveSheet.ChartObjects("Chart 2").Activate
    ActiveChart.Axes(xlValue).MajorGridlines.Select
    Selection.Delete
    ActiveSheet.ChartObjects("Chart 2").Activate
    ActiveChart.SeriesCollection(1).Select
    With Selection.Format.Line
        .Visible = msoTrue
        .Weight = 0.1
    End With
    ActiveChart.Legend.Select
    Selection.Delete

End Sub


Attribute VB_Name = "Module4"

Sub Fmax()
Attribute Fmax.VB_ProcData.VB_Invoke_Func = "j\n14"
'
' Fmax Macro
'

'
    Range("J3").Select
    ActiveCell.FormulaR1C1 = "Force (V)"
    Range("J4").Select
    ActiveCell.FormulaR1C1 = "Calibration"
    Range("J5").Select
    ActiveCell.FormulaR1C1 = "Force (uN)"
    Range("J6").Select
    ActiveCell.FormulaR1C1 = "Force (uN/myofibril)"
    Range("J7").Select
    ActiveCell.FormulaR1C1 = "CSA (uM^2)"
    Range("J8").Select
```

129

```
    ActiveCell.FormulaR1C1 = "Force (uN/uM^2)"
    Range("K2").Select
    ActiveCell.FormulaR1C1 = "act"
    Range("L2").Select
    ActiveCell.FormulaR1C1 = "rel"
    Range("K3").Select
    ActiveCell.FormulaR1C1 = "=R1C17-R2C17"
    Range("L3").Select
    ActiveCell.FormulaR1C1 = "=R1C30-R2C30"
    Range("L4").Select
    ActiveWindow.LargeScroll ToRight:=-1
    Range("K5").Select
    ActiveCell.FormulaR1C1 = "=R[-2]C/R[-1]C"
    Range("K5").Select
    Selection.AutoFill Destination:=Range("K5:L5"), Type:=xlFillDefault
    Range("K5:L5").Select
    Range("K6").Select
    ActiveCell.FormulaR1C1 = "=R[-1]C/R9C8"
    Range("L6").Select
    ActiveCell.FormulaR1C1 = "=R[-1]C/R9C8"
    Range("K7").Select
    ActiveCell.FormulaR1C1 = "=R[2]C[-3]*PI()*(2.5/2)^2"
    Range("K7").Select
    ActiveCell.FormulaR1C1 = "=R9C8*PI()*(2.5/2)^2"
    Range("L7").Select
    ActiveCell.FormulaR1C1 = "=R9C8*PI()*(2.5/2)^2"
    Range("K8").Select
    ActiveCell.FormulaR1C1 = "=R[-3]C/R[-1]C"
    Range("K8").Select
    Selection.AutoFill Destination:=Range("K8:L8"), Type:=xlFillDefault
    Range("K8:L8").Select

'
' ActRelLengthChange Macro
'
' Keyboard Shortcut: Ctrl+j
'
    Range("J11").Select
    ActiveCell.FormulaR1C1 = "ActRelLengthChange (V)"
    Range("K11").Select
    ActiveCell.FormulaR1C1 = "=R1C17-min(R1C29:R101C29)"
    Range("l11").Select
    ActiveCell.FormulaR1C1 = "=R1C17-max(R1C29:R101C29)"
'
' ForceLength Macro
'
'
    Range("J9").Select
    ActiveCell.FormulaR1C1 = "V/um"
    Range("J10").Select

    ActiveCell.FormulaR1C1 = "delF-L/L"
    Range("K10").Select
    ActiveCell.FormulaR1C1 = "=(R[-7]C/R[-1]C)/R8C8"
```

```
    Range("L10").Select
    ActiveCell.FormulaR1C1 = "=(R[-7]C/R[-1]C)/R8C8"

' umPerLen Macro
'

    Range("J12").Select
    ActiveCell.FormulaR1C1 = "ActRelLengthChange (um)"
    Range("J13").Select
    ActiveCell.FormulaR1C1 = "ActRelLengthChange (%)"
    Range("K12").Select
    ActiveCell.FormulaR1C1 = "=R[-1]C/R[-3]C"
    Range("K13").Select
    ActiveCell.FormulaR1C1 = "=R[-1]C/R8C8"
    Range("K13").Select
    Selection.Style = "Percent"
    Selection.NumberFormat = "0.000%"

    Range("l12").Select
    ActiveCell.FormulaR1C1 = "=R[-1]C/R[-3]C"
    Range("l13").Select
    ActiveCell.FormulaR1C1 = "=R[-1]C/R8C8"
    Range("l13").Select
    Selection.Style = "Percent"
    Selection.NumberFormat = "0.000%"


End Sub


Sub findvalues()
Attribute findvalues.VB_ProcData.VB_Invoke_Func = "d\n14"
'
' findvalues Macro
'

'
    Dim first50A As Double
    Dim last50A As Double
    Dim first90A As Double
    Dim last90A As Double

    Dim first50R As Double
    Dim last50R As Double
    Dim first90R As Double
    Dim last90R As Double

' find the first time the data passes 0.5 and save the corresponding time value
' to the just past 0.5 mark in the V3 cell
    Columns("T:T").Select
    Selection.Find(What:="1", After:=ActiveCell, LookIn:=xlValues, LookAt:= _
        xlPart, SearchOrder:=xlByRows, SearchDirection:=xlNext, MatchCase:=False _
        , SearchFormat:=False).Activate
    first50A = ActiveCell.Offset(0, -1).Value
```

131

```
    Range("V3").Select
    ActiveCell.FormulaR1C1 = first50A


' find the last time the data passes 0.5 and save the corresponding time value
' to the just before passing 0.5 mark in the V4 cell
    Columns("T:T").Select
    Selection.Find(What:="0", After:=ActiveCell, LookIn:=xlValues, LookAt:= _
        xlPart, SearchOrder:=xlByRows, SearchDirection:=xlPrevious, MatchCase:=False _
        , SearchFormat:=False).Activate
    last50A = ActiveCell.Offset(-1, -1).Value
    Range("V4").Select
    ActiveCell.FormulaR1C1 = last50A


' calculate the average time from the just before 0.5 and just after passing 0.5  and
' paste into the W3 cell
    Range("W3").Select
    ActiveCell.FormulaR1C1 = "=AVERAGE(RC[-1]:R[1]C[-1])"
    Range("X3").Select
    ActiveCell.FormulaR1C1 = "50% estimate average"


' find the first time the data passes 0.9 and save the corresponding time value
' to the just past 0.9 mark in the V5 cell
    Columns("u:u").Select
    Selection.Find(What:="1", After:=ActiveCell, LookIn:=xlValues, LookAt:= _
        xlPart, SearchOrder:=xlByRows, SearchDirection:=xlNext, MatchCase:=False _
        , SearchFormat:=False).Activate
    first90A = ActiveCell.Offset(0, -2).Value
    Range("V5").Select
    ActiveCell.FormulaR1C1 = first90A


' find the last time the data passes 0.9 and save the corresponding time value
' to the just before passing 0.9 mark in the V6 cell
    Columns("u:u").Select
    Selection.Find(What:="0", After:=ActiveCell, LookIn:=xlValues, LookAt:= _
        xlPart, SearchOrder:=xlByRows, SearchDirection:=xlPrevious, MatchCase:=False _
        , SearchFormat:=False).Activate
    last90A = ActiveCell.Offset(-1, -2).Value
    Range("V6").Select
    ActiveCell.FormulaR1C1 = last90A


' calculate the average time from the just before 0.9 values start and just before exceeding
' 0.9  and paste into the W5 cell
    Range("W5").Select
    ActiveCell.FormulaR1C1 = "=AVERAGE(RC[-1]:R[1]C[-1])"
    Range("X5").Select
    ActiveCell.FormulaR1C1 = "90% estimate average"


' find the first time the data passes 0.5 and save the corresponding time value
' to the just past 0.5 mark in the V3 cell
    Columns("AH:AH").Select
    Selection.Find(What:="0", After:=ActiveCell, LookIn:=xlValues, LookAt:= _
        xlPart, SearchOrder:=xlByRows, SearchDirection:=xlNext, MatchCase:=False _
        , SearchFormat:=False).Activate
    first50R = ActiveCell.Offset(0, -1).Value
```

```
    Range("AJ3").Select
    ActiveCell.FormulaR1C1 = first50R


' find the last time the data passes 0.5 and save the corresponding time value
' to the just before passing 0.5 mark in the V4 cell
    Columns("AH:AH").Select
    Selection.Find(What:="1", After:=ActiveCell, LookIn:=xlValues, LookAt:= _
        xlPart, SearchOrder:=xlByRows, SearchDirection:=xlPrevious, MatchCase:=False _
        , SearchFormat:=False).Activate
    last50R = ActiveCell.Offset(-1, -1).Value
    Range("AJ4").Select
    ActiveCell.FormulaR1C1 = last50R


' calculate the average time from the just before 0.5 and just after passing 0.5  and
' paste into the W3 cell
    Range("AK3").Select
    ActiveCell.FormulaR1C1 = "=AVERAGE(RC[-1]:R[1]C[-1])"
    Range("AL3").Select
    ActiveCell.FormulaR1C1 = "50% estimate average"


' find the first time the data passes 0.9 and save the corresponding time value
' to the just past 0.9 mark in the V5 cell
    Columns("AI:AI").Select
    Selection.Find(What:="0", After:=ActiveCell, LookIn:=xlValues, LookAt:= _
        xlPart, SearchOrder:=xlByRows, SearchDirection:=xlNext, MatchCase:=False _
        , SearchFormat:=False).Activate
    first90R = ActiveCell.Offset(0, -2).Value
    Range("AJ5").Select
    ActiveCell.FormulaR1C1 = first90R


' find the last time the data passes 0.9 and save the corresponding time value
' to the just before passing 0.9 mark in the V6 cell
    Columns("AI:AI").Select
    Selection.Find(What:="1", After:=ActiveCell, LookIn:=xlValues, LookAt:= _
        xlPart, SearchOrder:=xlByRows, SearchDirection:=xlPrevious, MatchCase:=False _
        , SearchFormat:=False).Activate
    last90R = ActiveCell.Offset(-1, -2).Value
    Range("AJ6").Select
    ActiveCell.FormulaR1C1 = last90R


' calculate the average time from the just before 0.9 values start and just before exceeding
' 0.9  and paste into the W5 cell
    Range("AK5").Select
    ActiveCell.FormulaR1C1 = "=AVERAGE(RC[-1]:R[1]C[-1])"
    Range("AL5").Select
    ActiveCell.FormulaR1C1 = "90% estimate average"
End Sub
Sub SlowPhase40to150()
Attribute SlowPhase40to150.VB_ProcData.VB_Invoke_Func = "s\n14"
'
' SlowPhase40to150 Macro
'
'Create ranges to copy and paste and then move them
    rangeX = "AP1:AP1000"
```

```
      rangeY = "AN1:AN1000"
      Application.Goto Reference:="R41C31:R151C33"
      Selection.Copy
      Range("AN1").Select
      Selection.PasteSpecial Paste:=xlPasteValues, Operation:=xlNone, SkipBlanks _
         :=False, Transpose:=False
      Application.CutCopyMode = False
      ActiveWindow.SmallScroll Down:=-6

' Create chart
      Range("AR1").Select
      ActiveSheet.Shapes.AddChart.Select
      ActiveChart.ChartType = xlXYScatter
      ActiveSheet.ChartObjects("Chart 3").Activate
      ActiveSheet.Shapes("Chart 3").Name = "Slow Phase"
      ActiveChart.SeriesCollection.NewSeries
      ActiveChart.SeriesCollection(1).XValues = Range(rangeX)
      ActiveChart.SeriesCollection(1).Values = Range(rangeY)

' create trendline
      ActiveChart.SeriesCollection(1).Select
      ActiveChart.SeriesCollection(1).Trendlines.Add
      ActiveChart.SeriesCollection(1).Trendlines(1).Select
      Selection.DisplayEquation = True
      Selection.DisplayRSquared = True

'create second range in chart (total relaxation)
      rangeX = "AG1:AG10000"
      rangeY = "AE1:AE10000"

      ActiveSheet.ChartObjects("Slow Phase").Activate

      ActiveChart.SeriesCollection.NewSeries
      ActiveChart.SeriesCollection(2).XValues = Range(rangeX)
      ActiveChart.SeriesCollection(2).Values = Range(rangeY)
      ActiveChart.SeriesCollection(2).Select
      Selection.MarkerStyle = -4142
      With Selection.Format.Line
         .Visible = msoTrue
         .ForeColor.ObjectThemeColor = msoThemeColorAccent1
         .ForeColor.TintAndShade = 0
         .ForeColor.Brightness = 0
      End With
      With Selection.Format.Line
         .Visible = msoTrue
         .Weight = 0
      End With
      ActiveChart.Axes(xlCategory).Select
      ActiveChart.Axes(xlCategory).MinimumScale = 0
      ActiveChart.Axes(xlCategory).MaximumScale = 1
      ActiveChart.Axes(xlValue).Select
      ActiveChart.Axes(xlValue).MinimumScale = 0.5
      ActiveChart.Axes(xlValue).MaximumScale = 1
```

```vb
'clean up chart
    ActiveChart.Axes(xlValue).MajorGridlines.Select
    Selection.Delete
    ActiveChart.Legend.Select
    Selection.Delete
    ActiveChart.SeriesCollection(1).Trendlines(1).Select
    Selection.Forward = 2

'resize chart
    ActiveSheet.Shapes("Chart 3").IncrementLeft 173.25
    ActiveSheet.Shapes("Chart 3").IncrementTop -141
    ActiveSheet.Shapes("Chart 3").ScaleWidth 1.1229166667, msoFalse, _
        msoScaleFromBottomRight
    ActiveSheet.Shapes("Chart 3").ScaleHeight 2.1875, msoFalse, msoScaleFromTopLeft

    ActiveSheet.ChartObjects("Slow Phase").Activate
    ActiveChart.SeriesCollection(1).Trendlines(1).DataLabel.Select
    Selection.Left = 298
    Selection.Top = 21
End Sub

Attribute VB_Name = "Module2"
Sub MakeEasyCoPy()
Attribute MakeEasyCoPy.VB_ProcData.VB_Invoke_Func = " \n14"
'
' MakeEasyCoPy Macro
'

'
    Range("A1:M2").Select
    Selection.Insert Shift:=xlDown, CopyOrigin:=xlFormatFromLeftOrAbove
    Range("a1").Select
    ActiveCell.FormulaR1C1 = "Fmax(Act)(uN/um2)"
    Range("b1").Select
    ActiveCell.FormulaR1C1 = "Fmax(Rel)(uN/um2)"
    Range("c1").Select
    ActiveCell.FormulaR1C1 = "50%Act"
    Range("d1").Select
    ActiveCell.FormulaR1C1 = "90%ACT"
    Range("e1").Select
    ActiveCell.FormulaR1C1 = "50%REL"
    Range("f1").Select
    ActiveCell.FormulaR1C1 = "90%REL"
    Range("g1").Select
    ActiveCell.FormulaR1C1 = "slow phase (1/s)"
    Range("h1").Select
    ActiveCell.FormulaR1C1 = "trelslow"
    Range("i1").Select
    ActiveCell.FormulaR1C1 = "deflection(act,%L)"
    Range("j1").Select
    ActiveCell.FormulaR1C1 = "deflection(rel,%L)"
    Range("k1").Select
    ActiveCell.FormulaR1C1 = "%Lchange(ACTtoRELmin)"
    Range("l1").Select
```

135

```
ActiveCell.FormulaR1C1 = "%Lchange(ACTtoRELmax)"
Range("a1:m2").Select

With Selection
    .HorizontalAlignment = xlGeneral
    .VerticalAlignment = xlBottom
    .WrapText = True
    .Orientation = 0
    .AddIndent = False
    .IndentLevel = 0
    .ShrinkToFit = False
    .ReadingOrder = xlContext
    .MergeCells = False
End With


Range("a2").Select
ActiveCell.FormulaR1C1 = "=R10C11"
Range("b2").Select
ActiveCell.FormulaR1C1 = "=R10C12"
Range("c2").Select
ActiveCell.FormulaR1C1 = "=R3C23"
Range("d2").Select
ActiveCell.FormulaR1C1 = "=R5C23"
Range("e2").Select
ActiveCell.FormulaR1C1 = "=R3C37"
Range("f2").Select
ActiveCell.FormulaR1C1 = "=R5C37"
Range("i2").Select
ActiveCell.FormulaR1C1 = "=R12C11"
Range("j2").Select
ActiveCell.FormulaR1C1 = "=R12C12"
Range("k2").Select
ActiveCell.FormulaR1C1 = "=R15C11"
Range("l2").Select
ActiveCell.FormulaR1C1 = "=R15C12"

Columns("M:M").Select
Selection.Insert Shift:=xlToRight, CopyOrigin:=xlFormatFromLeftOrAbove
Selection.Insert Shift:=xlToRight, CopyOrigin:=xlFormatFromLeftOrAbove
Selection.Insert Shift:=xlToRight, CopyOrigin:=xlFormatFromLeftOrAbove
Range("A1:L2").Select
Range("L1").Activate
Selection.Cut
Range("E1").Select
ActiveSheet.Paste
Range("A1").Select
ActiveCell.FormulaR1C1 = "Date"
Range("B1").Select
ActiveCell.FormulaR1C1 = "Experiment"
Range("C1").Select
ActiveCell.FormulaR1C1 = "Sample number"
Range("D1").Select
```

```
    ActiveCell.FormulaR1C1 = "trace"

    Range("B2").Select
    ActiveCell.FormulaR1C1 = "=R[6]C[6]"
    Range("A2").Select
    ActiveCell.FormulaR1C1 = "=R[35]C[7]"
    Range("C2").Select
    ActiveCell.FormulaR1C1 = "=R[7]C[5]"
    Range("D2").Select
    ActiveCell.FormulaR1C1 = "=R[37]C[4]"
    Range("D3").Select
End Sub
```

Licenses for reprint

<u>Racca et al, 2015 (CHAPTER 3 HUMAN SKELETAL MUSCLE in DISTAL
      ARTHROGRYPOSIS)</u>

**OXFORD UNIVERSITY PRESS LICENSE
TERMS AND CONDITIONS**

Mar 10, 2015

This is a License Agreement between Alice Ward Racca ("You") and Oxford University
Press ("Oxford University Press") provided by Copyright Clearance Center ("CCC"). The
license consists of your order details, the terms and conditions provided by Oxford
University Press, and the payment terms and conditions.

**All payments must be made in full to CCC. For payment instructions, please see
information listed at the bottom of this form.**

License Number   3585560276120

License date   Mar 10, 2015

Licensed content publisher Oxford University Press

Licensed content   Human Molecular Genetics
publication

Licensed content title   The embryonic myosin R672C mutation that underlies Freeman-Sheldon syndrome impairs crossbridge detachment and cycling in adult muscle:

Licensed content author   Alice W. Racca, Anita E. Beck, Margaret J. McMillin, F. Steven Korte, Michael J. Bamshad, Michael Regnier

Licensed content date   03/03/2015

Type of Use   Thesis/Dissertation

Institution name   None

Title of your work   Contractile Properties of Striated Muscle in Development and Disease

Publisher of your work   n/a

Expected publication date Mar 2015

Permissions cost   0.00 USD

Value added tax   0.00 USD

Total   0.00 USD

Total   0.00 USD

Terms and Conditions

STANDARD TERMS AND CONDITIONS FOR REPRODUCTION OF MATERIAL FROM AN OXFORD UNIVERSITY PRESS JOURNAL

1. Use of the material is restricted to the type of use specified in your order details.

2. This permission covers the use of the material in the English language in the following territory: world. If you have requested additional permission to translate this material, the terms and conditions of this reuse will be set out in clause 12.

3. This permission is limited to the particular use authorized in (1) above and does not allow you to sanction its use elsewhere in any other format other than specified above, nor does it

apply to quotations, images, artistic works etc that have been reproduced from other sources which may be part of the material to be used.

4. No alteration, omission or addition is made to the material without our written consent. Permission must be re-cleared with Oxford University Press if/when you decide to reprint.

5. The following credit line appears wherever the material is used: author, title, journal, year, volume, issue number, pagination, by permission of Oxford University Press or the sponsoring society if the journal is a society journal. Where a journal is being published on behalf of a learned society, the details of that society must be included in the credit line.

6. For the reproduction of a full article from an Oxford University Press journal for whatever purpose, the corresponding author of the material concerned should be informed of the proposed use. Contact details for the corresponding authors of all Oxford University Press journal contact can be found alongside either the abstract or full text of the article concerned, accessible from www.oxfordjournals.org Should there be a problem clearing these rights, please contact journals.permissions@oup.com

7. If the credit line or acknowledgement in our publication indicates that any of the figures, images or photos was reproduced, drawn or modified from an earlier source it will be necessary for you to clear this permission with the original publisher as well. If this permission has not been obtained, please note that this material cannot be included in your publication/photocopies.

8. While you may exercise the rights licensed immediately upon issuance of the license at the end of the licensing process for the transaction, provided that you have disclosed complete and accurate details of your proposed use, no license is finally effective unless and until full payment is received from you (either by Oxford University Press or by Copyright Clearance Center (CCC)) as provided in CCC's Billing and Payment terms and conditions. If full payment is not received on a timely basis, then any license preliminarily granted shall be deemed automatically revoked and shall be void as if never granted. Further, in the event that you breach any of these terms and conditions or any of CCC's Billing and Payment terms and conditions, the license is automatically revoked and shall be void as if never granted. Use of materials as described in a revoked license, as well as any use of the materials beyond the scope of an unrevoked license, may constitute copyright infringement and Oxford University Press reserves the right to take any and all action to protect its copyright in the materials.

9. This license is personal to you and may not be sublicensed, assigned or transferred by you to any other person without Oxford University Press's written permission.

10. Oxford University Press reserves all rights not specifically granted in the combination of (i) the license details provided by you and accepted in the course of this licensing transaction, (ii) these terms and conditions and (iii) CCC's Billing and Payment terms and conditions.

11. You hereby indemnify and agree to hold harmless Oxford University Press and CCC,

and their respective officers, directors, employs and agents, from and against any and all claims arising out of your use of the licensed material other than as specifically authorized pursuant to this license.

12. Other Terms and Conditions:

v1.4

Questions? <u>customercare@copyright.com</u> or +1-855-239-3415 (toll free in the US) or +1-978-646-2777.

Gratis licenses (referencing $0 in the Total field) are free. Please retain this printable license for your reference. No payment is required.

This Agreement between Alice Ward Racca ("You") and John Wiley and Sons ("John Wiley and Sons") consists of your license details and the terms and conditions provided by John Wiley and Sons and Copyright Clearance Center.

License Number	3552830411450
License date	Jan 19, 2015
Licensed Content Publisher	John Wiley and Sons
Licensed Content Publication	Journal of Physiology
Licensed Content Title	Contractility and kinetics of human fetal and human adult skeletal muscle
Licensed Content Author	Alice W. Racca,Anita E. Beck,Vijay S. Rao,Galina V. Flint,Scott D. Lundy,Donald E. Born,Michael J. Bamshad,Michael Regnier
Licensed Content Date	Jun 14, 2013
Pages	13
Type of use	Dissertation/Thesis
Requestor type	Author of this Wiley article
Format	Print and electronic
Portion	Full article
Will you be translating?	No
Title of your thesis / dissertation	Contractile Properties of Striated Muscle in Development and Disease
Expected completion date	Mar 2015
Expected size (number of pages)	200
Requestor Location	Alice Ward Racca
815 Mercer St., S184
Box 358056

SEATTLE, WA 98109
United States
Attn: Alice Ward Racca |
| Billing Type | Invoice |
| Billing Address | Alice Ward Racca
815 Mercer St., S184
Box 358056

SEATTLE, WA 98109 |

TERMS AND CONDITIONS

This copyrighted material is owned by or exclusively licensed to John Wiley & Sons, Inc. or one of its group companies (each a"Wiley Company") or handled on behalf of a society with which a Wiley Company has exclusive publishing rights in relation to a particular work (collectively "WILEY"). By clicking �accept� in connection with completing this licensing transaction, you agree that the following terms and conditions apply to this transaction (along with the billing and payment terms and conditions established by the Copyright Clearance Center Inc., ("CCC's Billing and Payment terms and conditions"), at the time that you opened your Rightslink account (these are available at any time at http://myaccount.copyright.com).

Terms and Conditions

- The materials you have requested permission to reproduce or reuse (the "Wiley Materials") are protected by copyright.

- You are hereby granted a personal, non-exclusive, non-sub licensable (on a stand-alone basis), non-transferable, worldwide, limited license to reproduce the Wiley Materials for the purpose specified in the licensing process. This license is for a one-time use only and limited to any maximum distribution number specified in the license. The first instance of republication or reuse granted by this licence must be completed within two years of the date of the grant of this licence (although copies prepared before the end date may be distributed thereafter). The Wiley Materials shall not be used in any other manner or for any other purpose, beyond what is granted in the license. Permission is granted subject to an appropriate acknowledgement given to the author, title of the material/book/journal and the publisher. You shall also duplicate the copyright notice that appears in the Wiley publication in your use of the Wiley Material. Permission is also granted on the understanding that nowhere in the text is a previously published source acknowledged for all or part of this Wiley Material. Any third party content is expressly excluded from this permission.

- With respect to the Wiley Materials, all rights are reserved. Except as expressly granted by the terms of the license, no part of the Wiley Materials may be copied, modified, adapted (except for minor reformatting required by the new Publication), translated, reproduced, transferred or distributed, in any form or by any means, and no derivative works may be made based on the Wiley Materials without the prior permission of the respective copyright owner. You may not alter, remove or suppress in any manner any copyright, trademark or other notices displayed by the

142

Wiley Materials. You may not license, rent, sell, loan, lease, pledge, offer as security, transfer or assign the Wiley Materials on a stand-alone basis, or any of the rights granted to you hereunder to any other person.

- The Wiley Materials and all of the intellectual property rights therein shall at all times remain the exclusive property of John Wiley & Sons Inc, the Wiley Companies, or their respective licensors, and your interest therein is only that of having possession of and the right to reproduce the Wiley Materials pursuant to Section 2 herein during the continuance of this Agreement. You agree that you own no right, title or interest in or to the Wiley Materials or any of the intellectual property rights therein. You shall have no rights hereunder other than the license as provided for above in Section 2. No right, license or interest to any trademark, trade name, service mark or other branding ("Marks") of WILEY or its licensors is granted hereunder, and you agree that you shall not assert any such right, license or interest with respect thereto.

- NEITHER WILEY NOR ITS LICENSORS MAKES ANY WARRANTY OR REPRESENTATION OF ANY KIND TO YOU OR ANY THIRD PARTY, EXPRESS, IMPLIED OR STATUTORY, WITH RESPECT TO THE MATERIALS OR THE ACCURACY OF ANY INFORMATION CONTAINED IN THE MATERIALS, INCLUDING, WITHOUT LIMITATION, ANY IMPLIED WARRANTY OF MERCHANTABILITY, ACCURACY, SATISFACTORY QUALITY, FITNESS FOR A PARTICULAR PURPOSE, USABILITY, INTEGRATION OR NON-INFRINGEMENT AND ALL SUCH WARRANTIES ARE HEREBY EXCLUDED BY WILEY AND ITS LICENSORS AND WAIVED BY YOU

- WILEY shall have the right to terminate this Agreement immediately upon breach of this Agreement by you.
- You shall indemnify, defend and hold harmless WILEY, its Licensors and their respective directors, officers, agents and employees, from and against any actual or threatened claims, demands, causes of action or proceedings arising from any breach of this Agreement by you.

- IN NO EVENT SHALL WILEY OR ITS LICENSORS BE LIABLE TO YOU OR ANY OTHER PARTY OR ANY OTHER PERSON OR ENTITY FOR ANY SPECIAL, CONSEQUENTIAL, INCIDENTAL, INDIRECT, EXEMPLARY OR PUNITIVE DAMAGES, HOWEVER CAUSED, ARISING OUT OF OR IN CONNECTION WITH THE DOWNLOADING, PROVISIONING, VIEWING OR USE OF THE MATERIALS REGARDLESS OF THE FORM OF ACTION, WHETHER FOR BREACH OF CONTRACT, BREACH OF WARRANTY, TORT, NEGLIGENCE, INFRINGEMENT OR OTHERWISE (INCLUDING, WITHOUT LIMITATION, DAMAGES BASED ON LOSS OF PROFITS, DATA, FILES, USE, BUSINESS OPPORTUNITY OR CLAIMS OF THIRD PARTIES), AND WHETHER OR NOT THE PARTY HAS BEEN ADVISED OF THE

POSSIBILITY OF SUCH DAMAGES. THIS LIMITATION SHALL APPLY NOTWITHSTANDING ANY FAILURE OF ESSENTIAL PURPOSE OF ANY LIMITED REMEDY PROVIDED HEREIN.

- Should any provision of this Agreement be held by a court of competent jurisdiction to be illegal, invalid, or unenforceable, that provision shall be deemed amended to achieve as nearly as possible the same economic effect as the original provision, and the legality, validity and enforceability of the remaining provisions of this Agreement shall not be affected or impaired thereby.

- The failure of either party to enforce any term or condition of this Agreement shall not constitute a waiver of either party's right to enforce each and every term and condition of this Agreement. No breach under this agreement shall be deemed waived or excused by either party unless such waiver or consent is in writing signed by the party granting such waiver or consent. The waiver by or consent of a party to a breach of any provision of this Agreement shall not operate or be construed as a waiver of or consent to any other or subsequent breach by such other party.

- This Agreement may not be assigned (including by operation of law or otherwise) by you without WILEY's prior written consent.

- Any fee required for this permission shall be non-refundable after thirty (30) days from receipt by the CCC.

- These terms and conditions together with CCC�s Billing and Payment terms and conditions (which are incorporated herein) form the entire agreement between you and WILEY concerning this licensing transaction and (in the absence of fraud) supersedes all prior agreements and representations of the parties, oral or written. This Agreement may not be amended except in writing signed by both parties. This Agreement shall be binding upon and inure to the benefit of the parties' successors, legal representatives, and authorized assigns.

- In the event of any conflict between your obligations established by these terms and conditions and those established by CCC�s Billing and Payment terms and conditions, these terms and conditions shall prevail.

- WILEY expressly reserves all rights not specifically granted in the combination of (i) the license details provided by you and accepted in the course of this licensing transaction, (ii) these terms and conditions and (iii) CCC�s Billing and Payment terms and conditions.

- This Agreement will be void if the Type of Use, Format, Circulation, or Requestor Type was misrepresented during the licensing process.

- This Agreement shall be governed by and construed in accordance with the laws of the State of New York, USA, without regards to such state�s conflict of law rules.

Any legal action, suit or proceeding arising out of or relating to these Terms and Conditions or the breach thereof shall be instituted in a court of competent jurisdiction in New York County in the State of New York in the United States of America and each party hereby consents and submits to the personal jurisdiction of such court, waives any objection to venue in such court and consents to service of process by registered or certified mail, return receipt requested, at the last known address of such party.

WILEY OPEN ACCESS TERMS AND CONDITIONS

Wiley Publishes Open Access Articles in fully Open Access Journals and in Subscription journals offering Online Open. Although most of the fully Open Access journals publish open access articles under the terms of the Creative Commons Attribution (CC BY) License only, the subscription journals and a few of the Open Access Journals offer a choice of Creative Commons Licenses:: Creative Commons Attribution (CC-BY) license Creative Commons Attribution Non-Commercial (CC-BY-NC) license and Creative Commons Attribution Non-Commercial-NoDerivs (CC-BY-NC-ND) License. The license type is clearly identified on the article.

The Creative Commons Attribution License

linking to the relevant Creative Commons web page.

To the fullest extent permitted by applicable law, the article is made available as is and without representation or warranties of any kind whether express, implied, statutory or otherwise and including, without limitation, warranties of title, merchantability, fitness for a particular purpose, non-infringement, absence of defects, accuracy, or the presence or absence of errors.

Creative Commons Attribution Non-Commercial License

The Creative Commons Attribution Non-Commercial (CC-BY-NC) License permits use, distribution and reproduction in any medium, provided the original work is properly cited and is not used for commercial purposes.(see below)

Creative Commons Attribution-Non-Commercial-NoDerivs License

The Creative Commons Attribution Non-Commercial-NoDerivs License (CC-BY-NC-ND) permits use, distribution and reproduction in any medium, provided the original work is properly cited, is not used for commercial purposes and no modifications or adaptations are made. (see below)

Use by non-commercial users

For non-commercial and non-promotional purposes, individual users may access, download, copy, display and redistribute to colleagues Wiley Open Access articles, as well as adapt, translate, text- and data-mine the content subject to the following conditions:

- The authors' moral rights are not compromised. These rights include the right of "paternity" (also known as "attribution" - the right for the author to be identified as such) and "integrity" (the right for the author not to have the work altered in such a way that the author's reputation or integrity may be impugned).

- Where content in the article is identified as belonging to a third party, it is the obligation of the user to ensure that any reuse complies with the copyright policies of the owner of that content.

- If article content is copied, downloaded or otherwise reused for non-commercial research and education purposes, a link to the appropriate bibliographic citation (authors, journal, article title, volume, issue, page numbers, DOI and the link to the definitive published version on **Wiley Online Library**) should be maintained. Copyright notices and disclaimers must not be deleted.

- Any translations, for which a prior translation agreement with Wiley has not been agreed, must prominently display the statement: "This is an unofficial translation of an article that appeared in a Wiley publication. The publisher has not endorsed this

translation."

Use by commercial "for-profit" organisations

Use of Wiley Open Access articles for commercial, promotional, or marketing purposes requires further explicit permission from Wiley and will be subject to a fee. Commercial purposes include:

- Copying or downloading of articles, or linking to such articles for further redistribution, sale or licensing;

- Copying, downloading or posting by a site or service that incorporates advertising with such content;

- The inclusion or incorporation of article content in other works or services (other than normal quotations with an appropriate citation) that is then available for sale or licensing, for a fee (for example, a compilation produced for marketing purposes, inclusion in a sales pack)

- Use of article content (other than normal quotations with appropriate citation) by for-profit organisations for promotional purposes

- Linking to article content in e-mails redistributed for promotional, marketing or educational purposes;

- Use for the purposes of monetary reward by means of sale, resale, licence, loan, transfer or other form of commercial exploitation such as marketing products

- Print reprints of Wiley Open Access articles can be purchased from: corporatesales@wiley.com

Further details can be found on Wiley Online Library
http://olabout.wiley.com/WileyCDA/Section/id-410895.html

Other Terms and Conditions:

v1.9

This is a License Agreement between Alice Ward Racca ("You") and Elsevier ("Elsevier") provided by Copyright Clearance Center ("CCC"). The license consists of your order details, the terms and conditions provided by Elsevier, and the payment terms and conditions.

All payments must be made in full to CCC. For payment instructions, please see information listed at the bottom of this form.

Supplier	Elsevier Limited The Boulevard,Langford Lane Kidlington,Oxford,OX5 1GB,UK
Registered Company Number	1982084
Customer name	Alice Ward Racca
Customer address	815 Mercer St., S184
	SEATTLE, WA 98109
License number	3552821311012
License date	Jan 19, 2015
Licensed content publisher	Elsevier
Licensed content publication	Journal of Molecular and Cellular Cardiology
Licensed content title	2-Deoxy adenosine triphosphate improves contraction in human end-stage heart failure
Licensed content author	None
Licensed content date	February 2015
Licensed content volume number	79
Licensed content issue number	n/a
Number of pages	8
Start Page	256
End Page	263
Type of Use	reuse in a thesis/dissertation
Portion	full article
Format	both print and electronic
Are you the author of this Elsevier article?	Yes

Will you be translating?	No
Title of your thesis/dissertation	Contractile Properties of Striated Muscle in Development and Disease
Expected completion date	Mar 2015
Estimated size (number of pages)	200
Elsevier VAT number	GB 494 6272 12
Permissions price	0.00 USD
VAT/Local Sales Tax	0.00 USD / 0.00 GBP
Total	0.00 USD
Terms and Conditions	

INTRODUCTION

1. The publisher for this copyrighted material is Elsevier. By clicking "accept" in connection with completing this licensing transaction, you agree that the following terms and conditions apply to this transaction (along with the Billing and Payment terms and conditions established by Copyright Clearance Center, Inc. ("CCC"), at the time that you opened your Rightslink account and that are available at any time at http://myaccount.copyright.com).

GENERAL TERMS

2. Elsevier hereby grants you permission to reproduce the aforementioned material subject to the terms and conditions indicated.

3. Acknowledgement: If any part of the material to be used (for example, figures) has appeared in our publication with credit or acknowledgement to another source, permission must also be sought from that source. If such permission is not obtained then that material may not be included in your publication/copies. Suitable acknowledgement to the source must be made, either as a footnote or in a reference list at the end of your publication, as follows:

"Reprinted from Publication title, Vol /edition number, Author(s), Title of article / title of chapter, Pages No., Copyright (Year), with permission from Elsevier [OR APPLICABLE SOCIETY COPYRIGHT OWNER]." Also Lancet special credit - "Reprinted from The Lancet, Vol. number, Author(s), Title of article, Pages No., Copyright (Year), with permission from Elsevier."

4. Reproduction of this material is confined to the purpose and/or media for which permission is hereby given.

5. Altering/Modifying Material: Not Permitted. However figures and illustrations may be altered/adapted minimally to serve your work. Any other abbreviations, additions, deletions and/or any other alterations shall be made only with prior written authorization of Elsevier

150

Ltd. (Please contact Elsevier at permissions@elsevier.com)

6. If the permission fee for the requested use of our material is waived in this instance, please be advised that your future requests for Elsevier materials may attract a fee.

7. Reservation of Rights: Publisher reserves all rights not specifically granted in the combination of (i) the license details provided by you and accepted in the course of this licensing transaction, (ii) these terms and conditions and (iii) CCC's Billing and Payment terms and conditions.

8. License Contingent Upon Payment: While you may exercise the rights licensed immediately upon issuance of the license at the end of the licensing process for the transaction, provided that you have disclosed complete and accurate details of your proposed use, no license is finally effective unless and until full payment is received from you (either by publisher or by CCC) as provided in CCC's Billing and Payment terms and conditions. If full payment is not received on a timely basis, then any license preliminarily granted shall be deemed automatically revoked and shall be void as if never granted. Further, in the event that you breach any of these terms and conditions or any of CCC's Billing and Payment terms and conditions, the license is automatically revoked and shall be void as if never granted. Use of materials as described in a revoked license, as well as any use of the materials beyond the scope of an unrevoked license, may constitute copyright infringement and publisher reserves the right to take any and all action to protect its copyright in the materials.

9. Warranties: Publisher makes no representations or warranties with respect to the licensed material.

10. Indemnity: You hereby indemnify and agree to hold harmless publisher and CCC, and their respective officers, directors, employees and agents, from and against any and all claims arising out of your use of the licensed material other than as specifically authorized pursuant to this license.

11. No Transfer of License: This license is personal to you and may not be sublicensed, assigned, or transferred by you to any other person without publisher's written permission.

12. No Amendment Except in Writing: This license may not be amended except in a writing signed by both parties (or, in the case of publisher, by CCC on publisher's behalf).

13. Objection to Contrary Terms: Publisher hereby objects to any terms contained in any purchase order, acknowledgment, check endorsement or other writing prepared by you, which terms are inconsistent with these terms and conditions or CCC's Billing and Payment terms and conditions. These terms and conditions, together with CCC's Billing and Payment terms and conditions (which are incorporated herein), comprise the entire agreement between you and publisher (and CCC) concerning this licensing transaction. In the event of any conflict between your obligations established by these terms and

conditions and those established by CCC's Billing and Payment terms and conditions, these terms and conditions shall control.

14. Revocation: Elsevier or Copyright Clearance Center may deny the permissions described in this License at their sole discretion, for any reason or no reason, with a full refund payable to you. Notice of such denial will be made using the contact information provided by you. Failure to receive such notice will not alter or invalidate the denial. In no event will Elsevier or Copyright Clearance Center be responsible or liable for any costs, expenses or damage incurred by you as a result of a denial of your permission request, other than a refund of the amount(s) paid by you to Elsevier and/or Copyright Clearance Center for denied permissions.

<div align="center">

LIMITED LICENSE

</div>

The following terms and conditions apply only to specific license types:

15. **Translation**: This permission is granted for non-exclusive world **English** rights only unless your license was granted for translation rights. If you licensed translation rights you may only translate this content into the languages you requested. A professional translator must perform all translations and reproduce the content word for word preserving the integrity of the article. If this license is to re-use 1 or 2 figures then permission is granted for non-exclusive world rights in all languages.

16. **Posting licensed content on any Website**: The following terms and conditions apply as follows: Licensing material from an Elsevier journal: All content posted to the web site must maintain the copyright information line on the bottom of each image; A hyper-text must be included to the Homepage of the journal from which you are licensing at http://www.sciencedirect.com/science/journal/xxxxx or the Elsevier homepage for books at http://www.elsevier.com; Central Storage: This license does not include permission for a scanned version of the material to be stored in a central repository such as that provided by Heron/XanEdu.

Licensing material from an Elsevier book: A hyper-text link must be included to the Elsevier homepage at http://www.elsevier.com . All content posted to the web site must maintain the copyright information line on the bottom of each image.

Posting licensed content on Electronic reserve: In addition to the above the following clauses are applicable: The web site must be password-protected and made available only to bona fide students registered on a relevant course. This permission is granted for 1 year only. You may obtain a new license for future website posting.

17.**For journal authors:** the following clauses are applicable in addition to the above: Permission granted is limited to the author accepted manuscript version* of your paper.

*Accepted Author Manuscript (AAM) Definition: An accepted author manuscript (AAM) is the author's version of the manuscript of an article that has been accepted for publication and which may include any author-incorporated changes suggested through the processes of submission processing, peer review, and editor-author communications. AAMs do not include other publisher value-added contributions such as copy-editing, formatting, technical enhancements and (if relevant) pagination.

You are not allowed to download and post the published journal article (whether PDF or HTML, proof or final version), nor may you scan the printed edition to create an electronic version. A hyper-text must be included to the Homepage of the journal from which you are licensing at http://www.sciencedirect.com/science/journal/xxxxx. As part of our normal production process, you will receive an e-mail notice when your article appears on Elsevier's online service ScienceDirect (www.sciencedirect.com). That e-mail will include the article's Digital Object Identifier (DOI). This number provides the electronic link to the published article and should be included in the posting of your personal version. We ask that you wait until you receive this e-mail and have the DOI to do any posting.

18. **Posting to a repository:** Authors may post their AAM immediately to their employer's institutional repository for internal use only and may make their manuscript publically available after the journal-specific embargo period has ended.

Please also refer to Elsevier's Article Posting Policy for further information.

19. **For book authors** the following clauses are applicable in addition to the above: Authors are permitted to place a brief summary of their work online only.. You are not allowed to download and post the published electronic version of your chapter, nor may you scan the printed edition to create an electronic version. **Posting to a repository:** Authors are permitted to post a summary of their chapter only in their institution's repository.

20. **Thesis/Dissertation**: If your license is for use in a thesis/dissertation your thesis may be submitted to your institution in either print or electronic form. Should your thesis be published commercially, please reapply for permission. These requirements include permission for the Library and Archives of Canada to supply single copies, on demand, of the complete thesis and include permission for Proquest/UMI to supply single copies, on demand, of the complete thesis. Should your thesis be published commercially, please reapply for permission.

Elsevier Open Access Terms and Conditions

Elsevier publishes Open Access articles in both its Open Access journals and via its Open Access articles option in subscription journals.

Authors publishing in an Open Access journal or who choose to make their article Open Access in an Elsevier subscription journal select one of the following Creative Commons user licenses, which define how a reader may reuse their work: Creative Commons Attribution License (CC BY), Creative Commons Attribution – Non Commercial - ShareAlike (CC BY NC SA) and Creative Commons Attribution – Non Commercial – No Derivatives (CC BY NC ND)

Terms & Conditions applicable to all Elsevier Open Access articles:

Any reuse of the article must not represent the author as endorsing the adaptation of the article nor should the article be modified in such a way as to damage the author's honour or reputation.

The author(s) must be appropriately credited.

If any part of the material to be used (for example, figures) has appeared in our publication with credit or acknowledgement to another source it is the responsibility of the user to ensure their reuse complies with the terms and conditions determined by the rights holder.

Additional Terms & Conditions applicable to each Creative Commons user license:

CC BY: You may distribute and copy the article, create extracts, abstracts, and other revised versions, adaptations or derivative works of or from an article (such as a translation), to include in a collective work (such as an anthology), to text or data mine the article, including for commercial purposes without permission from Elsevier

CC BY NC SA: For non-commercial purposes you may distribute and copy the article, create extracts, abstracts and other revised versions, adaptations or derivative works of or from an article (such as a translation), to include in a collective work (such as an anthology), to text and data mine the article and license new adaptations or creations under identical terms without permission from Elsevier

CC BY NC ND: For non-commercial purposes you may distribute and copy the article and include it in a collective work (such as an anthology), provided you do not alter or modify the article, without permission from Elsevier

Any commercial reuse of Open Access articles published with a CC BY NC SA or CC BY NC ND license requires permission from Elsevier and will be subject to a fee.

Commercial reuse includes:

☐ Promotional purposes (advertising or marketing)

☐ Commercial exploitation (e.g. a product for sale or loan)

□　　Systematic distribution (for a fee or free of charge)

Please refer to [Elsevier's Open Access Policy](#) for further information.

21. **Other Conditions**:

v1.7

VITA

Education

University of Washington, Seattle, WA, Bioengineering, Ph.D., Completion Date: 03/15

University of Washington, Seattle, WA, Bioengineering, M.S., Completion Date: 08/09

University of Washington (UW), Seattle, WA, Bioengineering, B.S., Completion Date: 08/08

Co-currently attended McNeese State University (MSU) & high school, Lake Charles, LA, Chemical Engineering, Completion Date: 05/05

Funding and Fellowships

Marie-Curie Individual Fellowship through the European Research Commission (06/15-06/17)

National Institutes of Health – NIAMS - Ruth L. Kirschstein National Research Service Award for Individual Predoctoral Fellow (04/12 – 04/15)

UW College of Engineering Cohn fellowship (declined) (09/09)

UW Mary Gates Research Scholarship (Supervisor: Michael Regnier, Dept. Bioengineering) (09/07-08/08)

UW Mary Gates Research Scholarship (Supervisor: Pierre Mourad, Applied Physics Laboratory) (09/06-08/07)

National Institutes of Health Clinical Research Experience for Engineers Summer Research Program (06/07 – 08/07)

UW Mary Gates Honors Scholarship (merit award) (09/05-08/07)

MSU Honors Scholarship (merit award) (08/03-05/05)

Publications

Racca AW, Beck AE, McMillin MJ, Korte FS, Bamshad MJ, Regnier M "Defects of embryonic myosin in Freeman-Sheldon syndrome cause prolonged relaxation of skeletal myofibers" Accepted at HMG.

Moussavi-Harami F, Razumova MV, **Racca AW**, Cheng Y, Stempien-Otero A, Regnier M (2014) "2-Deoxy adenosine triphosphate improves contraction in human end-stage heart failure" *J Mol Cell Cardiol*. **79C:**256-263.

Racca AW, Beck AE, Rao VS, Flint GV, Lundy SD, Born DE, Bamshad MJ & Regnier M (2013). Contractility and kinetics of human fetal and human adult skeletal muscle. *J Physiol* (Lond) **591**, 3049–3061.

Garcia JD, Gofeld M, Ray Illian P, Loeser JD, Kliot M, McClintic AM, **Ward AW**, Yao A & Mourad PD (2013). Intense focused ultrasound as a potential research tool for the quantification of diurnal inflammatory pain. *Ultrasonics* **53**, 84–89.

Manuscripts in Progress

Racca AW, Klaiman J, Pioner JM, Beck AE, Bamshad MJ, Regnier M "Force-length dependence and Ca^{2+} - mediated activation and relaxation kinetics in human fetal cardiac myofibrils" In preparation.

Pioner JM, Klaiman J, **Racca AW**, Murry, CE, Regnier M "Contractility of myofilaments in human induced Pluripotent Stem-cell derived cardiomyocytes" In preparation.

Pioner JM, Klaiman J, **Racca AW**, Murry, CE, Regnier M "Contractility of myofilaments in human induced Pluripotent Stem-cell derived cardiomyocytes from patient cell lines of myofilament and non-myofilament mutations" In preparation.

Abstracts and Presentations*

Pioner JM, **Racca AW**, […],Childers MK, Murry CE, Regnier M (2015) "Contractile Properties of Myofibrils from hiPSC-derived Cardiomyocytes of Patients with Duchenne Muscular Dystrophy" Biophysical Society meeting, February 7-11, 2015, Baltimore, MD.

Pioner JM, Yang KC , Papon L, **Racca AW**, […],Murry CE, Regnier M (2015) "Cell and Myofibril Contractile Properties of iPSC-derived Cardiomyocytes from a patient with an MYH7 Mutation associated with Familial Cardiomyopathy" Biophysical Society meeting, February 7-11, 2015, Baltimore, MD.

Moussavi-Harami F, Razumova MV, Cheng Y, **Racca AW**, Stempien-Otero A, Regnier M (2014) "2-Deoxy adenosine triphosphate improves contraction in human end-stage heart failure" American Heart Association BCVS, July 2014, Las Vegas, NV. Poster presentation

*Racca AW, Beck AE, Bamshad M, Regnier M (2014) "Differences In Activation And Relaxation Kinetics Of Human Fetal Skeletal And Cardiac Myofibrils" Biophysical Society meeting, February 15-19, 2014, San Francisco, CA. Poster Presentation. *Biophys. J 106 (2), 562a*

*Racca AW, Beck AE, Bamshad M, Regnier M (2014) "Prolonged Relaxation Kinetics In Distal Arthrogryposis Skeletal Muscle Myofibrils With A MYH3 R672CMutation" Biophysical Society meeting, February 15-19, 2014, San Francisco, CA. Poster Presentation. *Biophys. J*, **106** (2), 771a

*Racca AW, Beck AE, Rao V, Bamshad M, Regnier M (2013) "Kinetics Changes in Distal Arthrogryposis Skeletal Muscle with MYH3R672C mutation" Biomedical Engineering Society meeting, September 25-28, 2013, Seattle, WA. Platform Presentation

*Racca AW, Beck AE, Rao V, Bamshad M, Regnier M (2013) "Contractile Properties of Human Fetal Skeletal Myofibrils" Biophysical Society meeting, February 20-24, 2013, Pittsburg, PA. Poster Presentation. *Biophys. J* **104**(2), 483a

Beck AE, McMillin MJ, **Racca AW**, Gildersleeve HIS, Shively KMB, Regnier M, Bamshad MJ (2013) "Identifying the Genetic and Molecular Basis of Clubfoot" NIH/NICHD Structural Birth Defects working group, April 8-10, 2013, Bethesda, MD. Platform presentation.

*Ward AW, Beck AE, Bamshad MJ, Regnier M (2010) "Congenital contracture syndrome caused by mutation in embryonic myosin heavy chain characterized by significant changes in adult muscle contractility" Biophysical Society meeting, February 20-24, 2010, San Francisco, CA. Poster Presentation. *Biophys. J* **98** (3) 542a–543a

*Ward AW, Flint G, Beck AE, Bamshad MJ, Regnier M (2010) "Contractile Properties of Human Fetal Skeletal muscle proteins" Biophysical Society meeting, February 20-24, 2010, San Francisco, CA. Poster Presentation. *Biophys. J* **98**(3), 346a

Beck AE, **Ward AW**, McMillin MJ, Korte FS, Regnier M, Bamshad MJ (2010) "Defects of embryonic myosin in Freeman-Sheldon syndrome cause reduced force and prolonged relaxation of skeletal myofibers" David W. Smith Workshop on Malformations and Morphogenesis, August 27th – September 1, 2010. Platform presentation.

Beck AE, **Ward AW**, McMillin MJ, Korte FS, Regnier M, Bamshad MJ (2010) "Defects of embryonic myosin in Freeman-Sheldon syndrome reduce force and prolong relaxation of skeletal myofibers" American Society of Human Genetics, November 2-6, 2010, Washington, DC. Poster presentation.

Glass IA, Beck AE, **Ward AW**, Mason J, Eisenhower M, Rieder M, Regnier M, Bamshad MJ (2009). "RNA expression analysis of all genes from skeletal muscles from staged human conceptuses provides proof of principle for creating a transcriptional 'Fetal Atlas' " David W. Smith Workshop on Malformations and Morphogenesis, August 5th - 9th, 2009. Platform presentation.

Beck AE, **Ward AW**, Rieder M, Regnier M, Bamshad MJ (2009) "Transcriptional profile of the embryonic myosin heavy chain gene *MYH3* responsible for two congenital distal arthrogryposis syndrome subtypes" American Society of Human Genetics, October 20-24, 2009, Honolulu, Hawaii. Poster presentation.

Beck AE, McMillin MJ, Korte FS, **Ward AW**, Regnier M, Bamshad MJ (2008) "Contractility of individual myofibers is altered in individuals with myosin mutations that cause Freeman-Sheldon syndrome" American Society of Human Genetics, November 2008, Philadelphia, Pennsylvania. Poster presentation.

Beck AE, **Ward AW**, Tanner BCW, Kreutziger KL, Regnier M (2008) "Decreased Ca^{2+}-binding in a Skeletal Troponin C Mutant Disrupts Cooperative Interactions between Thin Filament Regulatory Units in Rabbit Psoas Muscle" Biophysical Society 2008. Platform Presentation. *Biophys. J* **94**(2), 321–324